A Discrete Roughness Index for Longitudinal Road Profiles

Eric Jose Zamora Alvarez

Thesis submitted to the faculty of the Virginia Polytechnic Institute and State University
in partial fulfillment of the requirements for the degree of

Master of Science
In
Mechanical Engineering

John B. Ferris
Tana Tjhung
Saied Taheri

December 7, 2015
Blacksburg, Virginia

Keywords: Discrete Roughness Index (DRI), International Roughness Index (IRI), road roughness, impulse response, moving average filter

A Discrete Roughness Index for Longitudinal Road Profiles

Eric Jose Zamora Alvarez

Abstract

Engineers of off-road equipment, on-road vehicles, pavement, and tires must assess the roughness of a terrain surface for the design of their products. The International Roughness Index (IRI), a standardized means of assessing longitudinal road roughness, quantifies roughness based on the average suspension travel for a particular vehicle at a prescribed speed. The Discrete Roughness Index (DRI) developed in this work address fundamental limitations of the IRI. Specifically, the DRI is calculated for each discretely measured location along a terrain surface and is applicable to vehicles traveling at varying speeds and using parameters other than the Golden Quarter-Car on which the IRI is based. The development of the DRI begins with a consistent discretization of the terrain surface, vehicle response, and the IRI. Next the Fractional Response Coefficient is developed, the properties of which are critical in the development of the DRI. The DRI is developed and its properties are discussed through theory and simulation of the ASTM E1926-08 profile. One important property of the average DRI is that it converges to the IRI as the distance between sampled points becomes smaller, for the particular case when the Golden Quarter-Car model is simulated at 80 kph. The DRI is not an alternative to the standard IRI, therefore, but a widely applicable roughness measure of which the standard IRI is a single specialized application.

Dedication

To my parents, my sister, and family for their support and motivation.

Acknowledgements

I would like to thank my advisor, Dr. John B. Ferris, for his tremendous support throughout my research. From day one, he has always had the time to provide academic and research guidance. Dr. Ferris showed me how to approach and organize theory, concepts, and code in an effective manner. I am also thankful to Dr.Tjhung for his time and support in guiding my research and to Dr. Taheri, who was always welcoming and willing to spend time to discuss about my research.

Special thanks to Fiat Chrysler Automobiles (FCA), Surface Systems & Instruments (SSI), and John Deere for sponsoring my research, for their input into my research, and for their time.

Special thanks to the Vehicle Terrain Performance Laboratory for allowing me to work in the lab. I appreciate the support from my friends and colleagues within the lab.

Lastly, I am thankful for the support from my family. None of this would have been possible without them. Their motivation to keep pushing forward inspired me to follow my goal of completing my degree.

Table of Contents

List of Figures

List of Tables

Nomenclature

IRI	International Roughness Index, a measure of roughness on road profiles
T	Total simulation time
L	Length of road profile
i	Location index (typically of an excitation)
j	Location index (typically of a response)
i_a	Location index halfway between index *i* and *i+1*
Δu	Constant intervals of distance traveled
t_j	Time at which the vehicle is located at j^{th} location
N	Number of discrete road samples
z_j	Suspension travel at time t_j
$\dot{z}_j$	Suspension velocity at time t_j
z_{Road}	Road elevation
Δz_{Road}	Change in road elevation
$\lvert\dot{z}\rvert$	Rectified suspension velocity
f_{ij}	Fractional response coefficient for response at time t_j due to excitation at time t_i
DRI_i	Discrete Roughness Index value at i^{th} measured road profile location
DRI_{avg}	Average Discrete Roughness Index over the length of the road profile
z_s	Sprung mass displacement
z_u	Unsprung mass displacement
Δz_i	Change in suspension response due to i^{th} road excitation
$\omega(n)$	Hanning function output
$I_{\min}$	First value of the impulse response that is less than 1 percent of the peak value
I_r	Trimmed impulse response
I_u	Unit impulse response
z_{step}	Step excitation height
Δt_{delay}	Time delay used to calculate the impulse response from a step response

1. Introduction

Due to the ever-changing road conditions, roughness indices are necessary to monitor the road conditions for ride, comfort, and safety. Roughness indices quantify the vehicle response to terrain excitations and are used for the development and testing of vehicles, tires, and pavement surfaces. All road profiles, new and old, exhibit roughness. The roughness gradually increases with age, the volume of traffic, weather conditions, and other forms of pavement distress. The increase in roughness is mostly caused by the vehicle and terrain interaction [1]. As a result of the roughness, higher loading conditions arise onto the vehicle suspension and components. Vehicle suspension components are subject to cyclic loading and fatigue damage from road roughness [2]. Road profiles with high degrees of roughness significantly impact the fatigue life of vehicle components. In previous years, the American Association of State Highway and Transportation Officials (AASHTO) has reported an estimated $76.8 billion in annual costs due to poor road conditions [1]. Driving on roads needing repair, on average, costs a driver $377 annually in additional vehicle costs. For urban areas with a large population (over 500,000), the additional vehicle costs range from $178 to $832 [3].

Faults, breaks, slab distortion (curling), and potholes are examples of events that contribute to the roughness of road profiles [4]. Faults are differences in the road elevation across a joint or crack. A break is a region on a road profile that begins with a decreasing slope in road elevation and ends with an increasing slope. Curling is the distortion of pavement into a curved shape [4]. A pothole is a dip or hole on the road caused by continual wheel loading on the pavement. Fatigue cracks form and cause portions of the pavement to break and leave holes on the pavement. The most commonly used roughness index to estimate the roughness due to these excitations or events is the International Roughness Index (IRI), which quantifies road roughness based on an average measure of the suspension travel per distance traveled. One of the limitations of the IRI is finding the exact cause of the roughness, since the suspension travel is averaged to obtain a single roughness statistic. The Discrete Roughness Index (DRI) developed in this work relates the roughness contribution from any excitation along a longitudinal road profile to any location of interest to provide the user with refined and localized measurements of roughness. From the DRI, two important roughness values are presented in this work. The first value consists of a roughness value calculated at each sampled elevation point

indicating the overall roughness caused by the elevation point (excitation) throughout the entire span of the road. The second value consists of a single value (the average of the former values) that summarizes the roughness for the road (similar to the IRI), which under certain scenarios, converges to the IRI. Future work will investigate the integration of nonlinear suspension and tire elements into the quarter car vehicle model used to calculate the DRI. The objective of this future study will be to simulate a refined representation of vehicles.

Due to the road roughness, vehicle owners typically replace their suspensions at approximately 100,000 miles for cars and 250,000 miles for trucks [1]. A procedure that uses the probability density function of the IRI for U.S. roads to estimate the service life of truck suspensions is outlined by Zaabar and Chatti [4]. With this in mind, car manufacturers aim to improve vehicle components such that they effectively respond to changes in road profiles. Manufacturers typically design their vehicles for the 90-95th percentile of road roughness [1],[5]. From IRI data reported, an IRI value of 3.9 m/km corresponds to the 93rd percentile of roughness distribution in the U.S. [1] while an IRI value of 3.2 m/km corresponds to the 87th percentile of the roughness distribution [4]. The typical IRI range for roads in the U.S. is between 1 and 5 m/km [1]. It is suspected, that in some instances, similar IRI values can correspond to different degrees of damage since the IRI is a linear roughness measure based on the suspension travel. That is, a doubled IRI value is the result of twice the suspension travel endured for a road profile. Since suspension travel does not necessarily equate to suspension damage, methods used to calculate suspension damage use the suspension loading history of the vehicle [1],[2]. Using the concepts from previously-developed damage estimates, within this work, as an extension of the DRI, a Discrete Damage Index (DDI) is introduced for further study.

1.1 Motivation for Research

One major issue faced by both vehicle engineers and pavement engineers is the ability to assess the roughness of a road surface. For the chassis engineer, the road surface is the primary excitation to the vehicle [6], from which loads, deformations, stresses and strains arise. Typically, vehicle engineers are only able to measure the actual chassis loads in the final stages of the design when it becomes difficult and expensive to modify the chassis. One method of assessing the road roughness is to measure the suspension travel of the vehicle by onboard instrumentation. This method, however, has reproducibility and reliability issues since

suspension and other vehicle components tend to wear and change over time. A preferred method of assessing road roughness is to use terrain excitations, along with vehicle and tire models, in road simulations to predict chassis loads and obtain estimates of the resulting fatigue damage [7]. The results obtained from these simulations allow engineers to make educated design decisions, which decreases the time and cost spent in vehicle development. Terrain excitation data is also useful for pavement engineers to characterize the road surface for quality, comfort, durability, and safety. These characteristics are critical to monitor over time for pavement maintenance and to better understand the use of materials and processes in road construction. Therefore, it is of great importance to describe and analyze road surface data in order to understand the pavement conditions of the road and the vehicle-to-road interaction.

The current practice of assessing road roughness is to describe the road surface in terms of a longitudinal road profile. The American Society of Testing and Materials (ASTM) defines a longitudinal profile as the perpendicular deviations of the pavement surface from an established parallel to the lane direction, usually the wheel tracks [8]. Since the early 1980s, the standard for road roughness has been the International Roughness Index (IRI). The IRI is a measure of the average rectified suspension travel of a 'golden quarter car' model when it is simulated to travel along a given road at 80 kph. The parameters of the golden quarter car model reflect those of a typical passenger vehicle. Although the golden quarter car model is both linear and time-invariant, the roughness measure (i.e., the IRI) is not. Consider first the fact that the vehicle response has a significant delay between the excitation (the actual event on the road, the roughness of which is to be characterized) and the response (the motion of the suspension). That is, the vehicle is a causal system in which the excitation must precede the response and the response continues for some time after the excitation has occurred. This delay between excitation and response is convolved with the nonlinear measure of vehicle response, the IRI. Since the IRI is a nonlinear measure of vehicle response, superposition cannot explicitly be used to combine or decompose the IRI in terms of a specific event in the road.

The IRI is usually applied to rather long sections of road (approximately 160 meters) and is standardized to a single speed [9],[10],[11]. This can lead to misinterpretations of certain sections of roads. For instance, a single large event in a section of relatively smooth road can result in the same IRI as a road that has moderate events scattered throughout the road section [10]. Therefore, in certain situations, the IRI cannot distinguish between road surfaces that

contain different events. To improve the IRI estimates in these situations, users typically set shorter, fixed profile lengths in increments to localize roughness [10],[12]. Similarly, the calculation of the IRI at the prescribed speed of 80 kph may lead to unrealistic roughness measures if vehicles do not typically travel at 80 kph on the road being evaluated. For example, vehicle speeds of 110 kph on highways and 50 kph on city streets are typical.

1.2 Problem Statement

The primary objective of this work is to develop a Discrete Roughness Index (DRI), which addresses some of the limitations of the IRI. The DRI is developed such that the roughness of each discretely-measured location along of the road profile is calculated. The DRI can be applied to vehicles simulated to travel at speeds other than 80 kph, and allows for the vehicle to vary speeds along the length of the road. It should be clear that vehicle parameters other than the Golden Quarter Car parameters can be used; the details are straightforward and not provided in this work. The IRI is limited in that it is based on a golden quarter car parameters, which aimed to capture the response of a generic vehicle on a road surface [13]. Finally, the DRI is consistent with the current IRI usage. Specifically, the average DRI, when simulating the Golden Quarter Car at 80 kph, converges to the IRI as the sampling interval decreases. This is not simply demonstrated empirically, but is true by the definition of the DRI. The proof of this property of the DRI is developed in the body of this work.

1.3 Thesis Statement

The Discrete Roughness Index (DRI) developed in this work addresses some of the IRI limitations by localizing roughness and providing widely-applicable measures of roughness for discrete road excitations on a longitudinal profile.

1.4 Main Contributions

In this work, a Discrete Roughness Index (DRI) is developed such that it can be used in cases when the velocity is varied, which is more representative of city-driving than at a prescribed speed of 80 kph which is the current practice with the IRI.

The objective of the DRI is to form a general framework for roughness measures that:

- Increases the application of roughness measures to cases of varying speeds
- Localizes the roughness to specific locations on the terrain surface

- Remains consistent with the IRI such that the IRI becomes a specific example within the more broadly applicable DRI developed in this work

1.5 Publications

The following journal paper has been submitted:

- Zamora Alvarez, E. J., Ferris, J. B., Scott, D., Horn, E., 2015, "Development of a Discrete Roughness Index for Longitudinal Road Profiles", International Journal of Pavement Engineering (under review)

1.6 Thesis Outline

The remainder of this work is developed as follows. First a brief history of roughness measures and the genesis of the IRI is presented, followed by the definition and properties of the IRI. Next, the derivation and the definition of the DRI are presented. In the derivation, one of the main steps involves the calculation of the vehicle suspension travel from the elevation of the road profile, from which the change in suspension travel along the road profile is calculated. The definition and the derivation of the fractional response coefficient is then presented, which relates the contributions from localized events in the road profile to the change in the suspension travel at instances along the road. The change in the suspension travel, the fractional response coefficient, and the spatial increment between sampled road data are used to obtain the DRI, which indicates the roughness at all locations along a road profile. The DRI is then evaluated on sample road profiles, including the triangular-pulse road profile defined in ASTM E1926-08 [11]. A discussion of the roughness data obtained by the DRI and future work follow.

2. Background

2.1 Road Roughness and Measurement

Over the years, terrain measurement has progressed from vehicle response systems to vehicle independent systems. In the 1920s, measures of roughness were obtained by measuring the suspension stroke via instrumentation installed on the car [14]. These systems were referred to as response-type road roughness measuring systems (RTRRMS), road meters, or response-type systems. An example of such system is the Mays Ride meter developed in 1967 [14]. Most ride meters used transducers that would measure the accumulated suspension travel of a host vehicle, which typically consisted of a passenger vehicle, light truck, a van, or a trailer. The accumulated suspension travel was recorded in inches and was then normalized by the distance traveled to obtain an average rectified slope of the road, indicating a measure of roughness. Major drawbacks of these systems were that the results were typically not reproducible since the measurements obtained were heavily dependent on vehicle parameters that contributed to the vehicle response. Such parameters included, but were not limited to, the tire pressures, tire sizes, spring rates, shocks, and other properties that were likely to change over time. This method therefore led to unstable results with respect to time and often, the measurements obtained only applied to the particular host vehicle used. Since the applicability and reproducibility of the roughness measures obtained via response-type systems was limited, there was a lack of a standard roughness scale.

In the 1960's, GM developed an inertial profilometer to obtain direct measurements of the terrain [6],[15],[16]. The objective was to combine the methodology from the rod and level surveying method along with the Dipstick method of measuring profile elevation in order to survey the elevation for large networks of roads [11]. The profilometer used a road-following wheel that extended below a car or trailer to measure the relative movement of the vehicle's body to the road surface [15],[16]. A signal from an accelerometer attached to the body of the vehicle was integrated twice to obtain the absolute vertical position of the body. The difference from the wheel measurement and the accelerometer signal resulted in the measurement of the road elevation. Terrain measurements obtained from inertial profilers allow for more reliable measurements since they eliminate the source of human error present in static measurements of terrain elevation (road and level and Dipstick methods).

Since then, many vehicle-independent measuring systems have been developed to improve on the system GM built. For instance, current profilers such as the ones shown in Figure 1 use non-contacting sensors (lasers) in place of the follower wheel to allow for testing at higher speeds. An inertial navigation system (INS) is also used to cancel out the vehicle body motion from the terrain elevation measurements. Early profilers were limited to low speeds because the follower wheel tended to bounce and was fragile [14]. Newer systems also have built-in corrections for minor variations of the longitudinal speed of the vehicle, which was previously restricted to a constant speed in early systems [14]. Once the profile has been measured, the second step in calculating the roughness is to input the road elevation data into a computer algorithm to obtain an index that will indicate the roughness of the road profile.

Figure 1. Illustration of current inertial road profilers

The unevenness of the terrain can be statistically described by roughness indices [17]. Roughness indices are an important indicator of pavement conditions. Over time, pavement conditions can have an adverse effect on vehicle costs, safety, vehicle handling, and on road users [17]. Roughness can be defined as changes in road profile heights for wavelengths ranging from 0.5 m to 50 m [18]. The majority of proposed roughness indices result in an estimate reflecting the ride quality of longitudinal road profiles by evaluating the comfort, safety, or the dynamic loading due to the excitations of the road on the vehicle. Some indices rely on physical measurements of the vibrational response of the vehicle while others use a simplified mathematical vehicle model to obtain a response of the vehicle due to the road. The vehicle response may include, but may not be limited to, the roll, pitch, longitudinal or lateral vibration of the vehicle. From the vehicle response, the indices can be used to identify sections of roads

where there is an increased concentration of roughness, signifying portions of the road that cause the greatest vehicle response.

According to Múčka, characteristics of an appropriate roughness index for longitudinal road profiles should reflect the roughness for a typical vehicle speed for a given road, reflect the response of a vehicle using parameters indicative of a typical fleet of car currently used, detect road sections of low quality in a spatial interval, indicate road quality in terms of the vehicle to human body interaction, and be relatively simple to calculate [17]. The Profilograph Index (PrI) and the IRI are the most commonly used roughness indices in the U.S. Annually, each state reports the IRI values of their highway networks in the Highway Performance Monitoring System (HPMS) in accordance with Federal Highway Administration regulations [18].

2.2 The Standard Roughness Index- The International Roughness Index (IRI)

The IRI was developed to address the reproducibility and quantization issues of roughness on road profiles. The drawbacks of the early Response-Type Road Roughness Measuring Systems (RTRRMS) were that the results were inconsistent since the methodology heavily relied on the properties of the tested vehicles used to obtain the suspension response. The National Cooperative Highway Research Program (NCHRP) conducted research of RTRRMS with the intention of defining a computer program to calibrate them. Since response-type systems were popular among states, mathematical models were developed to emulate the output of response-type systems such that the index resulted in units of slope. Research conducted by the NCHRP led to the development of a particular set of vehicle parameters to be used in the calculation of the IRI, called Golden Quarter Car parameters. Thus, the IRI resulted in a "virtual response-type system" [14]. Today, the IRI is one of the most commonly used roughness indices. The Federal Highway Administration (FHWA) requires the use of the IRI to annually update the database of their Highway Performance Monitoring System (HPMS) [19]. Currently, the IRI is the only roughness index that has shown reproducible results with the use of a variety of road measuring equipment [20].

The International Roughness Index is defined as the average, simulated, accumulated, absolute suspension travel for the Golden Quarter Car traveling along a single wheel track at 80 kph, as shown in Equation (1) .

$$IRI = \frac{1}{L}\int_0^T |\dot{z}|dt \tag{1}$$

The variable $\dot{z}$ represents the suspension velocity (velocity difference of the unsprung mass and the sprung mass) due to the road excitations. The integral of $|\dot{z}|$ represents the total rectified suspension travel for the time, *T*, required for the vehicle to travel a distance, *L*, along the road being considered. For paved roads, the IRI typically ranges from 0-12 m/km, where a low index indicates a smooth road profile and comfortable ride and a high index indicates many events and depressions along the road profile [11]. The IRI for unpaved roads typically ranges from 0-24 m/km [11].

In calculating the IRI, the road elevation data is first passed through a 250 mm moving average filter before the Golden Quarter Car model is simulated. The moving average filter simulates the ability of the tire to reduce particular excitations from the road that may include surface irregularities and cracks. This behavior is known as tire enveloping and bridging [9]. Therefore, through this filter, the sensitivity of the IRI algorithm to sharp small wavelength events decreases in order to simulate the physical tire behavior. Note that the quarter car model and the moving average filter are both Linear Time-Invariant (LTI) filters that are used in the calculation of the IRI [9]. Once the road profile is accurately measured and the moving average filter is applied, the quarter car model is used to calculate the suspension velocity response for the road profile. As shown schematically in Figure 2, when the suspension velocity response is integrated, the IRI accounts for the accumulated displacement difference, *z*, of the vehicle sprung mass, z_s, and the unsprung mass, z_u, in response to the road excitation inputs, z_{road}.

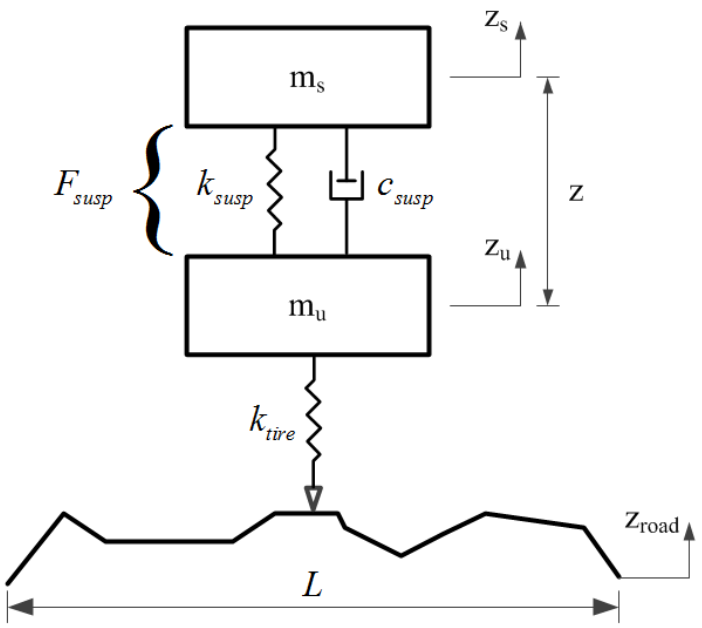

Figure 2. Schematic of quarter car model

Table 1 presents the golden quarter car parameters that are used in the calculation of the IRI. These parameters are chosen to make the simulation representative of a typical passenger car [10],[21]. The parameters are scaled according to the sprung mass of the vehicle in order to normalize the model for applicability into a larger range of vehicles. A constant vehicle speed of 80 kph is defined in the calculation of the IRI. The IRI is based on the parameters shown in Table 1 for a typical passenger car. Therefore, the functionality of the IRI is restricted to parameters pertaining to typical passenger cars. Part of the motivation for developing a roughness measure differing from the IRI is to have a wider applicability to all types of vehicles ranging from sports cars to commercial trucks.

Parameter	Value
Spring stiffness, k_{susp}	63.3 m_s
Tire stiffness, k_{tire}	653 m_s
Suspension Damping, c_{susp}	6 m_s
Unsprung mass, m_u	0.15 m_s

Table 1. Golden quarter car parameters normalized by the sprung mass, m_s

Depending on the selected baselength of the moving average filter, the IRI can either hide or reveal the changes in roughness throughout the length of the profile. The appropriate baselength chosen for the filter should reflect the points of interest along the road [20]. Different

interpretations of roughness can be obtained by selecting different baselengths of the moving average filter despite using the same IRI scale. As the baselength of the moving average filter increases, the greater the smoothing effect is on the road from the filter. By increasing the baselength, some of the road elevation content of the original profile can be lost. Decreasing the baselength allows for a greater refinement of localized events because the smoothing effect of the moving average is less. This would cause the IRI value to increase when compared to the previous case of increasing the baselength for the same road profile. A shorter baselength should be used to distinguish between specific road events. Short baselengths can reveal localized events in the road that could be obscured with longer baselengths. A longer baselength, such as 528 ft should be used to obtain a roughness statistic for networks of roads consisting of several miles in length [20]. Sayers recommends specifying roughness using two baselengths for pavement specifications. A long baselength, such as 528 ft, would be used to evaluate the entire length of road consisting of several miles, while a 20 ft baselength can also be used separately to monitor any events that may be obscured by the longer baselength [20].

Despite the widespread use of the IRI and the standard for measuring roughness that the IRI has established, the IRI exhibits some limitations that may need to be addressed. For instance, some limitations of the IRI are that the IRI can give similar roughness values for various sections of the road that vary significantly in road elevation. Another limitation is that the IRI is not applicable to all types of vehicles (mainly limited to passenger cars). The objective of the proposed DRI is to address improvements in some of the limitations of the IRI, specifically in the limitations discussed above.

Múčka discusses several other limitations of the IRI [18]. According to Múčka, the IRI has shown a limited ability to detect road quality on a highway after repairs were made. A possible reason for this was that the research development of the IRI was based on roads of low quality and low speeds. The IRI was developed when the maximum speed limit of 88.5 kph was in effect in the U.S. Another mentioned limitation is that the algorithm used to calculate the IRI has a weak sensitivity to wavelength contents below 2 m and above 20 m [18]. Therefore, despite the popular use of the IRI as a roughness statistic, there exist many areas of improvement to obtain refined measures of roughness.

2.3 Roughness Indices

Roughness indices have been developed to measure roughness, to evaluate the ride quality of a road profile, to calculate the vehicle response, and to localize roughness [18]. Of the roughness indices specifically outlined below, a majority are based on the IRI or have slight modifications to the IRI algorithm for calculating roughness. With some exceptions, most use a constant vehicle simulated speed and a simplified vehicle model. Many of the roughness indices also use vehicle parameters, such as the golden quarter car parameters, that are not indicative of the majority of current and actual fleets of vehicles. For each roughness index, a brief summary of the approach used to calculate roughness along with the associated limitations are provided. Table 2 summarizes the roughness indices discussed.

With respect to the Discrete Roughness Index (DRI) developed in this work, this developed index uses a quarter car model with the capability of integrating nonlinear suspension and spindle components to obtain refined representations of fleets of vehicles. Although a simplified vehicle model is used, the modularity of the constructed quarter car model allows for the substitution of various suspension models or tire models for a refined vehicle representation. The DRI can also be simulated at different constant speeds or in situations where the velocity is variable at each of the locations of the sampled road elevation points. Whereas a majority of the indices summarize the roughness of the road using a single statistic or value, one of the main features of the DRI is that the DRI evaluates the roughness at the location of each sampled road data point. Also, an average of these roughness values can be calculated to obtain an overall summary statistic for the entire road profile. A second distinguishing feature of the DRI is that in the calculation of the roughness at discrete locations, the DRI relates the contributions of previous excitations to the location of interest through the use of the estimated change in suspension travel, an impulse response function, and fractional response coefficients (Chapter 3). These two main features of the DRI are not examined in the indices outlined below.

2.3.1 Profilograph Index (PrI)

The PrI is used to measure the sum of deviations from a flat surface that occur beyond some tolerance over a road section of 100 m in length. The PrI is developed specifically for a particular measurement system, the profilograph, which only measures wavelengths in the range 0.3 m to 23 m [18]. This limited wavelength may result in an acceptable PrI rating for a road of

low ride quality. Another limitation is that since the index is based on a physical design and manufacturing of a particular measurement system, there are some repeatability and reproducibility concerns.

2.3.2 Spectrum Evenness Index (SEI)

The Spectrum Evenness Index (SEI) uses a 3-DOF quarter car model and is simulated at constant speeds of 80 kph for a truck and at 100 kph for a passenger car. The index is based on the frequency-weighted seat acceleration, the tire force, and the acceleration of the sprung mass. Limitations of the index include that a simple vehicle model is used and that since the power spectral density function is used to describe the road profile, some issues could arise in situations where the road profile is of an irregular shape because the power spectral density will not be able to approximate the irregular profile via a straight-line [18].

2.3.3 Truck Ride Index (TRI)

Truck Ride Index (TRI) uses a 3-DOF quarter truck model at a constant speed of 100 kph. The index indicates the frequency-weighted RMS vertical acceleration experienced at the driver's seat. This index has shown better correlation with ride comfort for heavy vehicles than the IRI [18]. Limitations of the TRI are that a constant velocity is used, a simple vehicle model is used, and only ride comfort is taken into account.

2.3.4 Longitudinal Evenness Index (LWI)

Longitudinal Evenness Index (LWI) or (LEI) evaluates the road profile based on ride comfort, ride safety, and the dynamic load of the road and sprung mass [22]. The LWI uses a passenger car model, a two-axle truck model, and a three-axle semitrailer model to obtain three vertical vehicle responses. The frequency weighted seat acceleration is obtained from the passenger car model, the tire force is obtained from the truck model, and the sprung mass acceleration is obtained from the middle axle of the three-axle semitrailer [18]. Each of these responses are weighted and the maximum value, based on a 100 m section, results in the LWI value [18]. Disadvantages of the LWI are that it may underestimate roughness and it is unclear which of the three responses influence the LWI value the most when evaluating the road profile.

2.3.5 Pavement Quality Index (PQI)

The Pavement Quality Index (PQI) is based on a 2-DOF quarter car model at a constant speed of 80 kph, which is very similar to the IRI to obtain the suspension response. The PQI takes into account ride quality with surface distress, but a disadvantage is that it has all of the limitations of the IRI, as mentioned previously. The PQI is a composition of two ratings: the Pavement Condition Rating (PCR) and the IRI [18].

2.3.6 Vehicle Response Index (VRI)

The Vehicle Response Index (VRI) was proposed in 2008 as an alternative index to the IRI, with the addition of variable velocity. The VRI uses the quarter car model for the calculation of the IRI and indicates a RMS value of the vehicle suspension response for wavelengths ranging from 0.5 m to 50 m [18]. The VRI has the same limitation as the IRI.

2.3.7 The Corrected Unevenness Index (C_w)

The Corrected Unevenness Index uses an 8-DOF truck model and a 12-DOF passenger car model to evaluate the ride comfort, safety, the dynamic load of the road, and the dynamic load of the sprung mass by taking into account the vertical acceleration of the driver's seat, the sprung mass acceleration, and the tire force [18]. Variable velocity can be used with this index. Limitations of the index are that it is limited in precisely locating the location of roughness in sections of the road profile, the index is for use in the frequency domain only, and it also exhibits the same issue of describing the road profile from the power spectral density as in the spectrum unevenness index [18].

2.3.8 Ride Quality Index (RQI)

The Ride Quality Index (RQI) uses measurements of the seat acceleration at various locations within a heavy vehicle to evaluate ride comfort. Variable velocities can be taken into account, but the RQI is limited to heavy vehicles [18].

2.3.9 Health Index (HI)

The Health Index (HI) uses the 2-DOF quarter car model to obtain a measure of the ride comfort by calculating the RMS values of the frequency-weighted acceleration of the sprung mass [18]. Limitations of the HI are that only ride comfort is considered, a constant velocity is used, and it is an alternative to the IRI meaning that it has the same limitations as the IRI.

2.3.10 Ride Condition Rating (RCR)

The Ride Condition Rating (RCR) calculates road roughness by calculating the root mean square of the vertical acceleration of a trailer axle [23]. The rating is based on a scale of 0-10, where a rating of 5 or 6 would indicate a need for repaving and a rating of 10 indicates a smooth road. Disadvantages of the RCR are that it is a response type road measuring metric and that it has less repeatability than the IRI [18].

2.3.11 Full-car Roughness Index (FRI)

The Full-car Roughness Index (FRI) uses full car model that captures the pitch, roll, bounce, and yaw of the vehicle to calculate a roughness measure [24]. A similar numerical approach of calculating the vehicle response by obtaining the state transition matrix and partial response matrix is used as in the IRI to compute the index value [24]. Results obtained showed that the vehicle speed and the footprint of the tire greatly influenced the calculated roughness measures [24]. Advantages of the FRI are that the index has less variance and higher repeatability than the IRI. However, some disadvantages include the greater computational effort required to calculate the FRI and the simplifications made in the full vehicle model, where the center of mass is assumed to be in the center of the rectangular frame [17]. Despite the numerous complex numerical models developed that include a higher number of degrees of freedom, such as roll and pitch, the vertical vibrational response of the vehicle remains the most significant for pavement excitations [25].

2.3.12 Roughness Index for Driving Expenditure (RIDE)

The Roughness Index for Driving Expenditure (RIDE) is calculated by taking the power spectral density of the sprung mass acceleration response of the reference vehicle to the road profile [17],[26],[27]. Some advantages of RIDE include that the index is related to ride comfort, it is suitable for identifying pavements that need resurfacing and it is sensitive to the excitation frequencies that are near the resonant frequencies of the sprung mass. Disadvantages of RIDE are that the index is heavily based on the vehicle parameters, such as the type of tires used, the sprung mass, the tire quality, and the dynamics of the vehicle suspension [17].

2.3.13 Half-car Roughness Index (HRI)

The Half-car Roughness Index (HRI) is similar to the IRI. The HRI utilizes both wheel track profiles from the vehicle instead of a single-wheel track profile [19]. The main difference between the HRI and IRI is that the HRI averages the two wheel profiles to obtain the measure of road roughness. Correlation studies by Sayer show that the HRI equals approximately 0.8 of the IRI value for paved roads [19]. For unpaved roads, the HRI is approximately 0.76 of the IRI value. The HRI exhibits the same limitations as the IRI.

2.3.14 Mean Roughness Index (MRI)

The Mean Roughness Index is similar to the HRI in that it uses both wheel track profiles. Instead of averaging the wheel track profiles, the IRI is computed for each profile and the resulting IRI values for the left and right wheel tracks are averaged to obtain the MRI [11]. The MRI also exhibits the same limitations as the IRI.

2.3.15 Dynamic Load Index (DLI)

The Dynamic Load Index measures dynamic truck-axle loading by calculating an index that is based on the variation of the road elevation in the frequency ranges of 1.5-4 Hz and 8-15 Hz [18]. The index focuses on these frequency ranges because the first set corresponds to truck bounce and the second range corresponds to axle bounce. These frequency ranges correspond to a truck speed of 96 kph. Limitations of this index are that it only focuses on the dynamic loading and that for heavy vehicles, the constants used to represent the variance of road elevation may not apply [18].

2.3.16 Heavy Articulated Truck Index (HATI)

The Heavy Articulated Truck Index is a profile-based roughness index that indicates sections of the road where there is poor ride quality for drivers and passengers of heavy trucks [18]. The index uses a 2-DOF quarter truck model to obtain a measure of the RMS suspension motion to evaluate ride comfort of heavy vehicles. A disadvantage of the index is that it is based on the IRI algorithm. The main differences are that different vehicle parameters and a different simulated vehicle speed are used.

Summarized in Table 2 are the discussed roughness indices, which are shown to compare the vehicle model used, the prescribed speed used to run the model, and the method used to evaluate roughness.

Roughness Index	Vehicle Model	Simulation Speed	Measures	Sensitive Wavelength Range
PrI	-	-	Physical measurement of road elevation deviations	0.3-23m
IRI	2-DOF Quarter Car	Constant 80kph	Relative Suspension Motion	1.2- 30 m
SEI	3-DOF Quarter Car	Constant 100 kph (car) 80 kph (truck)	Sprung mass acceleration, tire force, driver acceleration	-
TRI	3-DOF Quarter Truck	Constant 100 kph	RMS Vertical acceleration at driver to seat location	7.1-17.3 m [28]
LWI	2-DOF Truck 5-DOF semi-trailer 3-DOF Car	Constant 100 kph (car) 80 kph (truck)	RMS Seat acceleration, sprung mass vertical acceleration	1-40 m [29]
PQI	2-DOF Quarter Car	Constant 80kph	Relative Suspension Motion	-
VRI	2-DOF Quarter Car	Variable	RMS suspension motion	0.5-50 m
C_w	8-DOF Truck 12-DOF Car	Variable	RMS Seat Acceleration, sprung mass acceleration, tire force	-
RQI	-	Variable	RMS measurements of longitudinal and vertical acceleration of seat	0.61-15.24 m [28]
HI	2-DOF Quarter Car	Constant 80kph	RMS acceleration of sprung mass	1.2- 30 m
RCR	-	-	RMS vertical acceleration of trailer axle	-
FRI	Full Car	Constant 80kph	Relative Suspension Motion	-
RIDE	Reference vehicle	Constant 80kph	RMS acceleration of sprung mass	4.9-8.9m [28]
HRI	2-DOF Quarter Car	Constant 80kph	Relative Suspension Motion	1.2- 30 m
MRI	2-DOF Quarter Car	Constant 80kph	Relative Suspension Motion	1.2- 30 m
DLI	Profile-based	-	Truck-axle dynamic loading and road elevation variance	6.7-17.9 m 1.8-3.3 m
HATI	2-DOF Truck	Constant 100 kph	RMS vertical suspension motion	5-20 m

Table 2. A comparison of current roughness indices in use

2.4 Overview of the convolution integral and impulse response

Since the Quarter-Car model used in the calculation of the IRI is LTI, the convolution integral can be used to solve for the suspension response as a function of the road excitation,

which is briefly reviewed here. First consider a single event, specifically a unit impulse that occurs at time t_i. Next, consider the response of the suspension at some later time, t_j. The response of the suspension travel to this unit impulse is defined as the unit impulse response, $h(t_j - t_i)$ such as that shown in Figure 3. As the time elapsed between a particular response and an excitation increases, there is an oscillation and overall decrease in the magnitude of the impulse response.

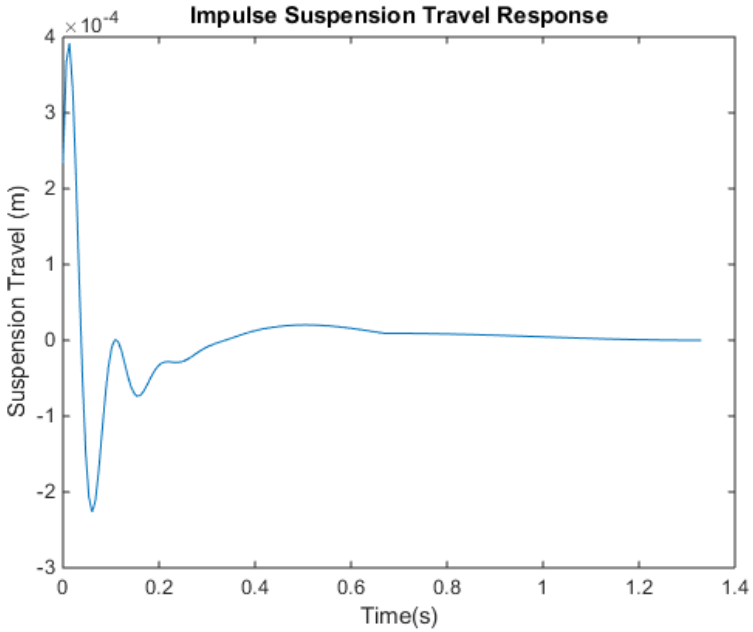

Figure 3. Unit impulse response

The unit impulse response is used to obtain the response of a LTI system at time t_j due to a single impulse of magnitude $F(t_i)\Delta t_i$ occurring at some previous time t_i. The fractional response, $\Delta z_i(t_j)$, is then the portion of the response at time t_j due to an impulse excitation at time t_i (a force, $F(t_i)$ that persists for the time interval Δt_i). This fractional response is shown in Equation (2) [30],[31].

$$\Delta z_i(t_j) = F(t_i)h(t_j - t_i)\Delta t_i \tag{2}$$

The total response of the system at time t_j is then the sum of the responses to excitations occurring before t_j, as shown in Equation (3).

$$z_j = z(t_j) = \sum_{i=1}^{j} \Delta z_i(t_j) = \sum_{i=1}^{j} F(t_i) h(t_j - t_i) \Delta t_i \tag{3}$$

If the limit is taken as Δt_i approaches zero, the convolution integral is obtained from the fundamental theorem of calculus as shown in Equation (4). The convolution integral is a mathematical operation of the input signal to an LTI system and its impulse response, which together, form the output of the system.

$$\lim_{\Delta t_i \to dt} \sum_{i=1}^{j} F(t_i) h(t_j - t_i) \Delta t_i = \int_0^{t_j} F(\tau) h(t_j - \tau) d\tau \tag{4}$$

Presently the discretized form of the convolution integral is used to calculate the suspension response as a function of the road excitation (Chapter 3).

2.5 Quarter car model dynamics for damage estimation application

For vehicle durability testing, the vertical road input is one the most important loading conditions [1],[4],[32]. For this reason, an analysis of fatigue damage is usually conducted by observing the response of a quarter car model at constant speeds on road profiles [2],[10]. Typical applications based on fatigue estimates include the explicit use of stresses and strains in the calculation of damage [10]. However, fatigue damage estimation methods exist based on the overall suspension loading of the vehicle instead of on a specific component [1],[2]. Although the quarter car model cannot exactly predict actual vehicle loads, the model captures important road characteristics for fatigue damage calculations [1],[2],[4]. One of the advantages of using the quarter car model is that the model is sensitive to the frequency range at which a vehicle typically encounters from road excitations. Thus, it captures the wavelengths that are relevant to motor vehicles. The quarter car model also emphasizes the frequencies around 1 Hz and 10 Hz, which are body and axle resonance, respectively [13]. The total force exerted on the sprung mass is input into a rainflow counting algorithm to estimate the damage in fatigue damage analyses [1],[2].

To recall, from previous measures of damage developed by [1],[2] the damage estimates are based on the loading history of the suspension of the vehicle. Figure 2 shows the region where the calculated suspension loads are located on the quarter car model (F_{susp}). Once the suspension loading response is obtained from the vehicle simulation, this loading history is filtered by a cycle counting method to obtain constant-amplitude cycles. This is necessary

because it is difficult to distinguish constant-amplitude cycles from the vehicle response since the terrain excitations are usually random in nature. The cycles counted are then input into a damage accumulation model to compute the damage.

2.6 Fatigue and life estimation

Fatigue is caused by cyclic changes in stress or strain. Fatigue is the resulting damage caused from the cyclic loading of a component [33],[34]. The damage process can consist of the generation of cracks, the propagation of cracks, and the failure of the component. Usually, a crack develops when the component experiences localized plastic deformation on a region of max stress. Over time, as the component endures a variable and cyclic loading history, the crack length increases, indicating prolonged damaged and eventual failure. To calculate fatigue life, there are three approaches that are commonly used. These approaches consist of the stress-life approach, the strain-life approach, and the crack growth approach.

Stages of fatigue include crack initiation and crack growth. In crack initiation, cracks usually originate from defects in the material structure. At the molecular level, these defects generate slip bands that spread along the maximum shear plane of the material [35]. The structural integrity of the material is therefore compromised. Under loading, cracks can increase in size and disrupt the stress flow. Usually, there is a large stress concentration at the crack tip, which causes crack propagation. Thereafter, cracks spread to the maximum tensile stress plane of the material. Some cracks remain small and the extent to which the crack grows depends on the energy required to overcome the grain barriers of the material [35].

For structural durability, stress or strain life analysis is conducted on a component. Stress life analysis is typically used for low stress and high cycle fatigue [36]. This type of analysis for estimating fatigue life can be used on engine components, transmissions, and other high speed rotating equipment. The stress-life approach is mostly used for load histories within the elastic range of the material. Advantages of the stress life approach is that it is simple to calculate, it is a good estimator for long life (high number of cycles), and that this approach has been extensively used and falls within a lot of fatigue test data. Disadvantages of this approach is that it is empirical and ignores the plasticity of the material [35]. Typical applications of the stress-life approach are for long life estimations, quick estimations, and for constant amplitude loading.

The Goodman line is one of the more conservative empirical curves to estimate alternating and mean stress effects on fatigue life and it is often used in practice [37]. The

Goodman relation is used to relate the alternating and mean stresses experienced by a part to the fatigue life of the part material. Thus, the Goodman line can be used to indicate whether a part will likely experience failure or not. For instance, if the combination of alternating and mean stresses lies to the right or above the Goodman line, part failure is likely to occur. Any alternating or mean stress configuration that lies below the line indicates that the part is not likely to fail. Examples of other empirical curves are the Soderberg, Gerber, and Morrow curves. The Soderberg curve is relatively more conservative than the rest and rarely used compared to the rest. Most fatigue test data tends to follow the Gerber and Goodman curves [38].

Strain life analysis is usually used for high stress, low cycle fatigue from road loads or other transient loading conditions. The strain life approach is suitable for time histories that contain large overloads or high stress concentrations. Plasticity and residual stresses can be modeled by this approach [35]. This method also is applicable to variable amplitude loading. Some of the disadvantages of using this approach is that it is more complex, some parts of the approach are empirical, and this approach only models the crack initiation. Typical applications are for long and short life, variable amplitude loading, and for components that experience infrequent large amplitude loading.

The crack growth approach models the growth of cracks for cyclic loading situations. This approach relates the presence of cracks and the effect cracks have on the strength of the part. Sequence loading effects can be tracked from this approach as well. Some of the weaknesses of this approach is that in estimating fatigue life, it is sensitive to the initial size of the crack, it is also sensitive to the geometry of the part, and it only investigates crack growth. Thus, the initiation of the crack is not taken into account. Applications for this approach would be to existing flaws or defects within the part and for the calculation of the residual life of the part after the initiation of the crack.

Fatigue analysis can also be conducted via finite element-based analyses. FEM is used to predict the stress and strain of individual components. Within the FEA software, virtual stress cycles [35] can be simulated. The fatigue life can also be predicted. Advantages of this method is that no prototype is required since all of the analyses are performed via simulations. It is also easy to modify existing features of the part of interest and observe the results. Disadvantages of this method are in some of the linear assumptions used for simplifying the model. Real world applications tend to exhibit nonlinearity. These analyses are also computationally expensive.

2.7 Fatigue analysis

Pseudo damage refers to a relative measure of the fatigue damage caused by the loading history of the vehicle [33]. For durability testing and modeling, a calculation of the pseudo damage from simple vehicle models allows for a quick comparison of relative damages caused by particular excitations from the terrain. The calculation involves the estimation of the fatigue life of the component(s) being investigated, the use of rain-flow counting, and the Palmgren-Miner rule to estimate the damage from the road excitations.

A general method to analyze fatigue data consists of conducting a computer simulation to generate a loading history (e.g. stress as a function of time), using a cycle-counting method to extract the variable loading amplitudes into constant amplitude loading cycles, and to then calculate the fatigue damage and life through a damage model such as the Palmgren-Miner rule. In many fatigue analysis methods, the suspension force was applied to a hypothetical structural suspension element with a cross sectional area in order to obtained a stress history [10]. This method uses a quasi-static approach in that it regards the suspension force as an input. The evaluation of road roughness through fatigue analysis methods have shown to be more sensitive in localizing short, rough sections of the road [10].

A fatigue damage index was defined by Johannesson et al., where the response considered is the force exerted on the sprung mass of the quarter car model [32]. Though the vehicle model is simplified and cannot be expected to exactly predict the loads experienced by a vehicle, the model serves to highlight the key road characteristics that play a role in the fatigue damage accumulation. The model uses suspension parameters representative of heavy vehicles. Since the vehicle-terrain interactions are random, it is necessary to extract constant amplitude cycles from a loading history in order to estimate the fatigue damage. This can be accomplished by a counting algorithm. Rainflow counting is one efficient counting method to convert a random loading history into constant amplitude loading cycles. Once these cycles are obtained, the Palmgren-Miner rule can be implemented to estimate the fatigue damage [4].

2.8 Cycle counting methods

The effects of a loading sequence on a component can be investigated by using cycle counting methods and through damage accumulation calculations. The objective of cycle

counting methods is to reduce complex variable amplitude loading histories into discrete constant amplitude events [34]. These events are then used to estimate fatigue damage.

Cycle counting methods are necessary for the calculation of the amplitude of a cycle when the amplitude varies with time. The loading parameter can include force, stress, strain, or other parameters of interest [39]. For a loading history with constant amplitude over time, it is relatively straightforward to determine the amplitude and the number of cycles. For variable amplitude loading, it is difficult to determine what exactly the amplitude of a cycle is or the length of a cycle. According to Yin et al., a good cycle counting method maximizes the ranges of a cycle [34]. In other words, the differences between the highest and lowest points on a loading history are more important than intermediate fluctuations.

2.8.1 One parameter cycle counting methods

For damage fatigue analysis, one-parameter cycle counting methods are inadequate because these methods do not relate the loading cycles, counted from a complex load history, to the local stress-strain hysteresis behavior [34]. Examples of one-parameter cycle counting methods are level crossing, peak-valley, and range counting methods and are explained in detail in [34].

A disadvantage of one-parameter cycle counting methods, such as simple range counting, is that this method does not take into account the sequence of the loading events or the material memory [33]. Yin defines a material memory event as a circumstance in which, under certain conditions, a closure of a stress-strain hysteresis loop is obtained. That is, when a stress-strain path is disrupted by a signal reversal, the path will continue from the point at which it was disrupted when the signal returns to the reversal value [33]. Other cycle counting methods, such as rainflow counting, are capable of retaining the material memory [33].

2.8.2 Two parameter cycle counting methods (Rainflow counting)

The rainflow cycle counting method is considered a two-parameter cycle counting method because it uses the two ranges from consecutive points to determine if there exists a cycle. According to Dowling (1979), rainflow counting methods lead to better fatigue life predictions [40]. Matsuishi and Endo in 1968 developed rainflow counting and a number of variations of this technique have since been developed [41]. This method was termed rainflow counting because of the similarity in raindrops dripping down a pagoda roof and running along

the roof edges. One of the benefits of using rainflow counting is that this method takes into account the entire loading history of the components and assumes that the structure of the component retains the effects of the loading history onto the structure (material memory) [33].

Rainflow counting is a useful cycle counting method for separating small oscillations from large oscillations without affecting the turning points. The output of a rainflow cycle counting algorithm is the max and min points of the cycle. These are then converted to amplitudes of the load. In fatigue damage calculations, small amplitude ranges can be disregarded because they don't cause cracks to propagate.

Once the time loading history has been transformed into a sequence of peaks and valleys, the rainflow counting method can be implemented by starting from either a peak or valley. The general rule is to follow the direction of the valley or peak ("flow" down like rain along a roof) until a reversal is reached. A reversal is essentially half of a cycle (from peak to trough or trough to peak). Then, generally speaking, the flow continues until the end of the time history or until the flow is interrupted by a previous flow or the flow reaches a peak of magnitude greater than the starting point.

2.8.3 Three-point rainflow counting

The three-point rainflow cycle counting method uses three consecutive points in a load history to determine if a cycle exists [34]. Take into consideration the magnitude of three consecutive points called S_1, S_2, S_3, where $\Delta S_1 = |S_1 - S_2|$ and $\Delta S_2 = |S_2 - S_3|$. As a general rule of thumb, if $\Delta S_1 > \Delta S_2$, no cycle exists from S_1 to S_2. If $\Delta S_1 \leq \Delta S_2$, then a cycle exists from S_1 to S_2. When a cycle is extracted, the value is recorded at the peak/valley of the first point and the value at the valley/peak of the second point is also recorded. Therefore, the output of a rainflow cycle counting algorithm would consist of the minimum and maximum values for each given cycle. The three-point method requires that the loading history contain only peaks and valleys and that it starts with either the peak or valley (whichever is greatest in absolute magnitude). Then, the rule discussed above is applied to every three consecutive points until a closed cycle is identified. Once a cycle is defined by two points, these two points are excluded and the previous (if it exists) and the following points are connected such that the procedure can be repeated. The range-pair counting method uses the same rule as discussed, but it does not require the load history to start with the max peak or lowest valley in magnitude [34].

2.8.4 Four-point rainflow counting

The four-point rainflow cycle counting method is similar to the three-point method, except that it uses four consecutive points to define a cycle. A general outline for the methodology of the four-point cycle counting method is defined below [34].

- First, four consecutive points are identified
- The inner range in defined as $\Delta S_I = |S_2 - S_3|$ and the outer stress range is defined by $\Delta S_O = |S_1 - S_4|$.
- If the inner range is less than or equal to the outer range $\Delta S_I \leq \Delta S_O$ and the points of the inner range are in between the points of the outer range, then S_2 to S_3 cycle is identified as a closed cycle.
- The two inner points are then excluded and the two outer points, S_1 and S_4, are connected.
- If there was no cycle formed in step 3, another check would be performed for the next four consecutive points.
- The process is repeated until there are no data points remaining

This counting method does not always form closed cycles with all of the data points. The data points that are remaining and that cannot define or form a cycle are the residue. Usually, these half cycles include the largest valley and peak from the history and may include other large events [42]. Therefore, it is possible that the most damaging events are not included within the rainflow algorithm. The residue can be treated as half of a complete cycle or treated as a full cycle. Treating the residue as a full cycle is a conservative approach in damage estimation [42]. To treat the residue from the four-point rainflow cycle counting method, the Cloormann/Seeger method can be used [43, 44]. This method results in all closed hysteresis loops [44].

Interestingly, the three-point rainflow cycle counts can be obtained from the four-point cycle counting method [34]. The procedure to obtain the three-point cycle counts is as follows:

- Use the four-point method to obtain the cycles and the residue
- Copy the residue and add to the original residue to form a sequence that is twice as long as the original residue
- Use the four-point method for this new residue sequence

- Use the defined cycles from step above and add to the original cycles found in the first step

Both of these cycle methods results in the same range-mean rainflow matrix. A rainflow matrix is a matrix showing the number of cycles in terms of the range and mean from the cycle counting. An advantage of using the four-point cycle counting method is that this method can also be used to reconstruct the load history from the cycles extracted. Another advantage is that the three-point rainflow matrix can be derived from the four-point rainflow cycles counted and the residue.

2.9 Overview of the Palmgren-Miner damage rule

The Palmgren-Miner rule is a simple cumulative damage model used to predict fatigue damage and failure. This is a commonly used approach in stress life calculations due to its simplicity and the fact that other nonlinear models require testing to validate the vehicle parameters being used, which may take longer to do. Fatigue damage is defined according to the cycle ratio, $\frac{n_i}{N_{f_i}}$, which is the cycle ratio of the number of load cycles to the corresponding fatigue life of that particular loading condition [34]. For the damage calculation, n_i is the number of cycles of a loading condition. The extent to which the fatigue life of the material is consumed depends on the level of operation of the loading condition and subsequent loading levels [45].

$$D = \frac{n_1}{Nf_1} + \frac{n_2}{Nf_2} + ... + \frac{n_k}{Nf_k} \tag{5}$$

From Equation (5), the total damage calculated can be simplified into the formulation shown in Equation (6). The material will fail due to fatigue damage when *D* is equal to 1 [46].

$$D = \sum_{i=1}^{k} \frac{n_i}{Nf_i} \tag{6}$$

2.10 Calculation of fatigue life from the Basquin relation

For high cycle fatigue, the Basquin relation can be used to describe the portion of the stress life curve for high cycle loading [47]. This relation describes the region of the S-N curve where the strains are elastic (low strain).

$$Nf_i = C^{-1}\left(F_{a_i}\right)^{-\beta} \tag{7}$$

In Equation (7), F_{a_i} is the stress amplitude, C is a material property constant, N_f is the fatigue life for an operating loading condition in cycles to failure, and β is the fatigue exponent [1],[2]. The fatigue exponent ranges from 4 to 25 [48]. In the transportation industry, a factor of 8 is commonly set for the structural materials used [48]. Typically, the fatigue exponent takes on the values between 3 and 8 [1]. The magnitude of the fatigue exponent dictates the quantity of damage caused by small and large cycles [2]. For a higher magnitude of the fatigue exponent, larger loads have a greater contribution to the total damage. The smaller the fatigue exponent, the greater the contribution of the smaller loads than larger load peaks to the damage. From the damage accumulation definition defined in Equation (6), the resulting damage formulation is shown in Equation (8) [1],[2].

$$D = C\sum_{i=1}^{k}\left(F_{a_i}\right)^{\beta} \tag{8}$$

From Equation (8), *k* is number of operational loading levels as defined by the number of bins from the rainflow counting.

2.11 Overview of calculating fatigue damage

The following is an overview of calculating fatigue damage:

- Obtain the loading history (suspension or spindle force) from the vehicle simulation
- Convert the loading history into local extrema (turning points)
- Input the turning points into the rainflow counting 4-point algorithm
- Calculate the amplitudes from the output cycle count
- Calculate the damage using the Palmgren-Miner rule from the cycle count

3. Development of the Discrete Roughness Index (DRI)

{A condensed version of this chapter has been submitted to the *International Journal of Pavement Engineering* and is currently under review}

One of the main objectives of a roughness index is to quantitatively describe the terrain and vehicle interaction. The most commonly used index is the International Roughness Index (IRI), which quantifies road roughness based on an average measure of the suspension travel per distance traveled. Many other roughness indices have developed a similar approach of using the suspension travel of a simulated vehicle to assess the surface roughness. One of the limitations of this approach is finding the exact cause of the roughness, since the suspension travel is averaged to obtain a single roughness statistic. The Discrete Roughness Index (DRI) presented in this chapter relates the contributions from any excitation along a longitudinal road profile to any response location of interest to provide the user with refined and localized measurements of roughness. In the development of the DRI, the road, the vehicle response, and the IRI are first discretized in a consistent manner. Next, the desired properties of a fractional response coefficient are defined and the fractional response coefficient is developed such that these properties are satisfied. Generally, the fractional response coefficient relates the contributions from localized events in the terrain surface to the change in suspension travel at instances along the surface. The DRI is then developed using the fractional response coefficient and the resulting properties of the DRI are explored. Of particular interest is the proof that the average DRI, when simulating the Golden Quarter-Car model at 80 kph, converges to the IRI as the sampling interval decreases. Finally, the DRI is validated on sample road profiles, including the triangular-pulse road profile defined in ASTM E1926-08 [11]. A discussion of the roughness data obtained by the DRI and concluding remarks complete this chapter.

3.1 DRI Discretization Process

3.1.1 Discretizing the Road

To begin the development of the DRI measure, it is assumed that accurately measured discrete sample points of the road elevation z_{Road} are available at constant intervals of distance traveled, Δu, which are shown schematically as small circles in Figure 4. Each location along the road at which a road elevation exists is indexed by a positive integer, i or j. An auxiliary set

of points are introduced that are located in the middle of these locations, at a distance $\Delta u/2$ from the nearest measured point, and are identified by index suffix, *a*.

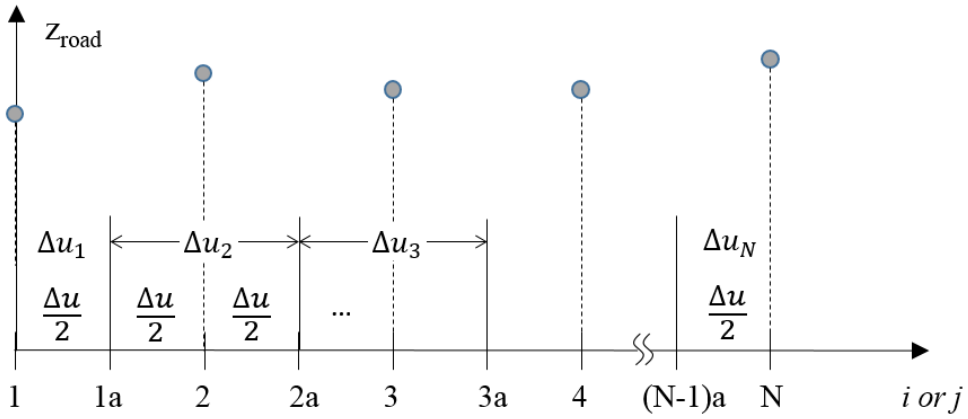

Figure 4. Indices of road elevation samples

It is clear that the true road profile is continuous and that these discrete measurements represent some small interval surrounding each discrete point. For example, the interval around the third measured point, defined as Δu_3, would span from index 2a to 3a and have length Δu. No extrapolation beyond the first and last measurements is made in this work, so that the interval about each discrete measurement is defined according to Equation (9).

$$\begin{aligned} \Delta u_j &= \frac{\Delta u}{2} && j = 1 \\ \Delta u_j &= \Delta u && j \in [2, N-1] \\ \Delta u_j &= \frac{\Delta u}{2} && j = N \end{aligned} \tag{9}$$

The length of the road, *L*, is then the sum of the length of these intervals, as shown in Equation (10).

$$L = \sum_{j=1}^{N} \Delta u_j = (N-1)\Delta u \tag{10}$$

It is then necessary to define the road excitation at each discrete location. Equation (11) discretizes the changes in road elevation such that there are *N* changes. This is accomplished by taking the average of the absolute forward difference and the absolute backward difference of the sampled road elevation data points. For the start and end points, half of the absolute forward difference and half of the absolute backward difference is calculated, respectively. The change

in road elevation plays a major role in defining the fractional response of the excitation on the suspension travel at a particular location along on the road profile.

$$\begin{aligned} \left|\Delta z_{road_i}\right| &= \left|\frac{z_{road_{i+1}} - z_{road_i}}{2}\right| && i = 1 \\ \left|\Delta z_{road_i}\right| &= \left|\frac{z_{road_{i+1}} - z_{road_i}}{2}\right| + \left|\frac{z_{road_i} - z_{road_{i-1}}}{2}\right| && i \in [2, N-1] \\ \left|\Delta z_{road_i}\right| &= \left|\frac{z_{road_i} - z_{road_{i-1}}}{2}\right| && i = N \end{aligned} \tag{11}$$

3.1.2 Discretizing the Vehicle Response

Once the road is properly discretized, the vehicle responses must be calculated, specifically the suspension travel. The details of how the vehicle is modeled and simulated is beyond the scope of this work, but some options are discussed as a means to direct future research. A simple example would be the quarter-car model shown in Figure 2 with constant coefficients for masses, spring stiffnesses, and damping. In this case, a continuous analytical solution can be determined. An alternative to the analytical solution is to use numerical simulation tools to determine the suspension response at discrete points. Given that some large modeling assumptions have already been made (e.g., that a real vehicle is adequately represented by a quarter-car model), proper numerical solution techniques will provide sufficiently accurate solutions for this application. In practice, an adaptive time step Runge-Kutta integrator would be used to determine the suspension response. These integrators can be programmed to deliver the suspension response at specified times and locations, or the responses provided by the integrator can be interpolated to find the responses at specific locations.

Regardless of the means used to calculate the suspension responses, the suspension response and the times at which these responses occurred (i.e., the time at which the vehicle traveled over these points) are calculated at both the original N measurement points (indexed by i or j) and the N-1 auxiliary points (indexed by i_a or j_a). The importance of knowing these times is critical since the DRI is developed such that it can be calculated even when the velocity varies over the length of the road. If the velocity varies and the spatial increment, Δu, is constant, then the time to travel between these indices must be permitted to vary. The time required to pass through the j^{th} interval is then Δt_j and defined in Equation (12).

$$\begin{aligned} \Delta t_j &= t_{ja} - t_j && j = 1 \\ \Delta t_j &= t_{ja} - t_{(j-1)a} && j \in [2, N-1] \\ \Delta t_j &= t_j - t_{(j-1)a} && j = N \end{aligned} \tag{12}$$

The DRI is a measure of the accumulated suspension travel, consistent with the seminal concept of the IRI. Although the suspension travel is continuous, it is calculated at discrete locations that represent some small interval surrounding each discrete point. For example, the suspension travel in the neighborhood around the third measured point, defined as Δz_3, would span from index 2a to 3a. An unbiased estimate of the change in the suspension travel is achieved by taking the absolute difference of the suspension travel calculated at the auxiliary points and the original measurement points. At the end points, either the absolute forward or backward differencing of the suspension travel is used. Therefore, for the purposes of estimating the suspension velocity, the change in suspension travel is estimated according to Equation (13).

$$\begin{aligned} \left|\Delta z_j\right| &= \left|z_{ja} - z_j\right| && j = 1 \\ \left|\Delta z_j\right| &= \left|z_{ja} - z_j\right| + \left|z_j - z_{(j-1)a}\right| && j \in [2, N-1] \\ \left|\Delta z_j\right| &= \left|z_j - z_{(j-1)a}\right| && j = N \end{aligned} \tag{13}$$

The estimated change in suspension travel and the time required for the vehicle to pass through the j^{th} interval are combined to estimate the suspension velocity in the j^{th} interval as given in Equation (14).

$$\begin{aligned} \left|\Delta z_j\right| &= \left|\dot{z}_j\right| \Delta t_j \\ \left|\dot{z}_j\right| &= \frac{\left|\Delta z_j\right|}{\Delta t_j} \end{aligned} \tag{14}$$

3.1.3 Discretizing the International Roughness Index (IRI)

In order to develop the DRI, the continuous form of the IRI (given in Equation (1)) is parsed in small intervals of time, Δt_j, that correspond to the intervals in which the road is discretized as shown in Equation (15).

$$IRI = \frac{1}{L}\int_0^T \left|\dot{z}\right| dt = \frac{1}{L}\left\{ \int_{t_1}^{t_{1a}} \left|\dot{z}\right| dt + \int_{t_{1a}}^{t_{2a}} \left|\dot{z}\right| dt + \ldots + \int_{t_{(N-1)a}}^{t_N} \left|\dot{z}\right| dt \right\} = \frac{1}{L}\sum_{j=1}^{N} \int_{\Delta t_j} \left|\dot{z}\right| dt \tag{15}$$

Clearly the magnitude of the suspension velocity, $|\dot{z}|$, is continuous within the discrete intervals. However, the estimated suspension velocity given in Equation (14) serves as an effective suspension velocity that is constant within each interval such that Equation (16) is true in the limit as Δt_j approaches zero.

$$\lim_{\Delta t_j \to 0} \int_{\Delta t_j} |\dot{z}| dt = |\dot{z}_j| \Delta t_j \tag{16}$$

Therefore, the discrete expression for the IRI is expressed in Equation (17).

$$\lim_{\Delta t_j \to 0} IRI = \frac{1}{L} \sum_{j=1}^{N} |\dot{z}_j| \Delta t_j \tag{17}$$

In the limit, the velocity of the suspension can be represented by Equation (14). It is assumed that the longitudinal velocity of the vehicle is nonnegative and therefore the time differences between successive responses must be nonnegative (i.e., $\Delta t_j \geq 0$), so that Equation (17) leads directly to Equation (18).

$$\lim_{\Delta t_j \to 0} IRI = \frac{1}{L} \sum_{j=1}^{N} \frac{|\Delta z_j|}{\Delta t_j} \Delta t_j = \frac{1}{L} \sum_{j=1}^{N} |\Delta z_j| \tag{18}$$

In this way, the IRI can be calculated either by Equation (17) or (18) depending on convenience. Also note that even if the calculation of the suspension response is derived from a linear time-invariant model, it is clear that the IRI is a nonlinear measure of roughness (due to the absolute value function). This is the first difficulty to overcome in defining a pointwise, discrete, roughness index. The second issue is that the suspension response occurs over a time period after the road excitation. This complicates the matter because at any moment in time the vehicle is responding to all the previous road excitations to some degree. This second issue motivates the development of a fractional response coefficient.

3.2 Properties of the fractional response coefficient

Consider the response of a vehicle at index *j*. At this moment, the vehicle is responding to all the previous road profile excitations, to differing degrees. Next, consider one such excitation occurring at index *i*. The fraction of the response at time *j* due to the excitation at location *i* is then defined as the fractional response coefficient, f_{ij}. Several constraints must exist

on this coefficient. Due to the causal nature of the vehicle dynamics, the response of the vehicle must occur after an event (the vehicle cannot respond to an event until it has occurred). This constraint is captured in Equation (19).

$$f_{ij} = 0 \qquad \forall i > j \tag{19}$$

The effect that an event has on the vehicle response at any moment in time can vary and, as provided in Equation (19), it is possible to have no effect at all. An event either affects the vehicle, or it does not. If it affects the vehicle, then the magnitude of that effect is to be quantified. In this way, the idea of a negative effect is meaningless and this constraint is written as Equation (20).

$$f_{ij} \geq 0\,, \ \forall i, j \tag{20}$$

The final requirement of the fractional response coefficient is that the sum of the coefficients must be equal to 1 over the entire domain of the road profile excitations (indexed by *i*) for every response location (indexed by j). That is, 100% of the response at any time must be attributable to some previous excitation. This constraint is written mathematically in Equation (21).

$$\sum_{i=1}^{N} f_{ij} = 1\,, \ \forall j \tag{21}$$

3.3 Defining the Fractional Response Coefficient

The coefficient f_{ij} is the fractional contribution from the excitation at location *i* at the response location *j*. That is, it is the fraction of the response at location *j* that is attributable to the excitation at location *i* and is defined in Equation (22), where the fractional response defined in Equation (2) plays a major role.

$$f_{ij} = \frac{\left|\Delta z_i(t_j)\right|}{\sum_{k=1}^{j}\left|\Delta z_k(t_j)\right|} \tag{22}$$

Although calculating the complete fractional response for each point is possible, it would be computationally expensive and, since many other simplifying assumptions have already been made, it would not provide additional insight into the development of a roughness index. As an alternative, a variation on the unit impulse response is used.

The derivation of the unit impulse response provided in Equation (2) is based on a force excitation exerted over a short period of time to form a unit impulse. In this work, the desired excitation is the road elevation, not an excitation force, so the unit impulse function is redefined as the suspension travel response due to an impulse in the road surface. The fractional response of the suspension travel is redefined as Equation (23).

$$\Delta z_i(t_j) = \Delta z_{road_i} h(t_j - t_i)\Delta t_i \tag{23}$$

The magnitude of the fractional suspension response depends on the time elapsed between the excitation (t_i) and the response (t_j). The fractional response coefficient is then estimated using the unit impulse response by substituting Equation (23) into Equation (22) thus forming Equation (24).

$$f_{ij} = \frac{\left|\Delta z_{road_i} h(t_j - t_i)\Delta t_i\right|}{\sum_{k=1}^{j}\left|\Delta z_{road_k} h(t_j - t_k)\Delta t_k\right|} \tag{24}$$

There is a subtle but critical difference in the way that the unit impulse response function is used in the convolution integral and how it is used in the definition of the fractional response coefficient developed herein. The convolution integral uses the sum of all the previous excitations (multiplied by the unit impulse response) to form the total response at any point in time. The fractional response coefficient uses the sum of the *magnitude* (the absolute value) of all the previous excitations (multiplied by the unit impulse response). The fractional response coefficient provides a quantitative measure of a particular excitation's effect on the system response at some response time relative to the other excitations for that particular response time.

3.4 Defining the Discrete Roughness Index (DRI)

The roughness attributable to a particular excitation is defined as the Discrete Roughness Index (DRI). The DRI for a particular location i is defined in Equation (25).

$$DRI_i = \sum_{j=1}^{N} \frac{1}{\Delta u_j} f_{ij}\left|\dot{z}_j\right|\Delta t_j \tag{25}$$

Note that Equation (25) is identical to the definition of the discretized IRI, given in Equation (17), with the addition of the fractional response coefficient developed in Equation (24). In the limit, the DRI can be written in terms of suspension travel as shown in Equation (26).

$$\lim_{\Delta t_j \to 0} DRI_i = \sum_{j=1}^{N} \frac{1}{\Delta u_j} f_{ij} \left| \Delta z_j \right| \tag{26}$$

3.5 Properties of the Discrete Roughness Index (DRI)

The usefulness of the DRI as a roughness measure is first demonstrated by developing the average DRI. It is shown that the average DRI, DRI_{avg}, converges to the IRI for the particular case when the simulated vehicle speed is constant at 80 kph and the Golden Quarter-Car model is used. The average DRI is shown in Equation (27).

$$\begin{aligned} DRI_{avg} &= \frac{1}{N} \sum_{i=1}^{N} DRI_i \\ &= \frac{1}{N} \sum_{i=1}^{N} \left(\sum_{j=1}^{N} \frac{1}{\Delta u_j} f_{ij} \left| \dot{z}_j \right| \Delta t_j \right) \\ &= \frac{1}{N} \sum_{j=1}^{N} \frac{1}{\Delta u_j} \left| \dot{z}_j \right| \Delta t_j \sum_{i=1}^{N} f_{ij} \end{aligned} \tag{27}$$

One of the properties of the fractional response is that the sum of the fractional response coefficients, f_{ij}, over all excitations, indexed by *i*, must sum to unity as given in Equation (21). Therefore the derivation of DRI_{avg} continues with Equation (28).

$$DRI_{avg} = \frac{1}{N} \sum_{j=1}^{N} \frac{1}{\Delta u_j} \left| \dot{z}_j \right| \Delta t_j \tag{28}$$

Since the first and last point in the summation differ from that of the middle points, a more explicit expression for Equation (28) is provided in Equation (29).

$$DRI_{avg} = \frac{1}{N} \left[\frac{1}{\Delta u_1} \left| \dot{z}_1 \right| \Delta t_1 + \sum_{j=2}^{N-1} \frac{1}{\Delta u_j} \left| \dot{z}_j \right| \Delta t_j \ldots \frac{1}{\Delta u_N} \left| \dot{z}_N \right| \Delta t_N \right] \tag{29}$$

Substituting Δu_j as defined in Equation (9) and Δt_j as defined in Equation (12), the following simplification is performed to obtain the discretized IRI equation as defined in Equation (17).

$$
\begin{aligned}
DRI_{avg} &= \frac{1}{N}\left[\frac{2}{\Delta u}\left|\dot{z}_1\right|\frac{\Delta t}{2} + \sum_{j=2}^{N-1}\frac{1}{\Delta u}\left|\dot{z}_j\right|\Delta t ... \frac{2}{\Delta u}\left|\dot{z}_N\right|\frac{\Delta t}{2}\right] \\
&= \frac{1}{N\Delta u}\left[2\left|\dot{z}_1\right|\frac{\Delta t}{2} + \sum_{j=2}^{N-1}\left|\dot{z}_j\right|\Delta t ... 2\left|\dot{z}_N\right|\frac{\Delta t}{2}\right] \\
&= \frac{1}{N\Delta u}\left[\left|\dot{z}_1\right|\Delta t + \sum_{j=2}^{N-1}\left|\dot{z}_j\right|\Delta t ... \left|\dot{z}_N\right|\Delta t\right] \\
&= \frac{1}{L}\left[\left|\dot{z}_1\right|\Delta t + \sum_{j=2}^{N-1}\left|\dot{z}_j\right|\Delta t ... \left|\dot{z}_N\right|\Delta t\right] \\
&= \frac{1}{L}\sum_{j=1}^{N}\left|\dot{z}_j\right|\Delta t = \lim_{\Delta t_j \to 0} IRI
\end{aligned}
\tag{30}
$$

By definition then, the average DRI converges to the IRI as the time steps become smaller whenever the DRI is simulated for a special case: using the Golden Quarter-Car model simulated at 80 kph. It should be clear, however, that the DRI is not limited to this special case, but merely demonstrates the compatibility with the standard IRI measure.

3.6 Obtaining the impulse response function, *h*

A quarter car vehicle model was simulated on a road with an impulse excitation to obtain an impulse response of the suspension travel. Initial static deflections for the sprung and unsprung mass are given for the initial conditions and once the vehicle reaches a steady state condition such that all of the vehicle states are approximately zero, the vehicle is simulated on a flat road with a step excitation. A sampling interval of the same width as the sampled road profile and a constant vehicle speed of 80 kph were used for the simulation.

To obtain the impulse response, a step excitation was used in the simulation. Such approach was considered because the Runge-Kutta integration solver used by MATLAB does not recognize the impulse excitation (single point) at a far distance along the road from the starting point. The impulse response was calculated by first obtaining the step response of the vehicle. Next, a time vector with a delay of 0.0001 seconds was defined by subtracting 0.0001 seconds from the original step response time vector. The step response was then interpolated with the new offset time vector values to obtain the delayed step response in terms of this newly defined time vector. To obtain the impulse response, the delayed step response was subtracted from the original step response. The impulse response was then normalized by the product of the

height of the step excitation and the delay in order to obtain the unit impulse response shown in Equation (31).

$$I_u = \frac{I_r}{z_{step}\Delta t_{delay}} \tag{31}$$

Since the impulse response eventually settles to zero, the impulse response was then trimmed to maintain the response to within a reasonable length. The trimmed length of the impulse response was defined by setting the last point of the response as the last point that was greater than one percent in magnitude of the maximum peak of the impulse response. This procedure causes the last point of the impulse response to result in a very small, but non-zero value. Therefore, a Hanning window was applied from the last point of the impulse response $I_{\min}$. Equation (32) was used to apply a Hanning window from $I_{\min}$. 98 additional points were added to the impulse response to obtain a smooth decay of the response to zero.

$$\omega(n) = I_{\min}\left(\frac{1+\cos(\pi n)}{2(N-1)}\right) \tag{32}$$

The impulse response for a quarter car model that uses golden quarter car parameters is shown in Figure 3. Note that for different vehicle parameters and simulated vehicle speeds, a different impulse response will be calculated by the algorithm that computes the DRI. The results shown were those for a golden quarter car vehicle model at a prescribed speed of 80 kph. These parameters were chosen for preliminary tests for the DRI. These results are further discussed in Section 3.7.

3.7 DRI Simulation Results

3.7.1 First simulation and explanation of the DRI on ASTM E1926-08

The first simulation shows the DRI results for the triangular pulse road defined in ASTM E1926-08 [11], shown as a solid line in Figure 5. The ASTM standard provides road surface heights at a constant spatial increment of 0.15m, prescribes a simulated constant vehicle speed of 80 kph and prescribes the use of the Golden Quarter-Car model. The road profile consists of 101 discrete road points. Only 27 of the 101 points of the road profile and the DRI plot are shown in Figure 5. The rest of the points consist of no elevation and the calculated DRI for these points is zero. For ease of explanation, the x axis of the plot was changed to discrete points instead of distance. Hence, each discrete point is an excitation of the road profile. Noticeable points on the

Figure are points 9 and 13. Discrete point 9 resulted in the highest DRI value. Discrete point 13 is the max road elevation and resulted in one of the lowest DRI values.

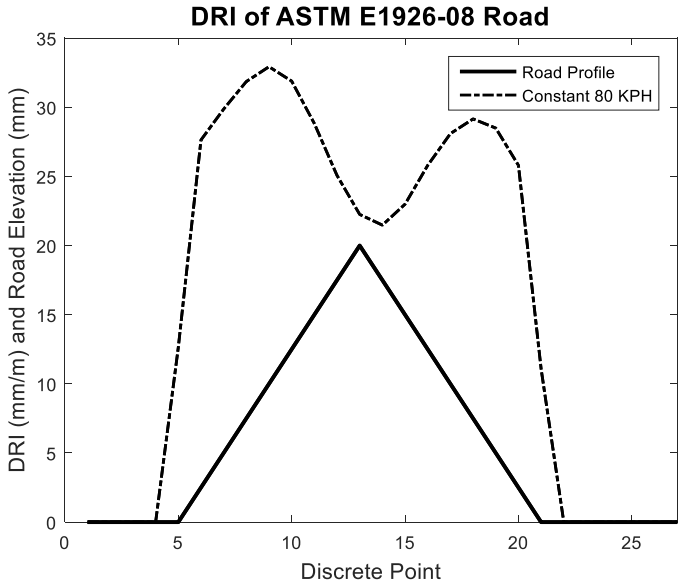

Figure 5. DRI plot of ASTM E1926-08 road profile at a constant 80 kph

Although it may seem counterintuitive as to why the highest road elevation point does not result in the highest DRI value, there are many factors to consider that influence the DRI calculation. One of the factors to consider is the change in the suspension response (defined in Equation (13)) of the vehicle over the triangular pulse event on the road. The plot on the right of Figure 6 shows the change in the suspension travel history for the complete road profile. Since, the road excitations lie within approximately the first 25 road data points, further attention is given to the left plot of Figure 6.

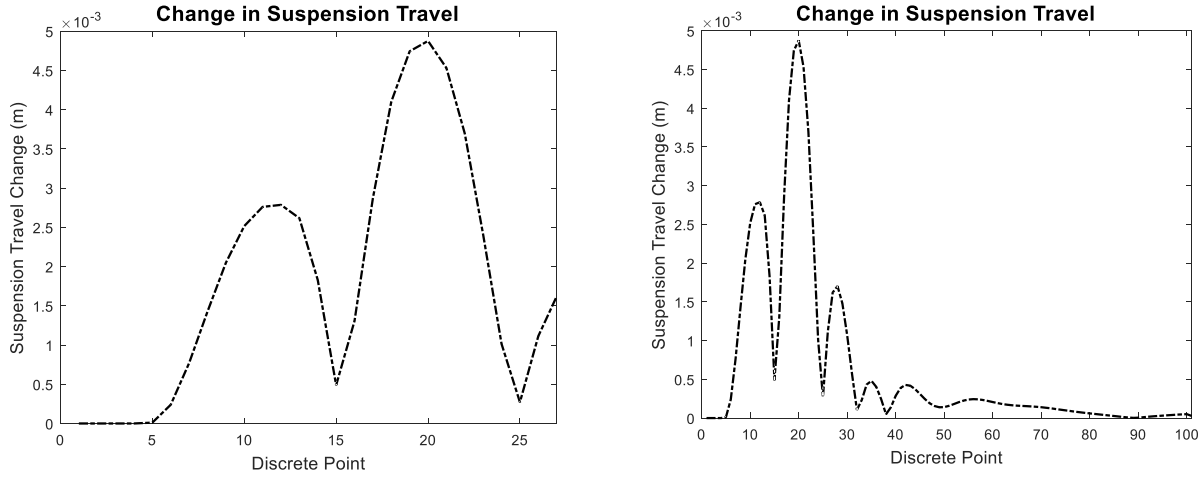

Figure 6. Change in suspension travel response for ASTM E1926-08 profile

The difference between the DRI values at points 9 and 13 is that DRI_9 captures the locations of the greatest change in suspension travel. To recall, from Equation (25), DRI_9 takes into account the change in suspension travel starting from point 9 and onward. Previous points are not considered since the fractional response coefficient, f_{ij}, will be zero due to the constraint set forth in Equation (19). Therefore, for DRI_{13}, only the change in suspension travel from point 13 and onward is taken into account. Thus, DRI_{13} does not include some of the peak values in the change in suspension travel values (points 9, 10, 11, and 12) as DRI_9. Instead, DRI_{13} mostly captures the points of the lowest change in suspension travel response around the peak elevation of the road profile.

Although DRI_9 and DRI_{13} capture the greatest peak of the change in suspension travel that occurs near points 17 through 22, the contribution of excitations 9 and 13 are not as significant at the locations of points 17 through 22 due to the magnitude of the impulse response and the fractional response coefficients pertaining to these discrete points. The magnitudes of the fractional response coefficient values and the magnitudes of the impulse response for excitations 9 and 13 are shown on Table 3 and Table 4, respectively.

Excitation, *i*	Response Location, *j*													
	9	10	11	12	13	14	15	16	17	18	19	20	21	22
9	0.149	0.223	0.238	0.199	0.123	0.046	0.014	0.053	0.075	0.082	0.075	0.062	0.047	0.033
13	0.000	0.000	0.000	0.000	0.111	0.167	0.168	0.136	0.087	0.035	0.012	0.047	0.072	0.091

Table 3. Fractional response coefficients for excitations 9 and 13

From Table 3, road excitation 9 has the greatest contributions at points 9 through 13 before decreasing to 0.046 at point 14. The reason for the decrease in the contribution is due to the decrease in the magnitude of the impulse response at location 14, which is 9.7 as shown in Table 4. To recall, the magnitude of the impulse response plays a major role in the calculation of the fractional response coefficient in Equation (24). Thus, as a major takeaway, DRI_9 results in a greater DRI value than DRI_{13} since the greatest contributions from 9 occur at the locations of the greatest change in suspension travel (Figure 6). Excitation 13, which is the peak of the road elevation profile, exhibits the greatest contributions at the locations of the lowest change in suspension travel. Although there is a peak in the change in suspension travel response near points 17 through 22, the contributions from excitations 9 and 13 have diminished significantly, which is shown in Table 3.

Excitation, *i*	Magnitude of Impulse Response at Location, *j*													
	9	10	11	12	13	14	15	16	17	18	19	20	21	22
9	21.0	35.0	38.9	34.2	23.1	9.7	3.3	13.4	20.0	22.6	21.3	17.9	12.9	8.2
13	0.0	0.0	0.0	0.0	21.0	35.0	38.9	34.2	23.1	9.7	3.3	13.4	20.0	22.6

Table 4. Magnitudes of the impulse response for excitations 9 and 13

Figure 3 illustrates the trend shown in Table 4. As the time elapsed between excitations and response locations increase, the magnitude of the impulse response decreases overall. Other factors shown on Equation (24) that influence the fractional response coefficient are the change in road elevation and the time duration of the excitation. Due to the nature of the road profile elevation and a constant vehicle speed of 80 kph, these factors did not contribute much to the DRI calculation when relatively comparing the values from excitations 9 and 13. Since the road profile is a triangular pulse with a constant slope in the rise and the decrease of the road elevation, the change in road elevation is the same for these points. Since a constant speed was used for this simulation, the duration of all the excitations is also the same. Therefore, for simulations in which the speed is constant and there is not much change in the road elevation, the impulse response and the change in the suspension travel response have a greater contribution in the calculation of the DRI values.

From the investigation conducted, the magnitude of the DRI values for each location along the road profile is significantly influenced by the change in the suspension travel at a location, the magnitude of the impulse response that relates the time elapsed between the excitation location and the location of the response, the change in the road elevation, and the duration of the excitation. Depending on the magnitude of these four factors, the magnitude of the DRI at a specific location will vary accordingly. For instance, to summarize, the maximum DRI value possible for a location is obtained when:

- The excitation of interest captures the greatest change in the suspension travel response
- The duration of the excitation is long, which is determined by the speed of the vehicle. (The slower the vehicle speed over the excitation, the longer the duration)
- The excitation exhibits the greatest change in road elevation

- The excitation exhibits the greatest contribution to the change in the suspension travel at instances where the vehicle model experiences the greatest changes in the suspension travel. For instance, the magnitude of the impulse response from the excitation is large at such locations. Usually, these locations are within close proximity to the excitation (due to the nature of the impulse response curve in Figure 3).

Table 5 shows the comparison of the IRI statistic used to summarize the roughness of the road profile and the average DRI value. To recall, the average DRI value is calculated by averaging the roughness at each discrete point. Thus, the average of 101 excitations results in a roughness value of 4.3154 mm/m. The main difference from the IRI and the average DRI is that the average DRI is an actual average of the roughness values obtained at each measured location of the road profile. The IRI is a statistic based on the average suspension travel per distance. The IRI statistic is not based on localized roughness, rather it is influenced by the amount of suspension travel throughout the entire road profile and the road distance traveled. One of the advantages of the DRI is that it is consistent with the roughness scale that the IRI adheres to. Closer convergence to the IRI can be obtained with a refined sampling interval, which is discussed in Section 3.8.1.

Simulated Speed	IRI (m/km)	Average DRI value (mm/m)	Percent Difference (%)
Constant 80 kph	4.3685	4.3154	1.216

Table 5. IRI and average DRI comparison

3.7.2 Investigation of road events on the DRI

Figure 7 shows the DRI for a plot with varying road events. Five distinct events are shown, the first of which is a similar triangular pulse found in ASTM E1926-08. A similar DRI curve is obtained for this event as previously shown.

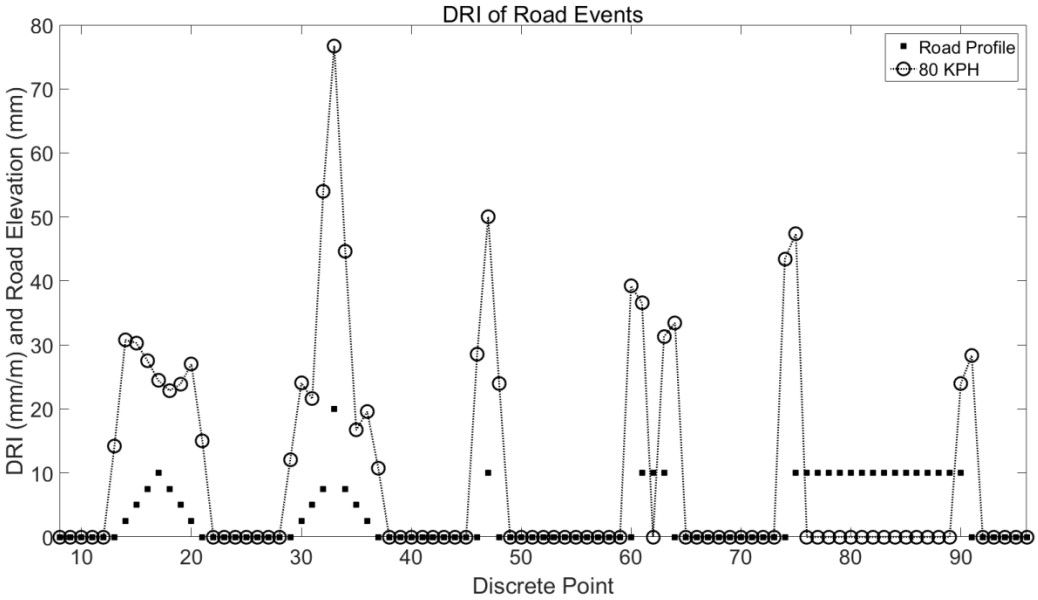

Figure 7. DRI of road profile containing varying events

The second event consists of a similar triangular pulse, with a peak elevation twice in magnitude as the previous triangular pulse. This event is significant because there is an abrupt change in the road elevation from discrete points 32 through 34. Point 33 exhibits the greatest change in road elevation, followed by points 32 and 34. Correspondingly, points 32 through 34 exhibit the highest fractional response coefficients. A significant contributor to the increased coefficient is the change in road elevation for these points. Thus, a higher rate of change in the road elevation can lead to a higher fractional response coefficient. Of course, the magnitude of the coefficient is also determined by the magnitude of the impulse response. Therefore, excitations within a close proximity of the response locations that exhibit a high rate of elevation change exhibit high fractional response coefficients. The greater the instances that an excitation matches its greatest contribution to the greatest change in the suspension travel, the higher the DRI value will be for that particular excitation. This is the explanation for the noticeable increase in the DRI plot at points 32 through 34.

The third event is a single point elevation of 10 mm. This event is essentially a one-point step excitation that generates three nonzero values. Two DRI values attribute from the estimation of the change in suspension travel at the auxiliary points (halfway between the nonzero and flat elevation) and the estimation of a road excitation (Equation (11)). The third DRI value is due to the excitation itself.

The fourth event is a step consisting of three elevation points of 10 mm. For this event, five nonzero DRI values are obtained. Again, two DRI values are due to estimating the change in the suspension travel at the auxiliary points (halfway between the zero and nonzero elevation points on both sides of the event and the definition of a road excitation). The remaining DRI values pertain to the nonzero elevation points that form the event. Notice that for the middle discrete point of the event (point 62), the DRI abruptly becomes zero. This is due to the lack of change in road elevation from the previous road elevation point. Since the slope is zero, this drives all of the fractional response coefficients to zero due to a lack of excitation. The last event is a longer step consisting of 15 elevation points of 10 mm, further illustrating the result that the DRI is zero when there is no road excitation (elevation change).

3.7.3 Simulation of ASTM E1926-08 at different constant vehicle speeds

The leftmost plot of Figure 8 shows the DRI of the road profile for constant speed scenarios. The first constant speed simulated was 40 kph (25 mph) which represents a typical residential zone speed. The second speed of 80 kph was used for comparison purposes, since it is the speed at which the IRI is computed. The third speed of 120 kph (75 mph) is representative of highway speeds.

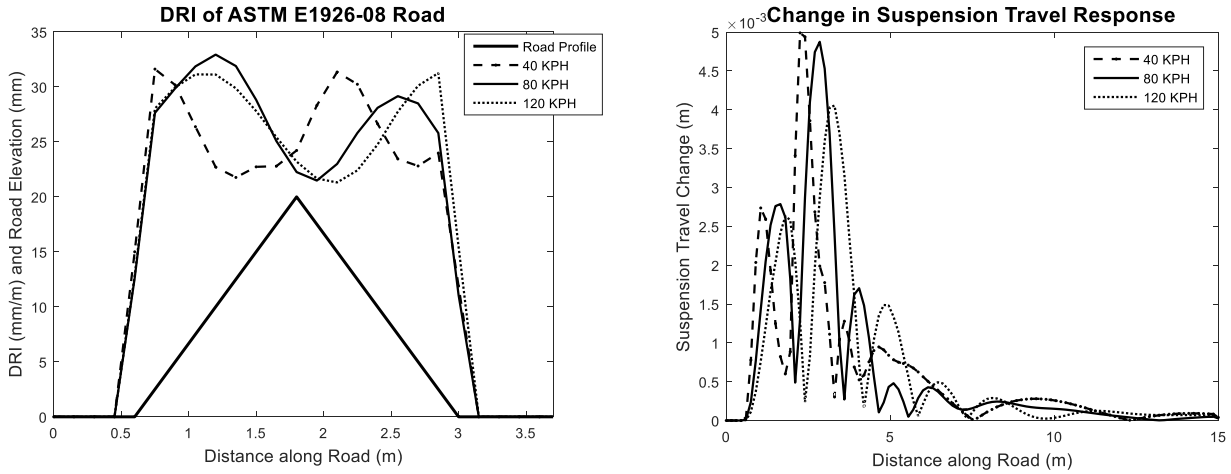

Figure 8. Simulation of ASTM E1926-08 profile at different constant speeds

As shown from the left plot of Figure 8, different regions of the road profile result in increased roughness based on the vehicle speed. For instance, the regions of the road where the roughness is at a peak for 80 kph, the roughness is relatively low for 40 kph. The roughness trend for 120 kph is similar to that of 80 kph. The main difference is that the roughness for 120

kph is slightly lower than that calculated for 80 kph. Part of the reason for the difference in the DRI plot is due to the horizontal offset applied to the change in the suspension travel response based on the vehicle speed. Thus, different portions of the road will result in greater or less roughness based on where the peaks of the change in suspension travel response align with the road profile. A general observation from the right plot of Figure 8 is that the greater the constant speed, the greater the extent to which the response is shifted to the right. The relative peak size of the response also reduces with an increase in speed. Therefore, with an increased constant speed, greater roughness is experienced at a delayed occurrence along the road when relatively compared to lower simulated vehicle speeds.

Vehicle Speed (kph)	40	80	120
Average DRI	4.1191	4.3154	4.2979

Table 6. Average DRI for each simulated constant vehicle speed

Table 6 shows the averaged DRI values for each vehicle speed. As a summary statistic of the road, the average DRI indicates that higher roughness is obtained at greater constant vehicle speeds. One of the advantages of the DRI is the duality of the DRI. Although the overall roughness statistic (similar to the IRI) may not indicate much based on the vehicle speed, the DRI plot allows for the interpretation of which regions of the road exhibit the greatest roughness based on the vehicle speed.

3.7.4 Varying speed simulation of ASTM E1926-08

Figure 9 shows the DRI of ASTM E1926-08 for three different vehicle speed scenarios. The first scenario (shown as a dash-dot curve) consists of a constant speed of 80 kph, which is the simulated speed of the golden quarter car model used to calculate the IRI. The second speed condition consists of a gradual increase in speed from 59 kph to 80 kph (36 mph to 50 mph). This speed represents the speed at which the vehicle encounters the triangular pulse excitation for approximately the first 3.2 m of the road profile. A reasonable speed range was chosen such that the speed can vary within 3.2 m. For the third speed condition, the initial speed of the vehicle is 80 kph and decreases to 59 kph at the end of the excitation. Only the first 3.2 m of the road profile is shown since the remaining 11.8 m of the road profile contains no elevation

content. The vehicle speed remains constant for the flat section and the magnitude consists of the speed at which the vehicle reaches the end of the of triangular pulse excitation.

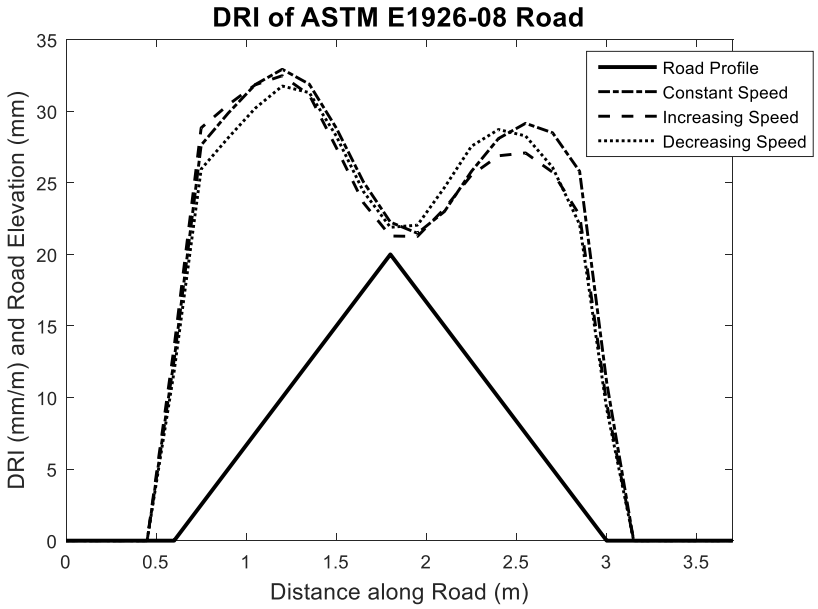

Figure 9. ASTM E1926-08 DRI Results

As opposed to the previous simulation, where the simulated vehicle speed remained constant, one minor factor that is varied is the duration of the excitation. Since the vehicle speed slightly varies, the time duration of each excitation changes as opposed to remaining constant as in the previous simulation. This simulation shows the ability of the DRI to compute roughness values dynamically under a changing speed. Small differences are noted in Figure 9 for a vehicle encountering the event at a rate of increasing or decreasing speed. Small changes in speed were implemented in this simulation due to the relatively short distance for the vehicle to accelerate or decelerate during the event. However, insight can still be gained from this simulation in that under an increasing speed, the first half of the event results in greater roughness than the second half. The opposite is true for the decreasing speed scenario in that less roughness is encountered initially while greater roughness is experienced near then end. All speed scenarios exhibit a decrease in roughness at approximately the same location as shown from Figure 9. The horizontal shift of the change in suspension travel response is not as large in magnitude relative to the previous simulation.

Table 7 shows the averaged DRI values for each speed scenario. From this statistic, there is a small, negligible difference in the roughness reported. However, from the DRI plot, one can gain insight as to the varying locations of increased or decreased roughness based on the speed

profile of the vehicle as mentioned above. When compared to the constant 80 kph simulation, the varying speed profile simulations result in an overall decreased roughness for the road profile.

Vehicle Speed (kph)	Increasing (59-80)	Constant 80	Decreasing (80-59)
Average DRI	4.1852	4.3154	4.1824

Table 7. Average DRI for each simulated vehicle speed scenario

3.7.5 Simulation of a measured profile (VTPL ILRaVTfac0914080)

This simulation was used to apply the DRI on an actual road measured by the Vehicle Terrain Performance Laboratory (VTPL) in Danville, VA. The purpose of this simulation was to test the DRI on real world data instead of on synthetic terrain profiles. This road was measured at a sampling interval of 0.1 m and contains a total of 4908 road data samples. Thus, the total length of the road measured is 490.7 m. A constant simulated vehicle speed of 80 kph was used in the simulation to compare the IRI statistic to the average DRI value. The rightmost plot of Figure 10 shows the DRI plot for the simulation.

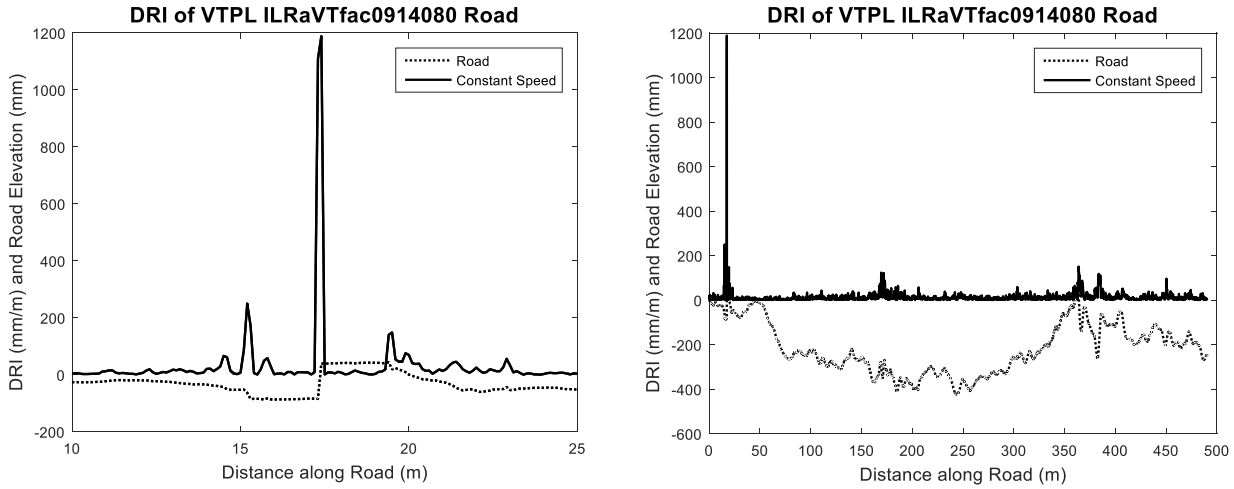

Figure 10. VTPL ILRaVTfac0914080 DRI results

The leftmost plot of Figure 10 shows a zoomed in region of the road profile (10-25 m). This region shows the detection of abrupt changes in the road elevation. For instance, at 17.3 m,

there is an event that resembles a step excitation. The step ranges from a minimum of -85.1 mm and becomes 39.3 mm within a longitudinal distance of 0.1m. Thus, this event is representative of a 124.4 mm (~5 in) bump on the road. This large change in elevation slope results in the largest DRI value for the entire road segment, signifying that this excitation captures a majority of the change in the suspension travel of the vehicle at instances where the excitation has a predominant effect (significant contribution) on the suspension travel. Subtle changes in the road elevation are also captured, as can be shown by the smaller peaks in the DRI plot at 15 m and 20 m along the road profile. Therefore, similar results are observed on the DRI based on the synthetic road obstacles generated on Figure 7.

Table 8 shows the summary road roughness statistics of the simulation. The high roughness values obtained for the IRI and average DRI indicate a rough road profile with many events that cause the suspension travel of the vehicle to vary significantly. Compared to Table 5, a decreased percent difference was obtained between the calculated IRI and average DRI values. Some of the main reasons for the closer agreement are due to the smaller sampling interval used (measured data was sampled at 100 mm) and the larger number of road samples (4908 as opposed to 101). Further discussion on the convergence of the two values is provided in Section 3.8.1.

	IRI	**Average DRI**	**Percent Difference (%)**
Constant 80 kph	12.9893	12.9786	0.082

Table 8. VTPL ILRaVTfac0914080 roughness results

3.7.6 Sample calculation of DRI at a response location

To recall, the DRI values are calculated from Equation (26). Therefore, the values shown on the figures represent the summation of the roughness from a particular excitation at each and every response location throughout the road profile. Computationally, DRI_i is computed by matrix multiplication of two matrices, which are the fractional response coefficient matrix and a column matrix of the change in suspension travel per incremental distance traveled. An example of the mathematical computational for a road profile with five excitations and response locations is shown in Figure 11 .

$$[DRI] = \begin{bmatrix} f(1,1) & f(1,2) & f(1,3) & f(1,4) & f(1,5) \\ f(2,1) & f(2,2) & f(2,3) & f(2,4) & f(2,5) \\ f(3,1) & f(3,2) & f(3,3) & f(3,4) & f(3,5) \\ f(4,1) & f(4,2) & f(4,3) & f(4,4) & f(4,5) \\ f(5,1) & f(5,2) & f(5,3) & f(5,4) & f(5,5) \end{bmatrix} \begin{bmatrix} \frac{\Delta z_1}{\Delta u_1} \\ \frac{\Delta z_2}{\Delta u_2} \\ \frac{\Delta z_3}{\Delta u_3} \\ \frac{\Delta z_4}{\Delta u_4} \\ \frac{\Delta z_5}{\Delta u_5} \end{bmatrix}$$

Figure 11. Calculation of DRI_i

For instance, to calculate the overall roughness from excitation 4 throughout an entire road profile consisting of 5 sampled points, the following calculation is performed as shown in Equation (33).

$$DRI_4 = f(4,1)\frac{|\Delta z_1|}{\Delta u_1} + f(4,2)\frac{|\Delta z_2|}{\Delta u_2} + f(4,3)\frac{|\Delta z_3|}{\Delta u_3} + f(4,4)\frac{|\Delta z_4|}{\Delta u_4} + f(4,5)\frac{|\Delta z_5|}{\Delta u_5} \tag{33}$$

By definition of the fractional response coefficient, the coefficients $f(4,1)$, $f(4,2)$, and $f(4,3)$ would be zero, which would eliminate the first three terms in the calculation. Therefore the calculation reduces to Equation (34).

$$DRI_4 = f(4,4)\frac{|\Delta z_4|}{\Delta u_4} + f(4,5)\frac{|\Delta z_5|}{\Delta u_5} \tag{34}$$

Through the calculation of the fractional response coefficient from Equation (24), the entire calculation can be expressed as shown in Equation (35). This represents a short example of the calculations performed to obtain the DRI plots shown in Figure 9 and Figure 10.

$$DRI_4 = \frac{\left|z_{road_4} h(t_4 - t_4)\Delta t_4\right|}{\sum_{k=1}^{4}\left|z_{road_k} h(t_4 - t_k)\Delta t_k\right|}\frac{|\Delta z_4|}{\Delta u_4} + \frac{\left|z_{road_4} h(t_5 - t_4)\Delta t_4\right|}{\sum_{k=1}^{5}\left|z_{road_k} h(t_5 - t_k)\Delta t_k\right|}\frac{|\Delta z_5|}{\Delta u_5} \tag{35}$$

Therefore, as shown from these calculations, the roughness caused by excitation 4 throughout the road profile is determined by the road elevation change at the location of excitation 4, the time of the duration of the excitation, the change of the suspension travel per incremental distance at the response location of interest, and the impulse response which relates the extent of the contribution of excitation 4 depending on the elapsed time between the excitation and the response location of interest. These factors contribute to the shape of the DRI

plot. For constant speed simulations, the time of the duration of the excitation will not play a role because the times in between excitations will be identical, which would reduce from the fractional response coefficient calculation. For such simulations, the magnitude of the road elevation, the impulse response, and the change of the suspension travel are the dominant factors in determining the shape of the DRI plot.

3.8 Discussion

3.8.1 Average DRI Convergence to the IRI

From the previous results shown, it has been noticed that the averaged DRI has not converged exactly to the calculated IRI values. This is due to the sampling interval used for the DRI calculations and simulations. A 0.15 m sampling interval results in a relatively large time elapsed for the simulated vehicle to travel between the sampled road points when compared to other smaller sampling intervals. To recall, from Equation (30), as the time difference between consecutive response locations approaches an infinitesimal value, the averaged DRI will converge closer to the IRI.

Considering a constant simulation speed of 80 kph, which is the standard simulated vehicle speed used in the calculation of the IRI, Table 9 shows four simulations results performed at four different sampling intervals for the unfiltered ASTM E1926-08 road profile. This road was tested using sampling intervals of 0.15 m, 0.10 m, 0.05 m, and 0.02 m. Since the sampling interval was decreased, the road elevation samples of the original road profile were increased through interpolation techniques to maintain the original distance of the road profile. A general observation from Table 9 shows that the percent error between the IRI and the average DRI decreases from 1.22 percent to 0.05 percent as the sampling interval between sampled road data points decreases in size.

IRI/DRI (mm/m)	Sampling Interval (m)			
	0.15*	**0.10**	**0.05**	**0.02**
IRI	4.3685	-	-	-
DRIavg	4.3154	4.3405	4.3589	4.3706
Error (%)	1.22	0.64	0.22	0.05

*original sampling interval of ASTM E1926-08 road profile

Table 9. ASTM E1926-08 roughness results at different sampling intervals

Table 10 shows that decreasing the sampling interval results in a smaller elapsed time for the vehicle to go from one sampled road elevation data point to the next. For the average DRI to be within 0.3 percent of the IRI for the roughness evaluation of the ASTM E1926-08 road profile, the time elapsed between the sampled data points must be such that the time is less than 2.25e-3 seconds. Table 10 also shows that decreasing the sampling interval results in the increase of the sample size of the road profile in order to obtain the original distance of the road as with the original sampling interval. This leads to an increase of the sample road elevation points used to calculate the DRI values, which requires greater computational effort. Depending on the specifications of the computer, Table 10 shows approximate computational times of the road profile under different sampling intervals. The computational time increases as the number sample points increases. Therefore, depending on the accuracy needed, there is a sacrifice of computational time.

	Sampling Interval (m)			
	0.15	**0.10**	**0.05**	**0.02**
Δt_j (s)	6.75e-3	4.5e-3	2.25e-3	9.0e-4
Sample size	101	151	301	751
Computation time (s)	1.9	3.1	9.5	52.4

Table 10. Comparison of parameters with smaller sampling interval

Figure 12 shows similar DRI curves of the profile roughness for smaller sampling intervals of the ASTM E1926-08 road. The curve with the smallest sampling interval (0.02 m) results in a smoother and continuous curve when compared to the 0.15 m sampling interval curve. A slight increase in roughness can be seen at the beginning nonzero elevation data points, while a reduction can be seen around the peak elevation. The reason for these slight increases and decreases is due to the refinement of the change in suspension travel response curve. Since more data points exist with a smaller sampling interval, there will be more points available at the locations of the peaks and valleys of the change in suspension travel response. This leads to greater refinement because more points will be able to sufficiently capture the entire change in the suspension travel response as opposed to a larger sampling interval, where significant portions of the response may be omitted due to a lack of sample points. Although more sample

points were synthetically generated, the outcome of this investigation was useful in showing the effect of roads sampled at small sampling intervals. Therefore, the advantage of an originally sampled dataset with a smaller sampling interval is that there is a greater refinement in terms of the roughness values calculated. To recall the results shown in Table 9, the average DRI converges to within 0.05 percent of the IRI at the sampling interval of 0.02 m.

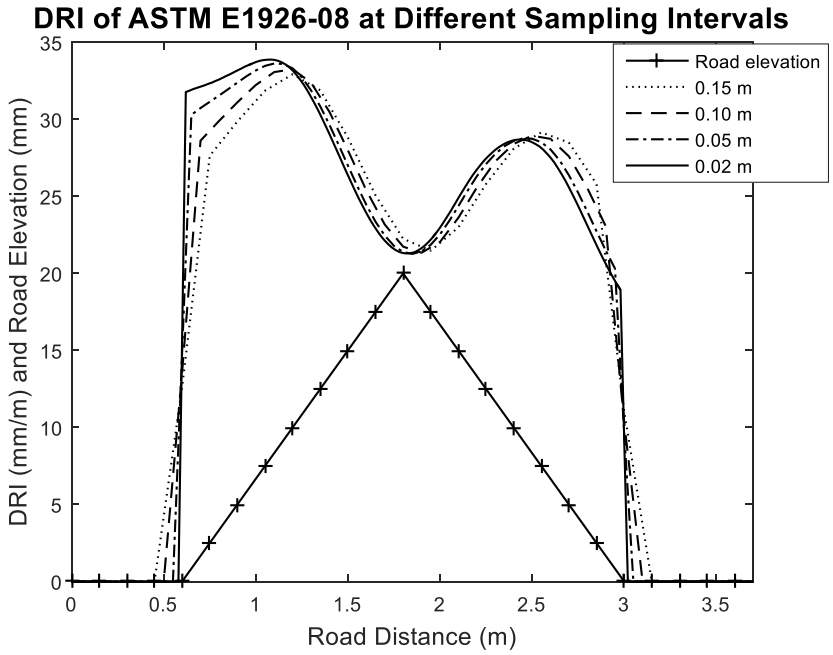

Figure 12. Refined DRI at smaller sampling intervals

3.8.2 Velocity Sensitivity of IRI and DRI

The following discussion is on the effect of different constant vehicle simulation speeds on roughness values. The first example shows the ASTM E1926-08 road, which to recall, was sampled at a sampling interval of 0.15 m. To observe the effect of different constant speeds on roughness, 17 simulations of the road profile from the speeds ranging from 10 kph to 170 kph in increments of 10 kph were conducted. Figure 13 shows the computed IRI values and the averaged DRI values calculated for each of these constant simulation speeds.

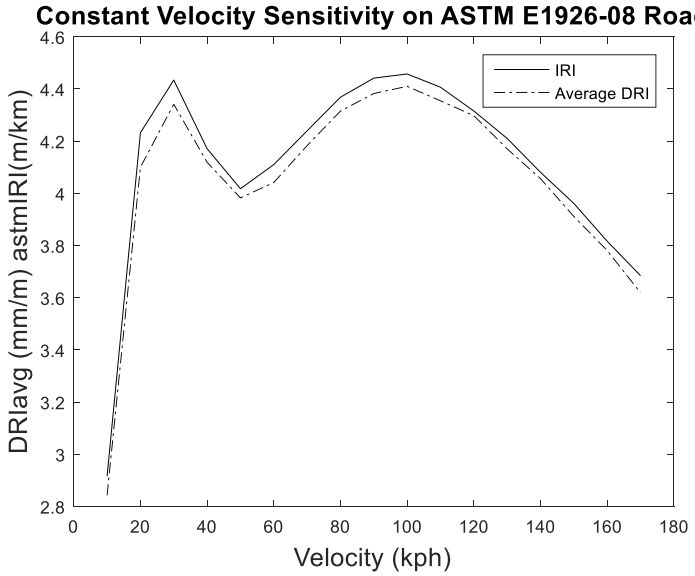

Figure 13. DRI and IRI roughness values at different simulation velocities

Notice that there is slight variation between the IRI and the averaged DRI values calculated. This is due to the relatively high sampling interval by which the road was sampled, as discussed in the Section 3.8.1. Other factors relating to the slight variation are due to the relatively low sampling number (101 elevation points) and little to no elevation content from the road profile. Interesting to note is that the resulting IRI value varies from approximately 2.9 to 4.5 m/km for the simulated vehicle speed range (10 kph to 170 kph).

Figure 14 shows the IRI and average DRI results for a road with a significantly different profile. This road was sampled at 0.1 m and contained 1518 samples (151.7 m long). For this road profile, the IRI and average DRI values converge closer than the previous road due to the smaller sampling interval. Also noticed is that higher convergence is obtained at higher speeds, which also agrees with the previous DRI convergence discussion in Section 3.8.1. The higher the simulated vehicle speed between sampled points, the smaller the elapsed time, allowing for higher convergence. At 10 kph, compared to the rest of the points in the Figure 14, this simulated vehicle speed results in the greatest elapsed time between samples, which explains the slightly lower convergence relative to the rest of the speeds.

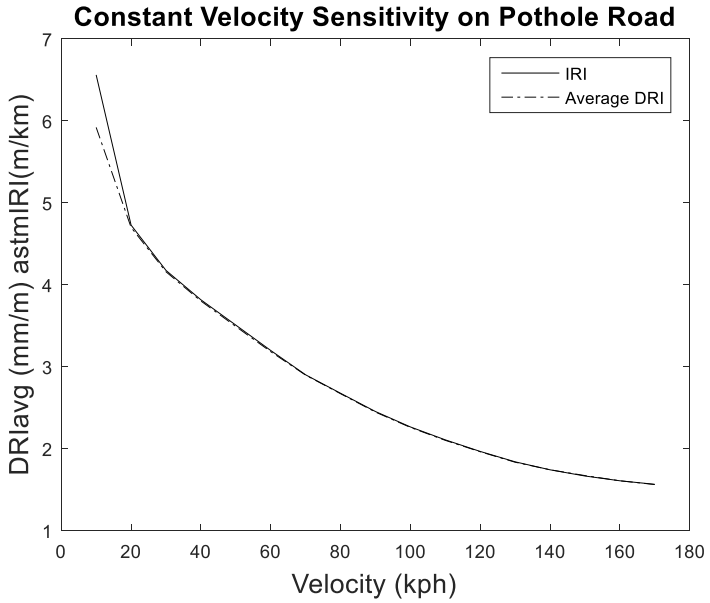

Figure 14. DRI and IRI roughness values at different simulation velocities

Figure 15 shows the simulation result for the road profile simulated from Figure 10. As was observed in the previous Figure 14, higher convergence is obtained for higher speeds. As an overall trend observed from the three road profiles, rougher values were usually obtained at lower speeds than at higher speeds. The only exception to this was the first road. Part of the reason for the slightly different result is due to the larger sampling interval (0.15 m) used for the first road. Thus, the distance or time elapsed between the sampled road points is much larger compared to the other roads that use a smaller sampling interval. As the speed of the vehicle decreases, the time elapsed increases. From Figure 3, the magnitude of the impulse response will be less due to the greater elapsed time between the sampled road points. Therefore, for the first road, the contributions from previous excitations will be less than if the vehicle were to have a greater speed. This decreases the overall roughness value calculated for the road.

As shown from the roughness values calculated at different velocities, there are many factors to consider when evaluating the roughness as discussed in Section 3.7.1. At particular speeds, certain factors may have a greater influence than others, which explains for the varying roughness values calculated at different speeds. This highlights one of the advantages of simulating and calculating the roughness at different and varying vehicle speeds rather than at a standard, constant speed. Limiting calculated roughness values to a particular, constant speed can limit or misinterpret the roughness values obtained for a particular segment of road.

Therefore it is important, when calculating roughness, to use a suitable speed that vehicles travel at along a particular road.

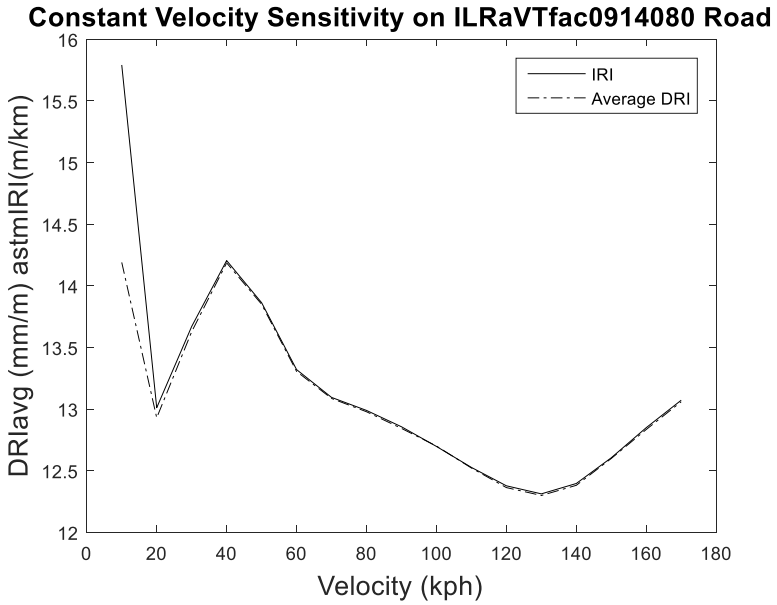

Figure 15. DRI and IRI roughness values at different simulation velocities

3.8.3 Grinding Application comparison to ProVAL

Profile Viewing and Analysis (ProVAL) is software that is used by many pavement contactors to analyze road data for roughness statistics. Within the ProVAL Smoothness Assurance Module (SAM), a grinding simulation can be performed to detect areas, based on the input road elevation data, where grinding may be necessary to smoothen the road to target specifications. According to the input specifications, the smoothness assurance grinding feature specifies the start and stop distances of grinding locations.

To compare the regions of the DRI that indicate relatively high roughness to the suggested grinding locations indicated by the grinding simulation in ProVAL, a grinding simulation of the unfiltered VTPL ILRaVTfac0914080 road profile was performed in ProVAL. Default grinding parameters were used in ProVAL. To recall, the road elevation profile and the DRI plot for this road profile is shown in Figure 10.

The results from the grinding simulation indicated that two grinding operations should be performed. The first operation consists from a start distance of 5.00 m to 14.30 m and the second grinding operation from 17.40 m to 22.00 m. Therefore, 13.9 m of the road profile (out

of 490.7 m) are subject to grinding as suggested by ProVAL. Figure 16 shows a zoomed-in DRI plot of the road profile and also highlights the grinding locations specified by the grinding simulation. Therefore, the Figure below only shows the section of the road where grinding may be necessary as specified by the grinding simulation. These sections are highlighted in yellow. The first grinding location contains relatively low DRI values, with the exception of increasing values near the end of the first grinding segment. The second grinding segment captures some of the high DRI values reported. In terms of overall location, the DRI and the grinding simulation both indicate locations of increased roughness along the road profile. However, as noted in Figure 16, the grinding simulation omitted an approximately 3.1 m portion of the road segment, where the DRI indicates high roughness.

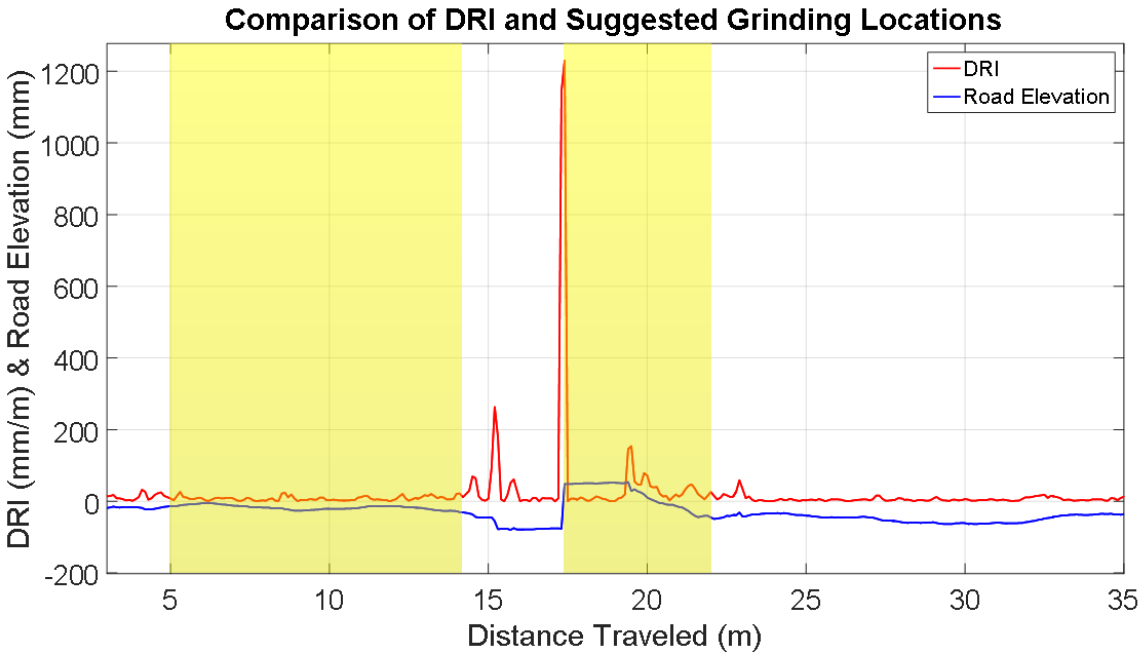

Figure 16. Comparison of ProVAL grinding locations (yellow) and DRI roughness

One observation from Figure 16 is that the ProVAL did not highlight the section 15 m into the road profile. From the road elevation shown, there is an abrupt change in elevation near 15 m, which results in a relatively high DRI value. Based on the DRI, this section may be suggested for grinding due to the relatively high DRI values calculated within this region. When evaluating the grinding suggestions from ProVAL, the first highlighted region in yellow contains

relatively low DRI values and based on the DRI, this section may not be necessary to grind when observing the road elevation curve. There are subtle changes in the road elevation for the region between 5 m to 14.30 m of the road profile. The second section between 17.4 m and 22.0 m captures a majority of the high roughness as indicated by the DRI.

For further study, a grinding strategy can be implemented that is based on the DRI plot as shown in Figure 16. The grinding strategy would effectively analyze whether a particular section of road may need grinding for smoothness assurance. This could be accomplished by observing the trends of the DRI plot and by developing grinding criteria that would indicate the most appropriate regions to grind. Once the grinding strategy is developed, comparison tests to the grinding strategy in ProVAL can be conducted to further evaluate the effectiveness of the DRI in grinding applications.

3.8.4 Implementation of moving average filter on DRI

The moving average filter can be applied to the DRI to simulate the bridging and enveloping behavior of the tire. These properties of the tire tend to mechanically filter out particular road excitations that a point follower tire model used in a quarter car simulation cannot filter alone. Therefore, before the road elevation samples are input into the quarter car vehicle simulation, the road is filtered by a moving average filter. The filter length, k, is calculated by Equation (36).

$$k = \max\left(1, round\left(\frac{base}{\Delta}\right)\right) \tag{36}$$

A filter length of 1 results in no averaging of the elevation points and the output is simply the same as the input. When the filter length is nonzero and greater than 1, there is a horizontal shift in the filtered output given by the variable ‘delay’ shown in Equation (37).

$$delay = \frac{k-1}{2} \tag{37}$$

An important observation to note is that when k is even, the delay results in a non-integer value. In terms of realigning the filtered profile to the original profile, a non-integer shift correction would be difficult to apply from a computing standpoint in MATLAB. Therefore, for even values of k, the filtered shifted output is averaged a second time by a filter length of 2 such that

the delay results in integer values. Table 11 shows the resulting delay and the applied moving average coefficients for filter lengths ranging from 2 to 6.

Filter Length	Original Delay	Resulting Delay (2^{nd} application)	Weighted Coefficients
2	0.5	1	$\frac{1}{4}, \frac{1}{2}, \frac{1}{4}$
3	1	1	$\frac{1}{3}, \frac{1}{3}, \frac{1}{3}$
4	1.5	2	$\frac{1}{8}, \frac{1}{4}, \frac{1}{4}, \frac{1}{4}, \frac{1}{8}$
5	2	2	$\frac{1}{5}, \frac{1}{5}, \frac{1}{5}, \frac{1}{5}, \frac{1}{5}$
6	2.5	3	$\frac{1}{12}, \frac{1}{6}, \frac{1}{6}, \frac{1}{6}, \frac{1}{6}, \frac{1}{6}, \frac{1}{12}$

Table 11. Corresponding moving average coefficients for each filter length

As an example, a 250 mm moving average filter (commonly used in the IRI calculation) and a sampling interval of 0.15 m result in a filter length of 2. Along the profile, a moving average would be applied such that the procedure shown in Equation (38) is carried out. That is, for the second and third road data points (z_2) and (z_3), the filtered results would be:

$$z_2 = \frac{z_1 + z_2}{2}, z_3 = \frac{z_2 + z_3}{2} \tag{38}$$

When compared to the original unfiltered road profile, the result for the second data point would be located 0.5 units to the right from the first data point (1.5 units on an absolute scale from zero). This leads to a delay of 0.5 (as shown in Equation (37)) with respect to the original, unfiltered profile, which is difficult to implement in MATLAB. Therefore, for even filter lengths, the filtered results are filtered a second time with a filter length of 2 to accumulate a second delay. This is shown in Equation (39).

$$\begin{aligned} z_{2,3} &= \frac{\frac{z_1 + z_2}{2} + \frac{z_2 + z_3}{2}}{2} \\ z_{2,3} &= \frac{1}{4} z_1 + \frac{1}{2} z_2 + \frac{1}{4} z_3 \end{aligned} \tag{39}$$

The second row shows the corresponding coefficients as originally shown in Table 11. The total delay for the two averages results in a 1 data point shift since the delay involved with a filter length of 2 is each 0.5. This would cause the result to occur on data point 2 (on an absolute scale). With the shift correction of 1, this averaging would represent the first data point of the sequence.

From this discussion, the effect of integrating a moving average filter into the calculation of the DRI is investigated. The IRI standard uses a moving average filter to simulate the enveloping behavior of a tire and to reduce the IRI sensitivity to the sampling interval [8]. The issue with using this standard filter is that the filtered road elevation data points are shifted by the filter when compared to the original elevation data. The horizontal shift is determined by the filter length of the filter. This phenomenon can be seen in Figure 17 below using a 250 mm moving average filter for the ASTM E1926-08 road for a 0.15 m sampling interval.

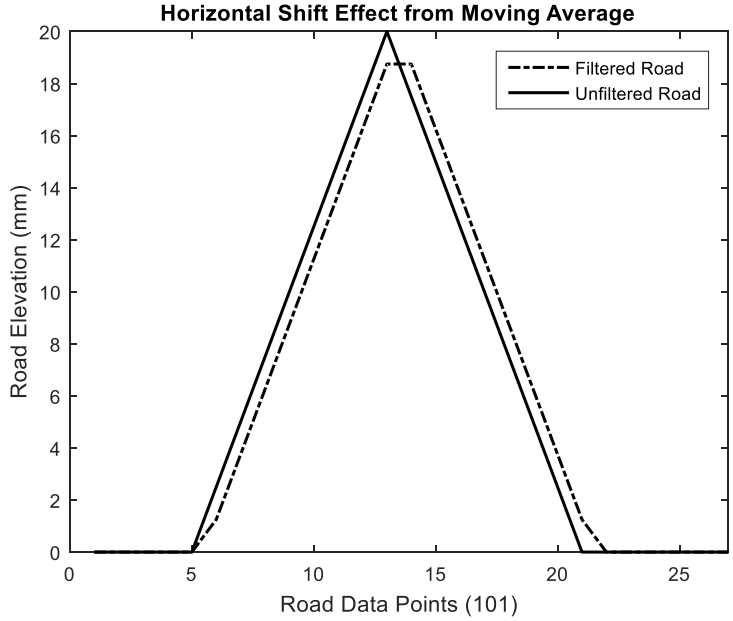

Figure 17. Horizontal shift effect from 250 mm moving average filter

This is a limitation because the indexing of the road profile is critical to the calculation of the DRI, since a roughness value is calculated for each road data point. In the calculation of the IRI, this is not a major limitation since the roughness values are averaged by the number of data points (taking into account the subtraction of data points from the filter length of the moving

average filter). In the calculation of the IRI, the roughness at a particular point is not of interest, since the suspension travel is averaged for a certain length of the profile. A second disadvantage of this approach would be that using this method alone would result in non-integer shift amounts for even-numbered filter lengths, which would cause programming difficulties to shift the data to match the original profile.

To address the non-integer shift issue, the smoothed points obtained from the filter can be further averaged with a filter length of 2 data points. The advantage of following this approach would be that the road elevation data would be shifted in whole number integers for even filter lengths. By implementing the shift correction, the filtered road profile data can be aligned with the original profile elevation. The disadvantage of this approach would be that a lower average DRI would be obtained when compared to the standard IRI of the filtered profile since the profile is filtered twice. Therefore, it is recommended to pre-filter the profile before inputting the road profile into the DRI algorithm. Figure 18 below shows the shift correction applied to the filtered road profile after the second filtering performed to obtain an integer shift.

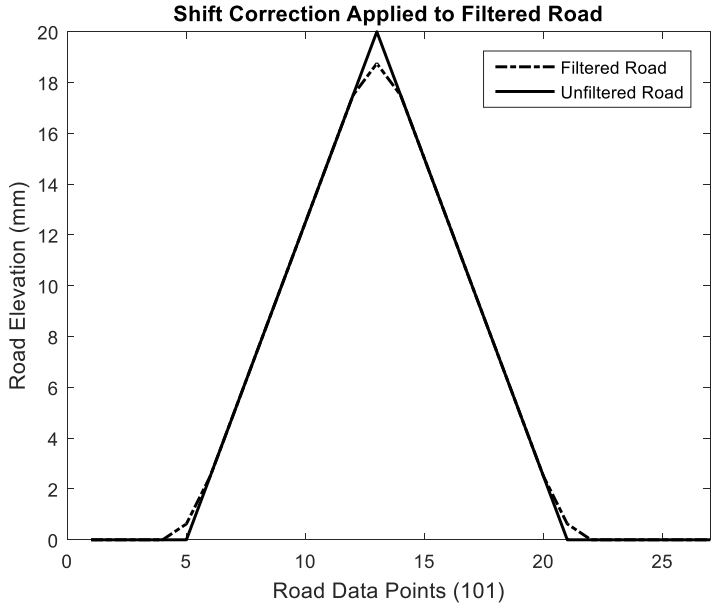

Figure 18. Shift correction applied to filtered road from 250 mm moving average filter

In essence, a different moving average filter is used to filter the road elevation data in order to appropriately use the moving average filter in the DRI calculation. The different filtering technique results in slightly different values (~2.98 percent difference when compared to

the filtered IRI for the ASTM E1926-08 road). Figure 19 below shows a comparison of the DRI curves for the ASTM E1926-08 road (filtered and unfiltered) for a constant simulated vehicle speed of 80 kph.

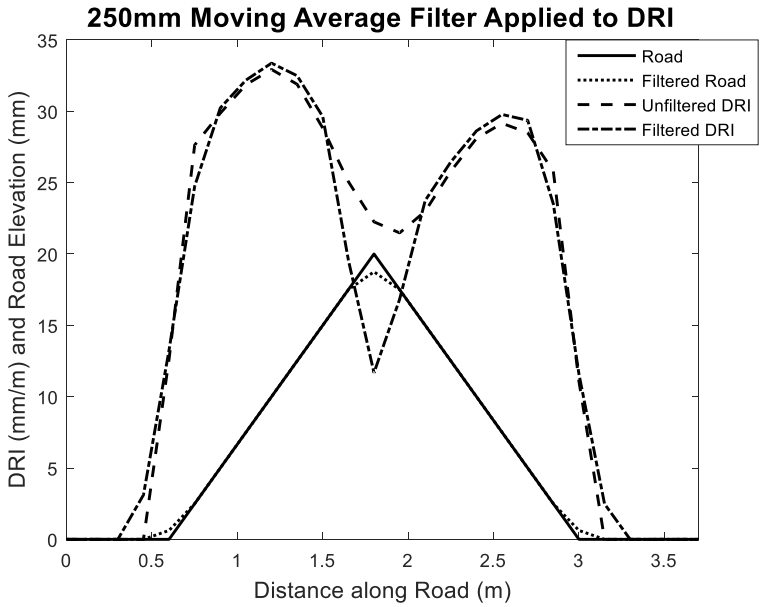

Figure 19. Moving average filter comparison for ASTM E1926-08 road profile

A noticeable decrease in roughness is observed at the peak elevation of the road profile for the 'Filtered' DRI curve. The application of the moving average filter reduced the elevation and the slope of the elevation around the peak of the road profile. Based on the investigation conducted to see the effect of the DRI plot on varying road events shown on Figure 7, this decrease in roughness is expected. Due to the reduction in the change in the road elevation around the peak, the DRI will decrease at such locations because a lower change in elevation will result in decreased fractional response coefficients for that excitation. The extreme case of the reduction in the change in elevation is zero, which signifies a flat profile. For flat portions where the change in elevation is zero, the DRI reduces to zero at such locations.

	Filtered IRI	**Filtered Average DRI**	**IRI (unfiltered)**	**Average DRI (unfiltered)**
Constant 80 kph	4.3562	4.2266	4.3685	4.3154

Table 12. ASTM E1926-08 road simulation with shift correction

Table 12 shows a comparison of the roughness statistics obtained from the unfiltered and filtered results. A slightly lower filtered, averaged DRI is obtained due to the necessary second filtering to align the filtered profile with the original profile. Again, the purpose of the realigning the profiles is to eliminate the horizontal shift caused by the application of a moving average onto the road profile.

Figure 20 shows a comparison of the DRI curves for the VTPL ILRaVTfac0914080 road (filtered and unfiltered) for a constant simulated vehicle speed of 80 kph. A specific portion of the road profile is shown due to the many excitations of the road profile. This section was chosen since it exhibits the greatest roughness.

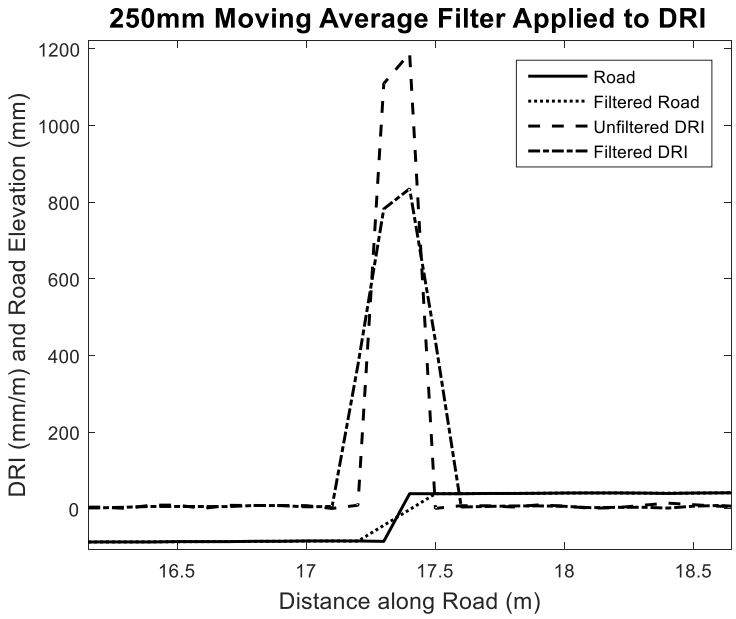

Figure 20. Moving average filter comparison for VTPL ILRaVTfac0914080 road profile

The application of the moving average filter reduces the slope of the elevation profile approximately from 17.3 m to 17.4 m along the road profile. Due to the reduction in the change of elevation in the road profile, this results in a reduction of the DRI value calculated for that particular location. Table 13 shows the filtered and unfiltered roughness statistics for the road profile. The results indicate that the application of the moving average filter results in a slight decrease in the overall roughness statistic used to summarize the road profile.

	Filtered IRI	Filtered Average DRI	IRI (unfiltered)	Average DRI (unfiltered)
Constant 80 kph	12.8861	12.8727	12.9893	12.9786

Table 13. VTPL ILRaVTfac0914080 road simulation with shift correction

Since a different moving average filtering technique is implemented with the DRI, it is expected that the calculated filtered averaged DRI results are slightly lower than the filtered IRI results for constant speed simulations. To recall the DRI convergence discussion, decreasing the sampling interval will cause the filtered DRI average to approach the filtered IRI value, but nonetheless, the average DRI will always be lower than the filtered IRI value since essentially the profile is averaged twice to appropriately apply the shift corrections to the road profile.

Another feature added to the moving average filter code was to trim the length of the filtered road by the delay because as the road is shifted to align with the original profile, the shift leaves a quantity of zeros (depending on the size of the shift) at the end of the road profile sampled data. Therefore, following the shifting correction, the resulting zeros are omitted from the road elevation data. Again, this only applies to when there is a delay due to the moving average filter. If there is a filter length of 1 or less, there is no delay.

3.9 Conclusion

Within this work, a roughness measure that relates the contribution of any excitation of the road to a particular response location has been developed. Namely, the purpose of the DRI is to provide a refined measure of localized roughness, allowing the user to pinpoint the main excitations or events on the road to the exact cause of the roughness. The DRI can distinguish between a relatively smooth road with a single, large excitation and a relative rough road with small excitations in magnitude. In certain situations, as described, the IRI calculation may result in the same roughness value for two distinct roads since it averages the suspension travel by the distance traveled. The DRI differentiates from the IRI because the DRI calculates a localized roughness value at each sampled road elevation point for situations when the vehicle maintains a constant velocity or when the velocity is variable. Thus, the roughness values obtained from the DRI can be applicable to highway or city driving scenarios. The IRI is also limited to constant speed and golden quarter car parameters (linear) applications. For further study, nonlinear elements, such as suspension or tire components, can be integrated into the modular quarter car

model used by the DRI to allow for a refined representation of fleets of cars. The characterization of road surfaces via refined measures of roughness will allow vehicle engineers to predict chassis loads, deformations, stresses, and strains on vehicle components. This will facilitate modifications to initial vehicle designs and prevent costly, late modifications to end designs. Thus, the DRI can be used in conjunction with the IRI and other roughness metrics to allow vehicle engineers and pavement engineers to effectively assess the roughness of a road surface.

4. Conclusions

4.1 Summary of Research

From this work, a Discrete Roughness Index was developed. The Discrete Roughness Index (DRI) provides a roughness measure at each discrete location along a terrain surface. The DRI can be used to distinguish the roughness between smooth surfaces with a single, large excitation and surfaces with uniform roughness, even when the surfaces would have the same IRI. One important property of the average DRI is that it converges to the IRI as the distance between sampled points become smaller, for the particular case when the golden quarter car model is simulated at 80 kph. The DRI is not an alternative to the standard IRI, therefore, but a widely applicable roughness measure of which the standard IRI is a single specialized application. The DRI can be calculated using vehicles traveling at varying speeds and using parameters other than the golden quarter car model making it applicable to highway, city, and off-road driving scenarios. In this way engineers of off-road equipment, on-road vehicles, pavement, and tires can assess the roughness of a terrain surface for the design of their products. This will facilitate improvements to initial designs and prevent costly modifications later in the design process.

4.2 Main Contributions

In this work, a Discrete Roughness Index (DRI) was developed such that it can be used in cases when the velocity is varied, which is more representative of city-driving than at a prescribed speed of 80 kph which is the current practice with the IRI.

The objective of the DRI was to form a general framework for roughness measures that:

- Increases the application of roughness measures to cases of varying speeds
- Localizes the roughness to specific locations on the roads
- Remains consistent with existing measures of roughness (such as the IRI) and broadens the applicability of these roughness measures to other vehicle parameters

4.3 Future Work

There are several areas for future work on the DRI. Some applications include the application of the DRI to damage estimates, the development of a grinding strategy based on the

DRI, and the development of a real-time algorithm of the DRI. In terms of the implementation of the DRI discussed in this work, future work consists of integrating nonlinear components into the simple vehicle models outlined within this work. The implementation of a constraint mode tire model is outlined in Appendix F. This particular model can be used to calculate the DRI and estimate pseudo-fatigue damage. This tire model captures tire deformation behavior along with the tire bridging and enveloping behaviors. Thus, refined estimates of roughness and damage can be obtained.

4.3.1 Preliminary investigation of damage and suspension travel

Preliminary pseudo damage estimates were calculated for various kinds of roads (synthetic and measured) to observe any correlations between the calculated suspension pseudo damage and the IRI (suspension travel). A constant 80 kph vehicle simulated speed was used as well as 'golden quarter car' parameters. Full results of the vehicle simulations performed are shown in Appendix E. Figure 21 highlights two road profiles, where one of them exhibits approximately twice the IRI and therefore twice the accumulated suspension travel. Interesting to note that the normalized pseudo damage per distance traveled (see Appendix E) does not increase by a factor 2. Rather, the road profile with twice the IRI exhibits a damage value that is 52.5 times greater in magnitude. These preliminary results highlight a particular instance where a doubled IRI does not necessarily indicate twice the damage endured for the vehicle.

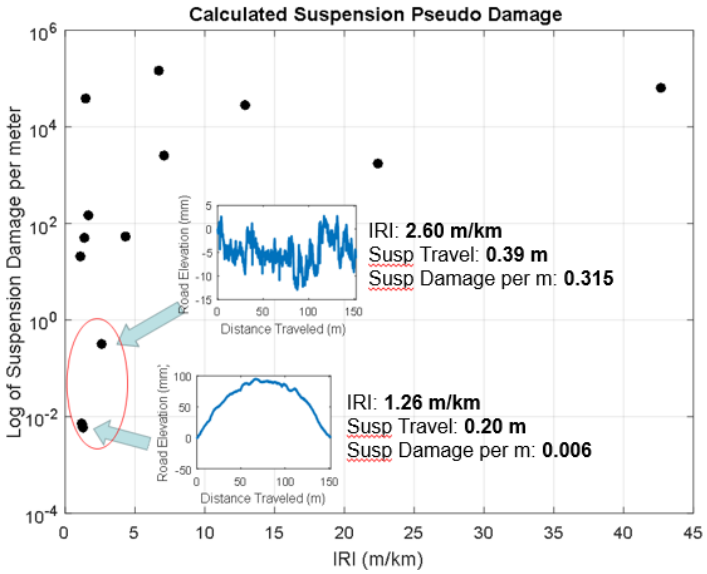

Figure 21. Doubling the IRI does not necessarily correlate to twice the damage

Figure 22 further illustrates the notion that larger values of the accumulated suspension travel for a road profile does not necessarily indicate greater damage. For instance, for the step road shown, the suspension travel of the vehicle was 0.61 m, and yet, this road resulted in one of the greatest damage estimates calculated. Therefore, it is not valid to assume a proportional relationship between the damage and the suspension travel.

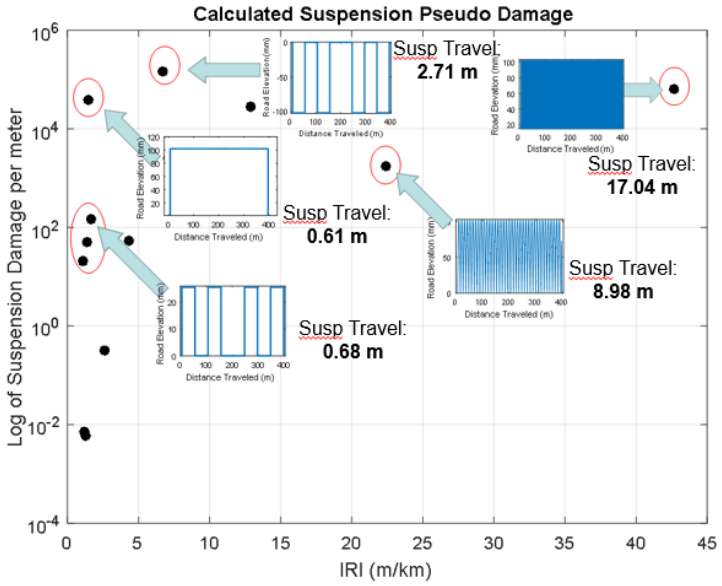

Figure 22. Suspension travel does not necessarily equate to greater damage

Figure 23 highlights the damage results for three road profiles with approximately similar IRI values. The calculated damage from each of these profiles ranges from a negligible to a substantial quantity of damage. Therefore, these results show that the IRI is not linearly proportional to the amount of damage. These preliminary results show that the suspension travel (IRI) does not reliably predict damage, signifying that the magnitude of the suspension travel does not necessarily equate to damage.

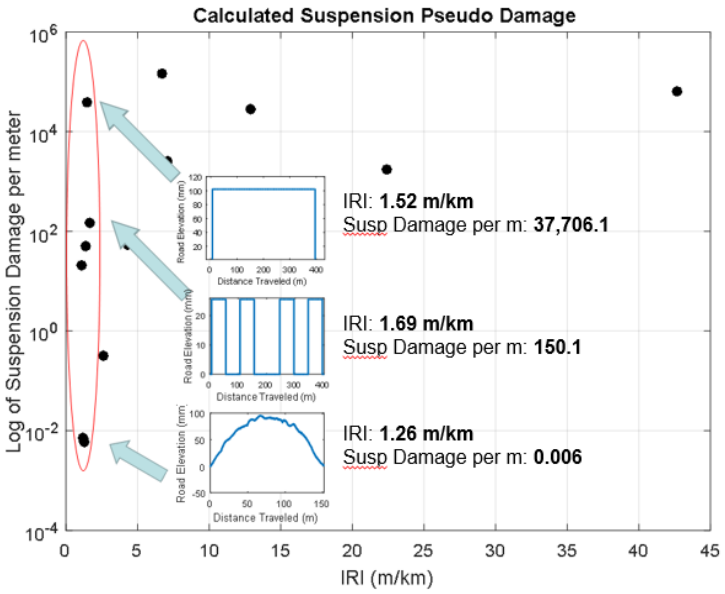

Figure 23. Damage comparison of roads with similar IRI values

Table 14 shows an extended list of roads with approximately similar IRI values that are plotted in Figures 21-23. The results from the step road are significant to draw to attention. Although the IRI is relatively low (1.52 m/km) and the accumulated suspension travel is approximately 0.6 m when a moving average filter is applied, the vehicle encounters relatively significant suspension and spindle damage.

Road	ASTM IRI (m/km)	Accumulated Suspension Travel (m)	Road Distance (m)	Susp PD per m	Spindle PD per m
Step Road	1.52	0.61	402.20	37,706.1	1.83e6
Square Bumps (25.6 mm)	1.69	0.68	402.20	150.1	7251.8
Square Bumps (20.4 mm)	1.35	0.54	402.20	50.1	2376.2
Square Bumps (17.0 mm)	1.12	0.45	402.20	20.5	946.9
MNRp00d9a1909020	1.21	0.19	151.50	0.007	0.135
MNRp00d9a1909080	1.24	0.19	151.50	0.006	0.090
MNRp00d9a1909010	1.26	0.20	151.50	0.006	0.134

Table 14. Comparison of approximately-similar IRI roads

When compared to one of the MNR profiles, the IRI for the step road is larger by a factor of 1.2, the accumulated suspension travel is approximately tripled, but the suspension and spindle pseudo damage estimates increase by 6.3e6 times and 1.83e7 times, respectively. The reason for the dramatic increase in the damage observed for the step road is due to the significant

suspension and spindle loads encountered during the impact points at the beginning and ending points of the step. For instance, from Figure 24, the suspension load increases to approximately 28 kN and the spindle load increases to 64 kN at the impact points. Although, for most of the road profile, the vehicle experiences negligible loading to the spindle or suspension, the loads encountered briefly at the beginning and ending of the event cause significant damage to the vehicle. This goes to show that the amount of suspension travel does not always correlate with the amount of damage done to the vehicle.

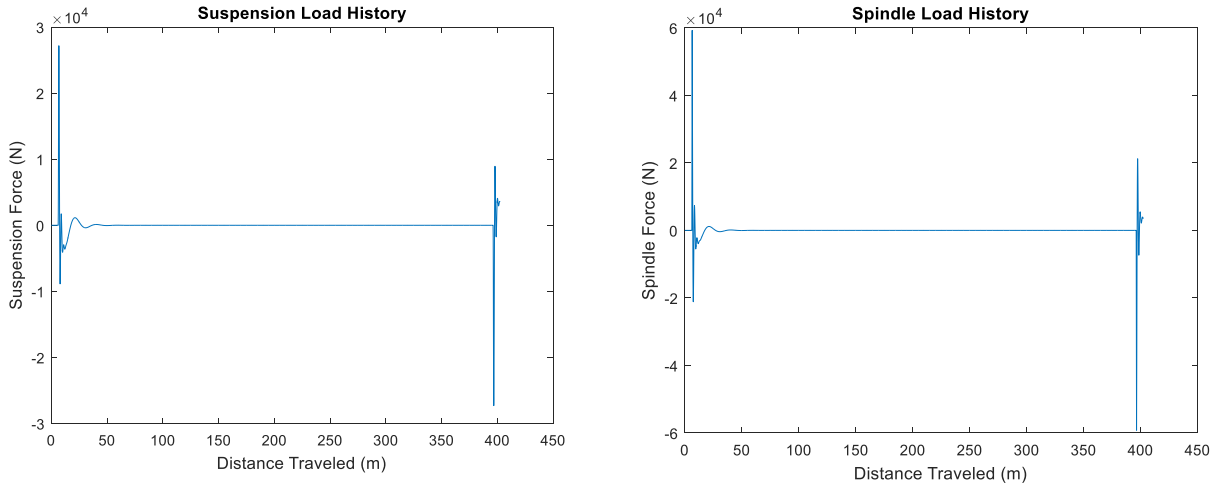

Figure 24. Suspension and spindle loading histories for step road

Figure 25 shows the suspension and spindle loading histories for MNRp00d9a1909080 road. Compared to Figure 24, the loading history in Figure 25 is scattered throughout the entire road profile, but much less in magnitude. For instance, in the suspension loading history, the peak magnitude for the step road is approximately 40 times larger than the peak magnitude of the MNRp00d9a1909080 road. Although the excitation is only encountered for a brief period in the step road, this excitation is more damaging than the relatively low and scattered loading present in the MNRp00d9a1909080 road.

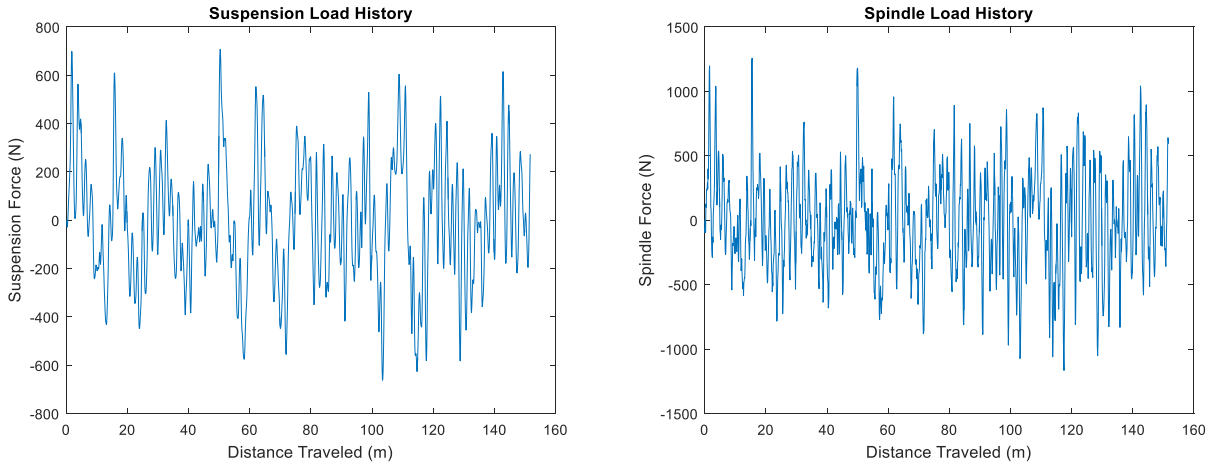

Figure 25. Suspension and spindle loading histories for MNRp00d9a1909080 road

Figure 26 shows a similar loading history when compared to Figure 24, with the exception that the elevation of the bump is four times less. The peak magnitude of the suspension loading history is approximately 7 kN, which is four times less than that from Figure 24. Interestingly, running the vehicle over four of the smaller bumps results in a pseudo-fatigue damage estimate that is 251.2 times less than the step road. Thus, although the accumulated suspension travel for step road (0.61 m) and for the square bumps (0.68 m) are similar, the estimated damage is very significant. This example shows that the IRI is unable to distinguish between the damage caused to the suspension of the vehicle for roads with similar suspension travel.

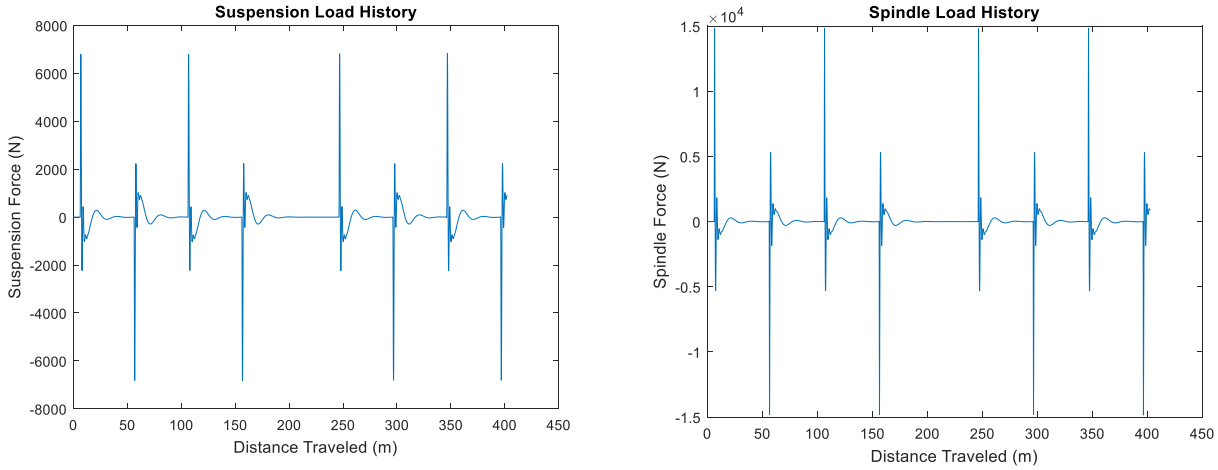

Figure 26. Suspension and spindle loading histories for square bumps (25.6 mm) road

Therefore, damage estimates based on the loading history of the vehicle serve as a consistent and more appropriate indication of damage than solely relying on the suspension motion of the vehicle.

4.3.2 Introduction of a Discrete Damage Index (DDI)

Since suspension travel is not indicative of suspension damage, it is proposed to develop a damage index that is based on the DRI and the concepts of damage discussed in Chapter 2. By replacing the suspension travel defined in Equation (25) with the formulations for the Palmgren-Miner rule and the Basquin relation, Equation (40) is obtained.

$$D_i = C\sum_{j=1}^{N} \frac{1}{\Delta u_j} f_{ij}\left(F_{a_i}\right)^{\beta} \tag{40}$$

In Equation (40), F_{a_i} are the cycle-counted loads of the suspension of the vehicle and D_i is the instantaneous damage at discrete locations on the profile. Further study will be necessary to define f_{ij}, which would relate the contribution of the cycle-counted load to the discrete road excitations on the road profile. For instance, depending on the definition of the cycle from the cycle counting method, the longitudinal span over which the cycle was defined would need to be correlated to the same longitudinal span along the road profile. In this manner, the load would be distributed over the pertaining span along the road profile via coefficients that will divide the load into particular amounts depending on the road elevation and other parameters that may influence the magnitude of the load.

The benefits of the DDI are that instantaneous measures of damage would be calculated for each discrete road excitation on a longitudinal profile. Therefore, refined estimates of damage would be obtained, which would localize regions of the road that are the most damaging to the vehicle. An added benefit of these estimates would be that the average of the measures of instantaneous damage calculated would equal to the total damage of the road profile, which would be equivalent to the current methods of calculating pseudo damage [1],[2],[32].

References

1. Zaabar, Imen, and Karim Chatti. "New mechanistic-empirical approach for estimating the effect of roughness on vehicle durability." *Transportation Research Record: Journal of the Transportation Research Board* 2227 (2011): 180-188.
2. Bogsjö, Klas, and Igor Rychlik. "Vehicle fatigue damage caused by road irregularities." Fatigue & Fracture of Engineering Materials & Structures 32.5 (2009): 391-402.
3. Robbins, Mary M., and Nam Tran. "Literature Review: The Effect of Pavement Roughness on Vehicle Operating Costs." (2015).
4. Zaabar, Imen, and Karim Chatti. "Identification of localized roughness features and their impact on vehicle durability." HVTT11, *International Heavy Vehicle Symposium: Balancing Competing Needs in Heavy Vehicle Transport Technology*. 2010.
5. Janas, Joe. "Relating road roughness to vehicle component fatigue: to establish the role of road roughness on vehicle component fatigue takes more than a Sunday cruise and seat-of-the-pants estimations.(Data Acquisition)." (2002).
6. Ferris, John B. and Jerry L. Larsen, Establishing Chassis Reliability Testing Targets Based on Road Roughness. *International Journal of Materials and Product Technology* 17.5-6 (2002):453-461.
7. Ahlin, Kjell, Johan Granlund, and Fredrik Lindstrom, Comparing road profiles with vehicle perceived roughness. *International Journal of Vehicle Design* 36.2-3 (2004): 270-286.
8. ASTM, *Standard Terminology Relating to Traveled Surface Characteristics*. 1989, American Society for Testing and Materials.
9. Sayers, Michael W., "On the calculation of international roughness index from longitudinal road profile." *Transportation Research Record, 1501* (1995): 1-12.
10. Howe, J. Gavin, et al. "Quarter car model stress analysis for terrain/road profile ratings." *International journal of vehicle design* 36.2-3 (2004): 248-269.
11. ASTM, *Standard Practice for Computing International Roughness Index of Roads from Longitudinal Profile Measurements*. 2008, American Society for Testing and Materials.
12. Sayers, Michael W., Thomas D. Gillespie, and William DO Paterson. *Guidelines for conducting and calibrating road roughness measurements*. No. Technical Paper 46. 1986.
13. Gillespie, Thomas D. "Everything you always wanted to know about the IRI, but were afraid to ask." *Road Profile Users Group Meeting*, Lincoln, Nebraska. 1992.
14. Sayers, Michael W., and Steven M. Karamihas. "The Little Book of Profiling." University of Michigan (1998).
15. Spangler, Elson B., and William J. Kelly. "Servo-seismic method of measuring road profile." *Highway Research Board Bulletin* 328 (1962).
16. Spangler, Elson B., and William J. Kelly. "GMR road profilometer-a method for measuring road profile." *Highway Research Record* 121 (1966).
17. Chemistruck, Heather M., et al. "Review of current developments in terrain characterization and modeling." *SPIE Defense, Security, and Sensing*. International Society for Optics and Photonics, 2009.
18. Múčka, Peter. "Current approaches to quantify the longitudinal road roughness." *International Journal of Pavement Engineering* ahead-of-print (2015): 1-21.

19. Sayers, Michael W. "Two quarter-car models for defining road roughness: IRI and HRI." *Transportation Research Record* 1215 (1989).
20. Sayers, Michael W. "Profiles of roughness." *Transportation Research Record* 1260 (1990).
21. Kropáč, Oldřich and Peter Múčka, "Be careful when using the International Roughness Index as an indicator of road unevenness". *Journal of Sound and Vibration*, 287.4(2005): 989-1003.
22. Arhin, S., Noel, E.C., and Lakew, M. "Establishing International Roughness Index for a Dense Urban Area – A case study in Washington, DC." WIT Press, 6th Sustainability City, pp. 275-286.
23. Hajek, Jerry, Thomas Kazmierowski, and Graham Musgrove, "Switching to International Roughness Index." *Transportation Research Record, 1643* (1998): 116-124.
24. Capuruço, Renato, et al., "Full-Car Roughness Index as Summary Roughness Statistic." *Transportation Research Record: Journal of the Transportation Research Board*, 1905 (2005):148–156.
25. Rouillard, Vincent. "Using predicted ride quality to characterise pavement roughness." *International Journal of Vehicle Design*, 36.2-3 (2004): 116-131.
26. Papagiannakis, A.T. *The Need for a New Pavement Roughness Index; RIDE*. SAE Technical Paper 973267, 1997.
27. Papagiannakis, A.T. and B. Raveendran, "International Standards Organization-Compatible Index for Pavement Roughness". *Transportation Research Record: Journal of the Transportation Research Board, 1643* (1998): 110-115.
28. Karahmihas, Steven M. "Critical Profiler Accuracy Requirements." Report UMTRI The University of Michigan Transportation Research Institute, Ann Arbor (2005).
29. Jordens, Rob, Bert de Wit, and Rijkswaterstaat DWW. "Measurements and Criteria: Essential Elements for Pavement Management." *Surface Characteristics of Roadways: International Research and Technologies, ASTM STP 1031* (1990): 355-365.
30. Inman, Daniel J. Engineering Vibration. 4th ed. Englewood Cliffs, N.J.: Prentice Hall, 2013.
31. Rao, Singiresu S. "Chapter 3: Harmonically Excited Vibration." *Mechanical Vibrations*. 5th ed. Upper Saddle River, N.J.: Prentice Hall, 2011.
32. Johannesson, Pär, and Igor Rychlik. "Modelling of road profiles using roughness indicators." *International Journal of Vehicle Design 66.4* (2014): 317-346.
33. Yin, Fengjie, Mark Cerkovnik, and Al Conle. "Assessment of Fatigue Damage from Variable Amplitude Loads in Risers." *The Twenty-fourth International Ocean and Polar Engineering Conference*. International Society of Offshore and Polar Engineers, 2014.
34. Lee, Yung-Li, Jwo Pan, Richard B, Hathaway, and Mark E. Barkey. Fatigue Testing and Analysis Theory and Practice. Burlington: Elsevier Butterworth-Heinemann, 2005.
35. "Fatigue and Durability: Explained." Seminar. HBM nCode, 2013. Lecture.
36. Purushothaman, Nammalwar, Paramsothy Jayakumar, Sandip Datta, Venkat Pisipati, and James Critchley. "A Robust Durability Process for Military Ground Vehicles." *Ground Vehicle Systems Engineering and Technology Symposium* (2009): 1-9.
37. "Fatigue." Elements of Metallurgy and Engineering Alloys #05224G. ASM International, 2008. 243-264.
38. "Fatigue Life Evaluation." Iowa State University. 4 Sept. 2015. <http://www.public.iastate.edu/~e_m.424/Fatigue.pdf>.

39. ASTM, *Standard Practices for Cycle Counting in Fatigue Analysis*. 1990, American Society for Testing and Materials.
40. Dowling, N. E. "Fatigue at notches and the local strain and fracture mechanics approaches." *ASTM STP 677* (1979): 247-273.
41. Matsuishi, M., and T. Endo. "Fatigue of metals subjected to varying stress." *Japan Society of Mechanical Engineers, Fukuoka, Japan* (1968): 37-40.
42. Sutherland, Herbert J. *On the fatigue analysis of wind turbines*. No. SAND99-0089. Sandia National Labs., Albuquerque, NM (US); Sandia National Labs., Livermore, CA (US), 1999.
43. Hammerum, Keld. *A fatigue approach to wind turbine control*. Diss. Technical University of Denmark, DTU, DK-2800 Kgs. Lyngby, Denmark, 2006.
44. Aalberts, Pieter J., and Martijn W. Nieuwenhuijs. "Full scale wave and whipping induced hull girder loads." *4th. Int. Conf. on Hydroelasticity, Wuxi, China*. 2006.
45. "Fatigue of Metals." 4 Sept. 2015. <http://www.sut.ac.th/engineering/Metal/pdf/MechMet/12_Fatigue of metals.pdf>.
46. Yongchen, Liu, Sun Li, and Xu Lichao. "A Net Map Method on Vehicle Structural Fatigue Damage Analysis." *Open Mechanical Engineering Journal 9* (2015): 92-98.
47. Kobayashi, Equo, et al. "Fatigue life prediction of biomedical titanium alloys under tensile/torsional stress." *Materials transactions 47.7* (2006): 1826-1831.
48. McNeill, Scot I. "Implementing the Fatigue Damage Spectrum and Fatigue Damage Equivalent Vibration Testing." *Shock and Vibration Symposium* (2008): 1-20.
49. Müller, Tobias, et al. *Identifying Vehicle Model Parameters Using Measured Terrain Excitations*. No. 2009-01-1197. SAE Technical Paper, 2009.
50. Ma, Rui, et al. "A planar quasi-static constraint mode tyre model." *Vehicle System Dynamics* (2015): 1-13.

Appendix A: Investigation of the ASTM IRI Algorithm

An in-depth investigation of the standard IRI calculation is provided as a reference to compare an alternate method of calculating the IRI that is based on the IRI standard. Motivation for recalculating the IRI will be presented in the following Section A.3. It is important to develop a greater understanding of the current methodology by which the IRI is calculated conceptually and numerically. According to Sayers, the International Roughness Index (IRI) is computed from a single-tracked longitudinal profile. It is recommended that the sampling interval between sampled road data points from a single-tracked profile is no greater than 300 mm [9]. This road profile data is filtered by a moving average filter and a quarter car model filter to calculate the IRI. The dynamics of the quarter car model are presented in Appendix A.1.

To recall, a simple quarter car model with golden quarter car parameters is used to calculate the IRI, which was shown in Figure 2. The method currently used to calculate the IRI does not explicitly solve for suspension and tire forces. The equation of motions are structured in a linear state space representation, which is discussed in Appendix A.1. Due to the linearity of this approach, this approach is mostly restricted to linear applications. Thus, a method has been proposed in Appendix A.3 to recalculate the IRI based on the IRI standard which is termed VTPL IRI. This method solves modular dynamic equations, which are shown in Appendix B.2, for the quarter car model in Figure 2 through the use of Runge-Kutta integration. These equations of motions are modular in that any suspension or spindle components can be integrated into the equations of motion, which would allow for the refined simulations of actual parameters used in current fleets of vehicles.

A.1 Linear State Space Representation of Quarter Car

For the ASTM calculation of the IRI, the equations of motion are expressed in state-space form of which is shown in Equation (41).

$$\begin{aligned} \dot{x} &= Ax + Bu \\ y &= Cx + Du \end{aligned} \tag{41}$$

In matrix form, Equation (41) can be rewritten in terms of the quarter car model parameters, as shown in Equation (42).

$$\begin{bmatrix} \dot{x}_1 \\ \dot{x}_2 \\ \dot{x}_3 \\ \dot{x}_4 \end{bmatrix} = \begin{bmatrix} 0 & 1 & 0 & 0 \\ -\frac{k_s}{m_s} & -\frac{c_s}{m_s} & \frac{k_s}{m_s} & \frac{c_s}{m_s} \\ 0 & 0 & 0 & 1 \\ \frac{k_s}{m_u} & \frac{c_s}{m_u} & -\frac{(k_t + k_s)}{m_u} & -\frac{c_s}{m_u} \end{bmatrix} \begin{bmatrix} x_s \\ \dot{x}_s \\ x_u \\ \dot{x}_u \end{bmatrix} + \begin{bmatrix} 0 \\ 0 \\ 0 \\ \frac{k_t}{m_u} \end{bmatrix} \begin{bmatrix} z_{road} \end{bmatrix}$$

$$y = \begin{bmatrix} -1 & 0 & 1 & 0 \end{bmatrix} \begin{bmatrix} x_s \\ \dot{x}_s \\ x_u \\ \dot{x}_u \end{bmatrix} + \begin{bmatrix} 0 \end{bmatrix} \begin{bmatrix} z_{road} \end{bmatrix} \tag{42}$$

For the calculation of the IRI, Golden Quarter car parameters are used, which are defined in Equation (43).

$$\begin{aligned} c &= \frac{c_s}{m_s} = 6 \\ k_1 &= \frac{k_t}{m_s} = 653 \\ k_2 &= \frac{k_s}{m_s} = 63.3 \\ \mu &= \frac{m_u}{m_s} = 0.15 \end{aligned} \tag{43}$$

Thus, the A and B matrices of the linear state space system can be rewritten as shown in Equation (44).

$$A = \begin{bmatrix} 1 & 0 & 0 & 0 \\ -k_2 & -c & k_2 & c \\ 0 & 0 & 1 & 0 \\ \frac{k_2}{\mu} & \frac{c}{\mu} & -\frac{(k_1 + k_2)}{\mu} & -\frac{c}{\mu} \end{bmatrix}$$

$$B = \begin{bmatrix} 0 \\ 0 \\ 0 \\ \frac{k_1}{\mu} \end{bmatrix} \tag{44}$$

According to Sayers, for a point i, the total response of the quarter car model system is equal to the sum of the homogeneous solution (free response) of the system at the previous $i-1$

point and the particular solution (forced response) to the road input between points $i-1$ and i [9]. Assuming that the input into the system is constant, the closed-form solution of the linear state space equation becomes Equation (45).

$$x_i = e^{A\Delta/V} x_{i-1} + A^{-1}\left(e^{A\Delta/V} - I\right)Bu \tag{45}$$

In Equation (45), Δ is the sampling interval used, V is the simulated constant vehicle speed of the quarter car model, and I is a 4x4 identity matrix. Sayers explains that the term $e^{A\Delta/V}$ is the state transition matrix defined as a 4x4 matrix and $A^{-1}\left(e^{A\Delta/V} - I\right)B$ is a 4x1 partial response array defining the force response with respect to the input, u. According to Sayers, there are initialization errors at the beginning of the simulation of the quarter car model to calculate the IRI [9]. Sayers mentions that this initialization error diminishes as the simulated car travels along the profile. For the constant simulated IRI prescribed speed of 80 kph, this initialization influences the quarter car model for about 20 m. From a computer study conducted, Sayers mentions that the sprung and unsprung mass initial positions should be set to the height of the road sample points 11m into the road profile [9]. Sayers also mentions that for interpolation methods, the best approximation of a sampled profile to a continuous one is to have a constant profile slope between road data samples [9]. Therefore, the road profile, road input, and initial conditions are input in terms of profile slope for the calculation of the ASTM IRI.

A.2 Investigation of the FORTRAN ASTM algorithm

From investigating the ASTM *FORTRAN* code used to calculated the IRI [9],[11], it was noted that the moving average filter operation, in terms of the road profile slope, is calculated by Equation (46).

$$s_{ps,i} = \frac{h_{p,i+k} - h_{p,i}}{k\Delta} \tag{46}$$

Where k is the filter length of the moving average filter. The filter length is defined as the number of points that are averaged before the next set of points are averaged. The filter length is found by Equation (47).

$$k = \max\left(\text{int}\left(\frac{base}{\Delta} \right) + 0.5, 1 \right) \tag{47}$$

To set up the initial conditions in terms of the road profile slope at 11 m down the road, Equations (48) and (49) are used. First, the corresponding data point at 11 m down the road is first computed by Equation (48).

$$i_{11} = \min\left(\text{int}\left(\frac{base}{\Delta} \right) + 0.5, nsamp \right) \tag{48}$$

Knowing the index of this point, the road elevation at this point can be obtained and therefore the profile slope for the initial conditions can be obtained from Equation (49).

$$x_{u_0} = x_{s_0} = \frac{h_{p,i_{11}} - h_{p,i_1}}{i_{11}\Delta} \tag{49}$$

Sayers suggests to use 0 for the initial velocities of the sprung and unsprung mass [9]. Therefore, the initial conditions in terms of profile slope are written as ($x_{s_0}, \dot{x}_{s_0}, x_{u_0}, \dot{x}_{u_0}$) and is rewritten as Equation (50).

$$ssInitCond = \left[\frac{h_{p,i_{11}} - h_{p,i_1}}{i_{11}\Delta}, 0, \frac{h_{p,i_{11}} - h_{p,i_1}}{i_{11}\Delta}, 0 \right] \tag{50}$$

The following is a description of how to convert the road data samples in terms of profile slope. Within the ASTM FORTRAN code, the variable 'UNITSC' is a main variable used in the conversion of elevation points to profile slope. 'UNITSC' is the product of the meters per unit of profile elevation height and the desired units of the IRI. For instance, in the code used, road elevation is usually converted to meters. Then, a typical unit in which the IRI is calculated is in m/km. Therefore, Equation (51) mathematically defines 'UNITSC.'

$$UNITSC = \left(\frac{m}{profileHeight} \right)\left(\frac{1000m}{1km} \right) = \left(\frac{m}{m} \right)\left(\frac{1000m}{1km} \right) = \frac{1000m}{km} \tag{51}$$

Another main variable used is SFPI. This variable is defined by Equation (52).

$$SFPI = \left(\frac{UNITSC}{k\Delta} \right) \tag{52}$$

Then, SFPI is multiplied by a forward difference of the road elevation that depends on the k, the filter length, which is incorporated into the equation shown above. This is done in a 'for loop'

for *n*-*k* data points. For a 0mm moving average filter, *k*=1. For a 250 mm moving average filter, *k*=2. The road profile mathematical equation is shown below, which is a reformulation of the moving average filter equation shown in Equation (46). Therefore, in essence, Equation (46) is a dual operation for calculating the profiling slope and smoothening the slope by using a moving average filter.

$$s_{ps,i} = SFPI\left(h_{p,i+k} - h_{p,i}\right) \tag{53}$$

The smoothed profile slope obtained from the Equation (53) is then filtered by the quarter car model filter to obtain the output, as defined by the C matrix, the difference in suspension displacement. The sprung suspension displacement is subtracted by the unsprung suspension displacement. However, since the road profile, road input, and the initial conditions were defined in terms of profile slope, the suspension displacement output is in terms of slope. This is actually indicative of the suspension velocity. To recall, Sayers discusses redefining the road elevation in terms of profile slope, transforms the initial conditions (shown in Equation (50)) and uses the quarter car model filter to filter the profile slopes.

Due to the filter length and the forward difference, Equation (54) is performed to recalculate the number of samples available after the filtering from the moving average filter/conversion to profile slope. Therefore, from this operation, there will be the loss of one sample point, regardless whether or not the road profile slope is filtered by the moving average filter. This is due to the forward difference applied to the road profile to obtain the road profile in terms of a slope profile.

$$n_{samp} = n_{samp} - k \tag{54}$$

Since these displacements are in terms of the slope, the absolute value of the summation of all the differences is taken to obtain the accumulated suspension travel per distance traveled and is then divided by the recalculated number of sample points due to the filtering, which was shown in Equation (54). The computational equation to calculate the ASTM IRI is shown in Equation (55).

$$IRI = \frac{\sum_{i=1}^{n_{samp}} \left| x_{u_i} - x_{s_i} \right|}{\left(n_{samp}\right)} \tag{55}$$

From the investigation, the IRI results in the loss of one sampled road data point due to the forward differencing used in converting the discrete road elevation points to an average profile slope. To overcome the loss of the sampled road point, the road profiles calculated by the IRI algorithm are usually zero-padded to prevent the loss of roughness content from the data.

When computing the DRI, this technique of forward differencing cannot be implemented since it necessary to evaluate the roughness at each *discrete* point. Therefore, in developing the DRI algorithm, it was necessary to generate roughness values for N points. To generate N points, as shown by Equation (30), the start and end indices of the DRI are multiplied by 2 (due to half of the longitudinal road distance considered for these indices). For the special case in which a constant velocity is used, the multiplicative factors of 2 for the beginning and end points reduce from Equation (30) due to half of the time considered for the vehicle to travel this distance under a constant speed. Thus, N roughness values for N discrete points are obtained. For varying velocities cases not applicable to the IRI, the time elapsed for the first and end points may not necessarily consist of half the time elapsed to reduce the multiplicative factor of 2 given to these indices (due to half of the distance traveled). Therefore, to remain consistent, the first and last indices are influenced by a factor greater than the rest of the indices.

A.3 Alternative Approach to the IRI Calculation

Part of the motivation to emulate the calculation of the IRI standard is to be able to introduce nonlinear elements into the suspension and tire components of the quarter car model. Since the IRI standard, as discussed in Appendix A.1, uses a state space system to calculate the IRI, it is limited to linear applications. Also, from the algorithm presented by Sayers, it is difficult to extract the suspension and tire forces exerted through the vehicle simulation. Thus, it is of great interest to modularize the code structure such that any suspension and tire force can be input into the system. Therefore, a new method of calculating the IRI is presented. The IRI calculated from this method will be termed the VTPL IRI. The main difference from this method and the ASTM method of calculating the IRI is that the VTPL IRI does not convert the elevation data into slopes, as presented in Appendix A.2. The road elevation points, depending if the road profile has been pre-filtered (0 mm moving average filter would be applied) or unfiltered (250 mm moving average filter), is first passed through a moving average filter. Then, a modular quarter car model is run through a terrain profile specified by discrete road elevation

points. Runge-Kutta integration is used to solve for the differential equations to find the suspension travel. Once calculated, the integral of the rectified suspension travel is calculated and divided by the road distance to obtain the IRI. Pseudo code explaining the details of configuration the vehicle simulation is outlined in Appendix D.

A.3.1 Comparison of ASTM IRI results to Raw VTPL IRI results

Table 15 shows a comparison of the IRI values calculated for measured and synthetic roads. The error is shown for each road. A corrected VTPL IRI is shown, which is discussed in Appendix A.3.2. The ASTM IRI values were calculated using the pseudo code provided in [11].

Road	Raw VTPL IRI (m/km)	Error	ASTM IRI (m/km)	Corrected VTPL IRI (m/km)	Error
ASTM Tri Pulse	4.3686	6.3488e-006	4.3685	4.3685	4.0932e-008
Pothole	2.6934	0.0071	2.6744	2.6744	2.1645e-008
ILRaVTfac0914070	7.1907	0.0047	7.2249	7.2249	3.0363e-008
ILRaVTfac0914080	12.9778	8.8396e-004	12.9893	12.9893	1.1462e-008
MNRp00d9a1909020	1.3272	0.0659	1.2452	1.2452	3.0159e-008
MNRp00d9a1909010	1.4100	0.0806	1.3048	1.3048	3.9438e-008
MNRp00d9a1909080	1.3582	0.0640	1.2765	1.2765	2.3665e-008
SSI Road (2.02 mi)	0.8283	0.0032	0.8257	0.8257	1.2539e-008

Table 15. Comparison of calculated IRI values

A.3.2 Application of a correction factor to obtain exact IRI convergence

Since the ASTM IRI code converts the road elevations into profile slopes and smoothens the profile using the moving average filter simultaneously, a shift in the road profile occurs within ASTM code. The shift is of no concern in terms of calculating the standard IRI because the indices of the road data points are unimportant since the profiles slopes are averaged to compute the IRI. For future uses of the VTPL IRI, the tracking of the indices is of great importance, particularly for the development of the DRI, where the indices are used to calculate the roughness of a discrete point. To recap, the ASTM IRI dually converts the road elevations into profile slopes and applies the moving average filter from Equation (46). This equation causes many shifts, depending on the baselength of the moving average filter. For instance, if no moving average filter is used (i.e. filter length of 1), Equation (46) results in only a horizontal backwards shift of 1 due to the forward differencing of the road elevations in order to convert to profile slope.

Figure 27 shows the backwards shift effect and the offset present in the suspension response results when no moving average filter is applied. The ASTM suspension response is offset with the VTPL suspension response by 1 data point. To obtain the plots shown below, the suspension velocity output of the VTPL algorithm was plotted with the suspension response output from the ASTM algorithm. The VTPL suspension response was approximately scaled in order to see that the two responses are offset by 1 data point. Interestingly, it was observed that the ASTM suspension response is shifted back 1 data point. This is due to the forward differencing applied within the ASTM algorithm in order convert the road profile in terms of slope before being filtered by the quarter car model. This is the case because as shown in the left suspension response plot of Figure 27 the ASTM curve shows a non-zero suspension response magnitude at point 5 along the road profile. In the right road elevation plot of Figure 27, there is no excitation (road elevation is 0) at point 5. This signifies that the suspension response curve is shifted backwards by 1 data point. Also to further verify this, the last data point (101) for the ASTM suspension response is zero, whereas a nonzero value is obtained from the VTPL response.

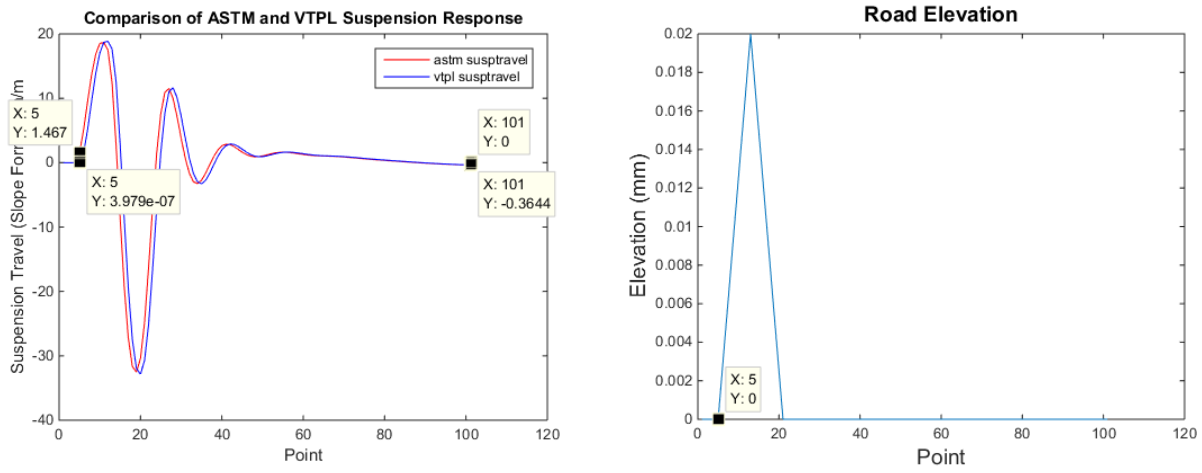

Figure 27. Comparison of ASTM and VTPL suspension travel response

If a 250 mm moving average filter and a spatial road increment of 0.15 m are used, the filter length becomes 2. In this scenario, the moving average filter forward averages two values before averaging the next two sequences of data points. However, in the ASTM code, this difference is stored as index i. Together with the forward differencing to obtain the profile slope, this results in an offset of 3 data points (1 shift from forward differencing, 2 shifts from

moving average filter), which can be seen in Figure 28. Therefore, the effect for the moving average filter with a filter length of 2 results in a further offset of 2 data points. In total, the ASTM suspension response is shifted back 3 data points in this situation.

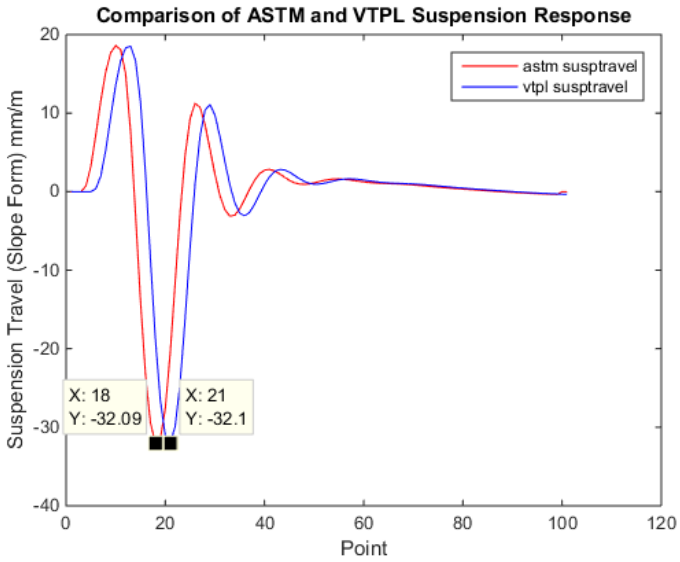

Figure 28. Comparison of horizontal shift in suspension response

Equation (56) is used to calculate the appropriate shift necessary to align the VTPL suspension response to the ASTM suspension response.

$$shift = 1 + k\,,\ \forall k \geq 2 \tag{56}$$

Therefore, the shift correction necessary to align the suspension responese is defined as the sum of 1 and the filter length for filter lengths greater than or equal to 2. The 1 in Equation (56) is due to the forward differencing used within the ASTM algorithm and the filter length is due to the number of points the moving average filter looks ahead and averages. For the filter length of 1, this is analogous to not using a moving average filter and therefore the only shift is due to the forward differencing in this situation.

Once the VTPL suspension response is appropriately aligned with the ASTM suspension response, the VTPL suspension response can be appropriately scaled to exactly match the ASTM suspension response. This is accomplished by dividing each element (corresponding index) of the VTPL suspension response by the ASTM suspension response to obtain an array of scaling factors as shown in Equation (57) . This is made possible due to the appropriate shifting correction applied previously.

$$sf = \frac{VTPL_{sr}}{ASTM_{sr}} \tag{57}$$

This VTPL suspension response is then divided by the appropriate array of scaling factors to convert to profile slope in order to match the ASTM response as shown in Equation (58).

$$sr_{ps} = \frac{VTPL_{sr}}{sf} \tag{58}$$

Figure 29 below shows that after the appropriate shifts are made and the VTPL suspension response is scaled appropriately into profile slope, the exact suspension travel as calculated by the ASTM is obtained.

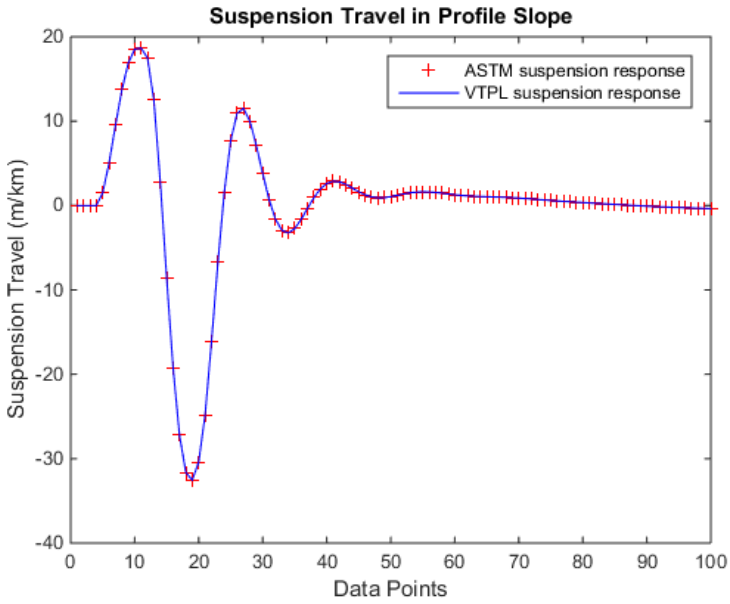

Figure 29. Correction factor applied to VTPL suspension response

The numerical results, with the correction factor applied, are shown for the triangular pulse simulated in ASTM E1926-08 in Table 16.

	0 mm moving average	250 mm moving average
ASTM IRI (m/km)	4.3685	4.3562
VTPL IRI (m/km)	4.3685	4.3562

Table 16. Exact convergence is obtained for ASTM IRI and VTPL IRI

From the in-depth investigation of the IRI, road data elevation points are converted into slopes of the profile, which are then input into the state space system defined earlier. With the VTPL

algorithm, this cannot be done because there will be inconsistent interpretations with the data. For instance, since the explicit tire and suspension forces are solved for, these equations will be inconsistent since profile slope instead of the actual displacement and velocities from the vehicle model states would be used to calculate the suspension and tire forces. For this reason, the shifting and appropriate scaling to the VTPL suspension response approach was followed. In essence, the VTPL calculates the suspension response using the road elevation points and then once all of the quarter car model states have been calculated, converts the suspension velocity response to profile slope through a scaling factor in order to match the ASTM IRI. This correction factor is only applied to the simulation of the quarter car model using a constant vehicle speed and golden quarter car parameters. For varying speeds and other nonlinear vehicle parameters, the correction factor to match the IRI cannot not be applied. Instead of applying the correction factor to the suspension velocity, the absolute value of the suspension velocity response is simply integrated to obtain the accumulated suspension travel and is then normalized by the total length of the road traveled (by definition as shown in Equation (1)).

As a side note, in one of the lines within the ASTM FORTRAN code, the variable IBASE is defined by Equation (59).

$$IBASE = MAX\left(INT\left(BASE / DX + 0.5,1\right)\right) \tag{59}$$

It has been observed that this line can lead to potential problems in inaccurately calculating the *IBASE*, which is the baselength of the moving average filter. For example, in the rare case of a 5 mm sampling interval with a 250 mm moving average filter, the line above incorrectly calculates the filterlength to be 51, in which it is not needed to add the 0.5 to make 51 since 250/5 is equal to 50, which is a whole number. The 0.5 in the code above is added for rounding purposes to the nearest integer since FORTRAN does not have a rounding function.

A.3.3 Conclusion

From this investigation, an alternative algorithm that can be used to calculate the IRI was discussed. This algorithm is modular in that nonlinear elements can be incorporated into the quarter car model, without relying on a state space system (IRI). Note that the applied correction factor is only used to obtain an *exact* convergence under a golden quarter quarter car model at 80

kph. This correctional factor cannot be used for the simulation of vehicle parameters differing from the golden quarter car parameters. For such parameters, the correction factor will not be applied. However, this algorithm will allow for the simulation of refined vehicle parameters that can be more representative of actual fleets of cars.

Appendix B: Vehicle models used in simulation

B.1 1-DOF Vehicle Model

Figure 30 shows a 1-DOF vehicle model. This model does not contain a suspension. A spring follower along with a damper is used to model the tire characteristics of the model. The damping of the tire is set to three percent. This model can be used to calculate pseudo damage and the IRI. Since this model does not have a suspension, the roughness calculated from this model is likely to be very high.

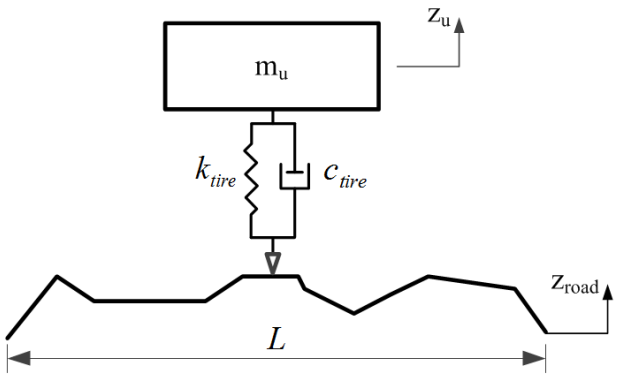

Figure 30. 1-DOF vehicle model

The equations of motion for the vehicle model are as follows:

$$\ddot{z}_u = \frac{F_{tire}}{m_u} \tag{60}$$

$$F_{tire} = k_{tire}\left(z_{road} - z_u\right) + c_{tire}\left(\dot{z}_{road} - \dot{z}_u\right) \tag{61}$$

Equation (62) defines the tire force found from the terrain excitations, where c_{tire} is set to 3%.

$$c_{tire} = 0.03\left(2\sqrt{m_{un}k_{tire}}\right) \tag{62}$$

$$\dot{z}_{road} = \left(\frac{dy}{du}\right)\left(\frac{du}{dt}\right) \tag{63}$$

Equation (63) also defines a component used to calculate the tire force, where $\frac{dy}{du}$ is equal to the rate of change in road elevation per spatial coordinate traveled and $\frac{du}{dt}$ is equal to the vehicle velocity.

1-DOF Static Deflection Equations:

$$z_u = \frac{-m_u g}{k_{tire}} \tag{64}$$

$$\dot{z}_u = 0 \tag{65}$$

B.2 2-DOF Vehicle Model (Quarter Car Model)

Figure 2 shows the quarter car model used to calculate the DRI. The equations of motions for the model are shown below. The vertical acceleration of the sprung mass is calculated by Equation (66).

$$\ddot{z}_s = \frac{F_{susp}}{m_s} \tag{66}$$

Equation (67) is used to calculate the unsprung mass vertical acceleration.

$$\ddot{z}_u = \frac{F_{tire} - F_{susp}}{m_u} \tag{67}$$

The tire force is defined as shown in Equation (68).

$$F_{tire} = k_{tire}\left(z_{road} - z_u\right) \tag{68}$$

Equation (69) defines the suspension force.

$$F_{susp} = k_{susp}\left(z_u - z_s\right) + c_{susp}\left(\dot{z}_u - \dot{z}_s\right) \tag{69}$$

2-DOF Static Deflection Equations:

$$z_s = -\left(\frac{m_s g}{k_{susp}} + \frac{\left(m_s + m_u\right)g}{k_{tire}}\right) \tag{70}$$

$$\dot{z}_s = 0 \tag{71}$$

$$z_u = \frac{-\left(m_s + m_u\right)g}{k_{tire}} \tag{72}$$

$$\dot{z}_u = 0 \tag{73}$$

B.3 7-DOF Vehicle Model (Full Car Model)

The 7-DOF model shown has been modeled and validated by Müller, Tobias, et al [49]. This model has been used for IRI and pseudo-fatigue damage estimations.

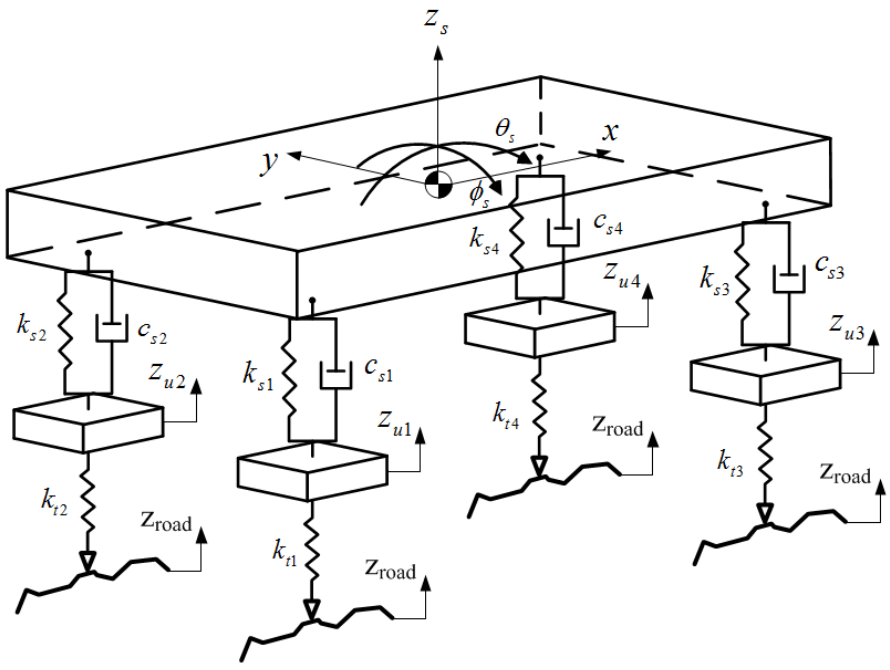

Figure 31. 7-DOF full car model

The corners of the vehicle are defined as follows:

- 1: Left Front
- 2: Right Front
- 3: Left Rear
- 4: Right Rear

Mathematically, the 7-DOF model has 14 states, which are defined as follows:

- 1: sprung mass position
- 2: sprung mass velocity
- 3: roll position
- 4: roll velocity
- 5: pitch position
- 6: pitch velocity
- 7: corner 1 unsprung mass position
- 8: corner 1 unsprung mass velocity
- 9: corner 2 unsprung mass position
- 10: corner 2 unsprung mass velocity
- 11: corner 3 unsprung mass position
- 12: corner 3 unsprung mass velocity
- 13: corner 4 unsprung mass position
- 14: corner 4 unsprung mass velocity

The equations of motion for the 7-DOF model are as follows:

The sprung mass vertical acceleration is defined by Equation (74).

$$\ddot{z}_s = \frac{1}{m_s}\left(F_{susp1} + F_{susp2} + F_{susp3} + F_{susp4}\right) \tag{74}$$

The pitch angle acceleration of sprung mass is defined by Equation (75).

$$\ddot{\theta}_s = \frac{1}{I_{yy}}\left[a\left(F_{susp1} + F_{susp2}\right) - b\left(F_{susp3} + F_{susp4}\right)\right] \tag{75}$$

The roll angle acceleration of sprung mass is defined by Equation (76).

$$\ddot{\phi}_s = \frac{t}{I_{xx}}\left(-F_{susp1} + F_{susp2} - F_{susp3} + F_{susp4}\right) \tag{76}$$

The next set of equations of motion define the vertical acceleration of the unsprung masses for each corner as shown in Equation (77).

$$\begin{aligned}
\ddot{z}_{u1} &= \frac{1}{m_{u1}}\left(F_{tire1} - F_{susp1}\right) \\
\ddot{z}_{u2} &= \frac{1}{m_{u2}}\left(F_{tire2} - F_{susp2}\right) \\
\ddot{z}_{u3} &= \frac{1}{m_{u3}}\left(F_{tire3} - F_{susp3}\right) \\
\ddot{z}_{u4} &= \frac{1}{m_{u4}}\left(F_{tire4} - F_{susp4}\right)
\end{aligned} \tag{77}$$

The set of equations shown for Equation (78) define the definition of the suspension forces.

$$\begin{aligned}
F_{susp1} &= k_{susp1}\left(z_{u1} - z_{sc1}\right) + c_{susp1}\left(\dot{z}_{u1} - \dot{z}_{sc1}\right) \\
F_{susp2} &= k_{susp2}\left(z_{u2} - z_{sc2}\right) + c_{susp2}\left(\dot{z}_{u2} - \dot{z}_{sc2}\right) \\
F_{susp3} &= k_{susp3}\left(z_{u3} - z_{sc3}\right) + c_{susp3}\left(\dot{z}_{u3} - \dot{z}_{sc3}\right) \\
F_{susp4} &= k_{susp4}\left(z_{u4} - z_{sc4}\right) + c_{susp4}\left(\dot{z}_{u4} - \dot{z}_{sc4}\right)
\end{aligned} \tag{78}$$

Equation (79) defines the sprung mass vertical displacement contribution to each of the four corners of the vehicle.

$$\begin{aligned}
z_{sc1} &= z_s + a\sin\left(\theta_s\right) - 0.5t\sin\left(\phi_s\right) \\
z_{sc2} &= z_s + a\sin\left(\theta_s\right) + 0.5t\sin\left(\phi_s\right) \\
z_{sc3} &= z_s - b\sin\left(\theta_s\right) - 0.5t\sin\left(\phi_s\right) \\
z_{sc4} &= z_s - b\sin\left(\theta_s\right) + 0.5t\sin\left(\phi_s\right)
\end{aligned} \tag{79}$$

Equation (80) defines the sprung mass velocity contribution to each of the four corners.

$$\begin{aligned}
\dot{z}_{sc1} &= \dot{z}_s + a\cos\left(\theta_s\right)\dot{\theta}_s - 0.5t\cos\left(\phi_s\right)\dot{\phi}_s \\
\dot{z}_{sc2} &= \dot{z}_s + a\cos\left(\theta_s\right)\dot{\theta}_s + 0.5t\cos\left(\phi_s\right)\dot{\phi}_s \\
\dot{z}_{sc3} &= \dot{z}_s - b\cos\left(\theta_s\right)\dot{\theta}_s - 0.5t\cos\left(\phi_s\right)\dot{\phi}_s \\
\dot{z}_{sc4} &= \dot{z}_s - b\cos\left(\theta_s\right)\dot{\theta}_s + 0.5t\cos\left(\phi_s\right)\dot{\phi}_s
\end{aligned} \tag{80}$$

Equation (81) defines the spindle/tire forces at each corner.

$$\begin{aligned} F_{tire1} &= k_{tire1}\left(z_{road1} - z_{u1}\right) \\ F_{tire2} &= k_{tire2}\left(z_{road2} - z_{u2}\right) \\ F_{tire3} &= k_{tire3}\left(z_{road3} - z_{u3}\right) \\ F_{tire4} &= k_{tire4}\left(z_{road4} - z_{u4}\right) \end{aligned} \tag{81}$$

7-DOF Static Deflection Equations:

Corner 1:

Sprung mass contribution to corner 1:

$$m_{s1} = \frac{1}{2}\left(\frac{m_s b}{a+b}\right) \tag{82}$$

Unsprung mass deflection:

$$z_{u1} = \frac{\left(m_{s1} + m_{u1}\right)g}{k_{tire1}} \tag{83}$$

Corner 2:

Sprung mass contribution to corner 2:

$$m_{s2} = \frac{1}{2}\left(\frac{m_s b}{a+b}\right) \tag{84}$$

Unsprung mass deflection:

$$z_{u2} = \frac{\left(m_{s2} + m_{u2}\right)g}{k_{tire2}} \tag{85}$$

Corner 3:

Sprung mass contribution to corner 3:

$$m_{s3} = \frac{1}{2}\left(\frac{m_s a}{a+b}\right) \tag{86}$$

Unsprung mass deflection:

$$z_{u3} = \frac{(m_{s3} + m_{u3})g}{k_{tire3}} \tag{87}$$

Corner 4:

Sprung mass contribution to corner 4:

$$m_{s4} = \frac{1}{2}\left(\frac{m_s a}{a+b}\right) \tag{88}$$

Unsprung mass deflection:

$$z_{u4} = \frac{(m_{s4} + m_{u4})g}{k_{tire4}} \tag{89}$$

Sprung Mass:

Sprung mass deflection:

$$z_s = \left[\left(\frac{m_s g}{k_{susp1} + k_{susp2} + k_{susp3} + k_{susp4}}\right) + z_{u1} + z_{u2} + z_{u3} + z_{u4}\right] \tag{90}$$

For the initial conditions for the 7-DOF model, all of the sprung and unsprung mass deflections will be negative for the sprung mass and unsprung masses positions (going down due to gravity). Sprung mass roll, pitch, velocity, and unsprung velocities are zero for the initial conditions.

Appendix C: Taylor Series Expansion

To estimate the suspension travel, a Taylor series approximation is used. The estimated change in suspension travel and the time for the vehicle to pass through the j^{th} interval are used to estimate the suspension velocity in the j^{th} interval. Let $g(t)$ represent the suspension travel. Then, the general form of the Taylor series polynomial centered at t_j can be expressed in Equation (91).

$$g(t) = g(t_j) + g_j'(t - t_j) + \frac{1}{2!} g_j''(t - t_j)^2 + ... \tag{91}$$

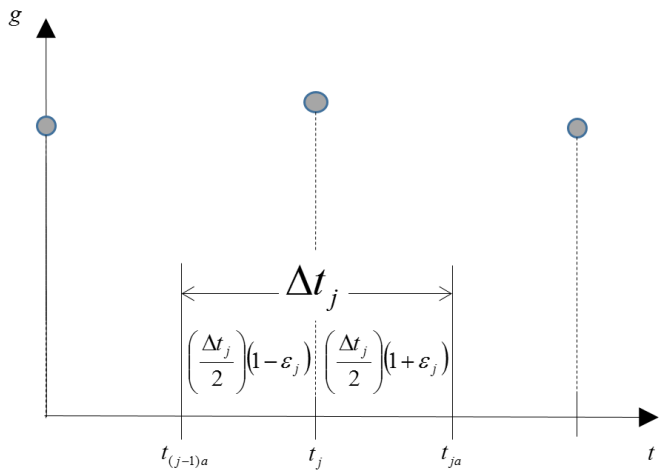

Figure 32. Suspension response plotted as a function of time

Equation (92) shows that the suspension travel can be estimated at the auxiliary point, $t = t_{ja}$, shown in Figure 32.

$$\begin{aligned} g(t_{ja}) &= g_j + g_j'(t_{ja} - t_j) + \frac{1}{2!} g_j''(t_{ja} - t_j)^2 + ... \\ g(t_{ja}) &= g_j + g_j'\left(\frac{\Delta t_j}{2}\right)(1+\varepsilon_j) + \frac{1}{2!} g_j''\left(\frac{\Delta t_j}{2}\right)^2 (1+\varepsilon_j)^2 + ... \\ g(t_{ja}) &= g_j + \frac{1}{2} g_j'(\Delta t_j)(1+\varepsilon_j) + \frac{1}{8} g_j''(\Delta t_j)^2 (1+\varepsilon_j)^2 + ... \end{aligned} \tag{92}$$

A second estimation can be obtained at $t = t_{(j-1)a}$ centered at t_j as shown in Equation (93).

$$\begin{aligned} g(t_{(j-1)a}) &= g_j + g_j'(t_{(j-1)a} - t_j) + \frac{1}{2!} g_j''(t_{(j-1)a} - t_j)^2 + ... \\ g(t_{(j-1)a}) &= g_j + g_j'\left(-\frac{\Delta t_j}{2}\right)(1-\varepsilon_j) + \frac{1}{2!} g_j''\left(-\frac{\Delta t_j}{2}\right)^2 (1-\varepsilon_j)^2 + ... \\ g(t_{(j-1)a}) &= g_j - \frac{1}{2} g_j'(\Delta t_j)(1-\varepsilon_j) + \frac{1}{8} g_j''(\Delta t_j)^2 (1-\varepsilon_j)^2 + ... \end{aligned} \tag{93}$$

Now that there are approximations for the auxiliary points of $t = t_{ja}$ and $t = t_{(j-1)a}$, two systems of equations can be constructed to solve for g_j' and g_j''. These two equations are constructed by adding and subtracting the two approximations as shown in Equation (94) and Equation (95), respectively.

$$g(t_{ja}) + g(t_{(j-1)a}) = 2g_j + g_j'\Delta t_j\varepsilon_j + \frac{1}{4}g_j''(\Delta t_j)^2 \tag{94}$$

$$g(t_{ja}) - g(t_{(j-1)a}) = g_j'\Delta t_j + \frac{1}{2}g_j''(\Delta t_j)^2\varepsilon_j \tag{95}$$

Solving Equation (95) for g_j'' and substituting into Equation (94), Equation (96) shows the result obtained for g_j'.

$$g_j' = \frac{g(t_{ja}) - g(t_{(j-1)a})}{\Delta t_j} + \frac{-2\varepsilon_j\left[g(t_{ja}) + g(t_{(j-1)a}) - 2g_j\right]}{\Delta t_j} \tag{96}$$

From Equation (96), the zeroth order term is taken for the estimation of the suspension travel such that the result shown in Equation (97) is obtained when g_j is redefined as z_j.

$$\dot{z}_j = \frac{z(t_{ja}) - z(t_{(j-1)a})}{\Delta t_j} \tag{97}$$

Equation (97) is simplified in Equation (98), which is the result shown from Equation (14).

$$\dot{z}_j = \frac{\Delta z_j}{\Delta t_j} \tag{98}$$

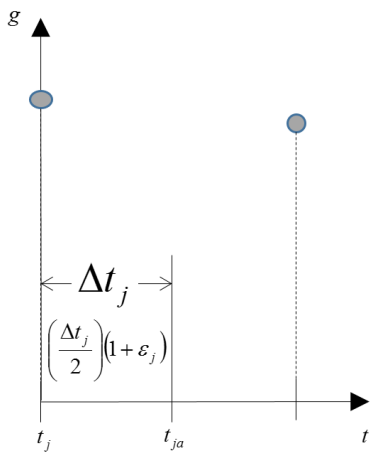

Figure 33. Suspension response at auxiliary point

For the beginning point as shown in Figure 33, Equation (92) can be reformulated as Equation (99).

$$g(t_{ja}) = g_j + g_j'(t_{ja} - t_j) + \frac{1}{2!} g_j''(t_{ja} - t_j)^2 + ...$$
$$g(t_{ja}) = g_j + g_j'(\Delta t_j)(1 + \varepsilon_j) + \frac{1}{2!} g_j''(\Delta t_j)^2 (1 + \varepsilon_j)^2 + ... \quad (99)$$

Using the first order approximation of the Equation (99), a slight variation of Equation (96) is obtained, assuming ε_j is small.

$$g_j' = \frac{g(t_{ja}) - g(t_j)}{\Delta t_j} \quad (100)$$

Equation (100) simplifies into Equation (98) as well when g_j is redefined as z_j. The same technique shown applies for the end point.

Appendix D: Implementation of DRI in Simulation

The DRI algorithm consists of several functions. The following is an overview of each of the functions in the order that they are executed in the code.

- The first function consists of initializing the basic parameters that are used in the code. This function is called 'init_params'

  Within this function, various variables are predefined. All of the variables are stored in a data structure 'S.Params.' This allows for a very convenient callout of the variables in other functions because the data structure S is simply imported into the function instead of individually calling out the variables. The quarter car model parameters such as the sprung mass (msprung), the unsprung mass (munsprung), the suspension stiffness (ksprung) and damping (csprung), and the stiffness of the unsprung mass (ktire) are defined. Gravity is set at 9.807 m/s^2.

  The variable filterBase refers to the base length of the moving average filter used in the 'moving_average_filter' function. The units of this variable is in meters.

The variable uIncrement refers the constant spatial increment between sampled road elevation data points. The units are in meters.

The variable velocity consists of a column vector that consists of the discrete velocities of the vehicle at each of the sampled road data elevation points. This is assumed to be known. For the IRI, calculation, the default is set to 80. The units of the individual velocities within the vector are in kph and are then converted to m/s.

The variable astmVelocity is the velocity that the ASTM algorithm uses to calculate the IRI.

The variable options is used to set the Runge-Kutta solver tolerances to control the accuracy of the solution. Change to smaller tolerances to increase the accuracy of the solution, however, the computing power necessary to solve the differential equations significantly increases along with speed reductions in the algorithm.

Variables are also defined that are used in the 'define_steady_state' function.

Variables are also defined that are used in the 'define_impulse_response' function.

- The second function consists of defining the road elevation profile used in the simulation. This function is called 'define_zRoad'

Within this function, a .mat or .erd file can be loaded from actual data acquisition trips or the road elevation profile can be manually defined by inputting the road elevations in a column vector.

Once the road profile is selected, each of the road elevation points is subtracted by the first elevation point to get the road profile in terms of relative heights with the first point set as an absolute reference. The output of this function is the road elevation profile (zRoad).

- The third function, optional, consists of calculating the IRI according to the ASTM standard. This function uses an independent function to calculate the IRI and is based on the FORTRAN code defined in [11]. The variables associated with the internal algorithms of this code is not associated with the DRI algorithm. Therefore, this function is optional and can be commented out. This function is just used as a reference to compare the average DRI to the IRI standard for convergence purposes. This function is called 'calc_ASTM_IRI.'

- The fourth function, filters the road profile by a moving average filter. This function is called 'moving_average_filter.' The first two lines of the function involve calculating the filter length of the filter according to the specified base length and spatial increment between data points. Most common baselengths used for the filter are 0 mm (no filtering) and 250 mm. To change the baselength of the moving average filter, go to the 'init_params' function and change the filterBase function to 0 or 0.25. Within the moving average filter function, the delay involved, if any, by the filter and the filter coefficients are also calculated. These topics are covered in detail in the Chapter 3. The road is then filtered according to the coefficients calculated earlier by the filter command. One of the important tasks of this function is to shift the filtered road profile back to its original location since the application of the filter involves a shifting for particular base lengths specified. A second alternative to this function is to simply import the filtered profile using the define_zRoad function and set the baselength for the moving average filter to zero.

- The fifth function, optional, involves increasing the sampling rate of the elevation data by specifying a desired spatial increment in which to upsample the data such that the original data can be interpolated at the values specified by the desired spatial increment. This function is called 'upsample_for_IRI_convergence.' This function is optional and is used only to check that the average DRI converges to the IRI at sufficiently small sampling intervals.

- The sixth function is called ‘define_steady_state.’ The purpose of this function is to obtain the steady state behavior of the quarter car model. Initially, since gravity is taken into account, the vehicle tire and suspension deflects due to gravity, resulting in a transient state. The quarter car model is run on a flat road until the deflection and movement of the quarter car model is below a specified tolerance. Once the tolerance is obtained, the positions and velocities of the quarter car model are recorded and these are defined as the steady state conditions for the quarter car model (initial conditions), which are output as a variable named ssInitCond.

    - For this function, the initial static deflections due to gravity are input for the initial positions of the sprung and the unsprung mass. The initial velocities of the unsprung and sprung masses are assumed to be zero. An initial value of -1 is given to a variable named ‘keepGoing.’ This variable toggles between -1 or 1. It switches to 1 when the vehicle states reach a steady state condition, such that all of the vehicle states are approximately zero. The tolerance is determined by a multiplier and the smallest number that the cpu can calculate (eps). An example of this number is 2.2204e-16.

    - The bulk of this function consists of a flat road vehicle simulation that is looped such that the road keeps extending until the vehicle reaches a steady state condition. In the simulation, the vehicle states, which are the positions and velocities of the unsprung and sprung mass are calculated. Before the road is extended, the final vehicle states at the end of the road are recorded and checked to see if they are within the desired tolerance. If they do not fulfill the specified steady state tolerances, the vehicle states are passed on as the initial conditions for the next extended portion of the road. The process is repeated via a while loop that is controlled by the variable ‘keepGoing’. When ‘keepGoing’ is positive (toggles to 1), the loop is terminated and the final vehicle states are saved as ‘ssInitCond’, which are the vehicle steady state initial conditions. These conditions are used for all vehicle simulations, such as the actual vehicle road simulation of the road profile of interest and for the impulse response simulation.

- The seventh function is called 'veh_road_simulation.' This is one of the main functions of the algorithm and this function consists of several functions within that are used to calculate the vehicle states in response to the road elevation profile.

    - Within this function there are several variable names. The uVector variable is a row vector of the spatial increments of the road covering the entire distance. For example, if the spatial increment was 0.15 m, the uVector consists of these accumulated spatial increments (i.e., 0.15, 0.30, 0.45, etc.) up until the ending distance of the road.
    - uVectorDummy is similar to the uVector variable, except that it covers twice the distance of the uVector. This is done to ensure that the vehicle, during the simulation, covers the actual distance of the road of interest (specified by the uVector). The reason this method is employed is because one of the inputs into the differential equation solver involves time, which is estimated (especially for variable velocity scenarios). Thus the time it takes the vehicle to reach the end of the road is estimated. To ensure that the vehicle goes through all of the points of the road profile, the time is overestimated and this is why an extended length of the road is used (uVectorDummy).
    - Since the incremental distance vector is extended, the road elevation and velocities vectors must also be increased to the same length. These are referred to as zRoadDummy and uVelocityDummy.
    - To estimate the amount of time the vehicle takes to reach the end of the road, a constant acceleration is assumed between road data sampled points. As a rough estimate, the following equation is used to obtain an initial estimate of the time. In the code, there are two variables called uLowVelocity and uHighVelocity, which are averaged according to the equation below. The result of the equation below is called deltaTimes in the code. To ensure that enough time is given in the simulation for the vehicle to reach the end of the road, 50% of the calculated time is also added to the initial estimate of time added. This result is called estTspan.

Therefore, in the differential equation solver (ode45), the time span for the solution is from 0 seconds to estTspan interval.

$$\Delta t_j = \frac{2\Delta u}{v_o + v_f}$$

- The next major function within the veh_road_simulation function is called 'calc_veh_response.' Within this function, all of the variables mentioned above, along with some of the parameters stored in the 'S' data structure are imported. Inside of this function, the ode45 command is called to solve the differential equations for the quarter car model. Ode45 internally calls another function called 'two_dof_model' which contains the equations of motions for the quarter car model.
    - Within the 'two_dof_model' function, the equations of motion of the quarter car model are specified to find the displacements and velocities of the sprung and unsprung masses, which are grouped into an x_dot vector. This x_dot vector is integrated to give the states of the quarter car model in response to the road input. Thus, the output of the ode45 function is T and X, which represent the time in the simulation at which the positions and velocities of the quarter car model were calculated. The X matrix represents the states of the quarter car model. The first column of X is the sprung position, the second column is the sprung velocity, the third column is the unsprung position, the fourth column is the unsprung velocity, and the fifth column is the distance along the road that the quarter car model has traveled.
    - The fifth state is determined by the interpolation of the velocity of the vehicle at the variable time step, t, that the ode45 solver uses. Thus, using the uVector and the uVelocity vectors, the two_dof_model function uses interpolation to find the velocity at the 't' ode45 uses and then integrates this velocity to find the distance of the vehicle.

Once the ode45 commands iteratively solves the equation of motions of the quarter car model for every adaptive time step it uses, a variable called halfuVector is defined. This halfuVector is essentially the uVector, except that half of the spatial increment is taken for the first nonzero value and the last value of the vector. This halfuVector represents the auxiliary points located along the longitudinal road profile as defined in Chapter 3. This will result in a vector that is greater than the uVector by 1 element.

Next, a search procedure for 'NaN' is conducted. NaN stands for 'Not a number' in Matlab and the software reports this value when a solution is non-existent or infinity. The reason this search procedure is conducted is to omit the NaN's that may be generated by the overestimation of the time span for the vehicle to reach the road. For instance, the vehicle may reach the end of the road such that there are no road elevation data left to simulate, but the solver has not each the end of the time span specified. Therefore, the solver continues to solve the differential equations without road elevation data, which results in NaN. Symbolically, what occurs is that the vehicle has gone off the defined road in space. Therefore, this search is conducted to omit these data points.

Following this search, the states of the quarter car model and the times at which these states were solved at are calculated by interpolating the T and X vectors and the matrix from ode45 at the halfuVector data points. This halfuVector data points is the index defined in Chapter 3.

Once the data is obtained at the halfuVector, the same interpolation technique is used to calculate the states and times at the uVector points. These states and times are used to recalculate the tire and suspension forces at the locations of the road data elevation points (uVector).

Therefore, the outputs of the 'veh_road_simulation' are the interpolated states, times, suspension forces, and tire forces according to the locations specified by

the uVector. The interpolated states and times at the locations specified by the halfuVector, called newhalfStates, is also output.

- The suspension travel of the quarter car model from driving on the road profile is then calculated by subtracting the second column of the newHalfStates from the fourth column. Mathematically, this is subtracting the sprung position of the model from the unsprung position to obtain the suspension travel.

- Then, the change in the suspension travel is calculated by using a function called 'calculate_change_in_susp_travel'. The reason for interpolating according to the halfuVector was to estimate the suspension travel at these points. The suspension travel is also calculated at the location of the road elevation samples. This function uses these two estimates of the suspension travel to calculate the change in the suspension travel according to Equation (13). The result is that each change in suspension travel can be associated to a particular point of the road elevation vector (zRoad). The output is called deltaSuspTravel.

- Next follows another main function of the DRI algorithm. This function is called 'define_unit_impulse_response.' This function calculates the impulse response of the quarter car model through simulation of an impulse excitation. The impulse response will be used in the calculation of the fractional response coefficient.

    - The first function called within this function is called 'create_stepRoad.' Inside of this function, a step road is created according to the parameters specified earlier in the 'init_params' function. The first couple of lines in the 'create_stepRoad' function consists of identifying the number of data points (1,2,3,4, etc.) of where the end location of the road will consist of and where would the step location occurs according to the sampling interval of the road.

      For example, if the end location of the step road is 20 m and the sampling interval is 0.15 m, the round command will output 133. A +1 needs to be added to the

result in 134 points because this number represents the number of data points that form the distance. There are 133 intervals or segments, but there is always one more point than there are segments or intervals in between. The same procedure is followed to find the step location.

Next, now that the step location and the end location of the step have been defined, this range of data points is populated with the elevation of the step as defined by the stepHeight parameter in the 'init_params' function. The step road is called izRoad. The last two commands within this function consists of defining the uVector for this road and the uVectorDummy for the road (which signifies the same meaning as in the veh_road_simulation function).

- The next couple of lines within the 'define_unit_impulse_response' function look very similar to the procedure used in the 'veh_road_simulation' function. The uVelocityDummy, the estTspan, and the izRoadDummy vectors are all defined since ode45 will also be used to simulate the vehicle over the step Road created. At this point, there may be confusion as to why a step road instead of an impulse road is being simulated. More on this discussion will follow. To solve the vehicle states for the step road a similar function as in the veh_road_simulation function is used, which is called 'calc_veh_impulse_response.' This outputs T and X (as explained earlier) for the step road simulation.
- Next a uVectorTrim variable is defined, which is similar in concept to the uVector. This uVectorTrim represents a distance vector from the location at which the step occurs to the end location of the road.
- The next two lines are used to interpolate the states and times from the ode45 results at the locations specified by the uVectorTrim.
- Next, another function called 'calc_unit_impulse_response' is implemented. Within this function, the suspension travel response is calculated at the interpolated states by subtracting the sprung position from the unsprung position. This is called vehResp.

A critical step within this function is the definition of a timeDelay. This time delay will be used to obtain the same step response as the vehResp, but delayed according to the delay variable, as defined in the 'init_params' function. The time vector for the delayed step response is obtained by subtracting the delay to each of the elements in the time vector corresponding to the vehResp response, which is called timeResp. The delayed time vector that is calculated is called timeDelay.
Now, the respDelay (the delayed response) is obtained by the interpolation of the timeResp and vehResp at the locations of the timeDelay vector.

To obtain the impulse response, the respDelay (the delayed step suspension travel response) is subtracted from the vehResp (the original step suspension travel response). This results in the appropriate impulse response (since vehResp is greater than respDelay due to the offset in time).
Now that the impulse response has been calculated, the unit impulse response is calculated by the following equation.

$$I_u = \frac{I_r}{z_{step}\Delta t_{delay}}$$

As shown from the equation, the unit Impulse response is obtained by dividing the impulse response by the product of the height of the step excitation and the amount of time by which the response was delayed.

Since when the vehResp and respDelay were subtracted, one element of the respDelay could not be calculated since the interpolation command cannot interpolate outside of the time associated, the first value of the impulse is a NaN. To omit the NaN, the unitImpulse response is defined from the second point until the end.

One of the last functions that are called within this function is called the 'trim_and_smooth_impulse_response' function. The purpose of this function is to shorten the impulse response because the last portion of the response is essentially zero, but continues for large span of data points.

- Within this function, the first step is find the magnitude of the max point of the impulse suspension travel response.
- The next step is to find the last point of the suspension response that is 1 percent of the maximum value of the response.
- The response is then trimmed from the first point to the index of the last point that corresponds to 1 percent of the max value of the response.
- Next a Hanning window is applied from the last point of the trimmed response in order to smoothen the decay to zero. This avoids any abrupt omission from the impulse response. Without including the last point from the trimmed response, 98 points from the Hanning window are added to the impulse response to smoothen the response. For reference, the following equation was used to apply the Hanning window.

$$\omega(n) = I_{\min}\left(\frac{1+\cos(\pi m)}{2(N-1)}\right)$$

- Therefore the output of this function is the fully defined unitImpulseTrim response.

Now that the impulse response has been fully defined, the time vector associated with this response needs to be refined. First, the 2 points until the end of the original time vector of the original suspension travel step response is defined as the newTimeVector. Then, the first value of this time vector is subtracted from each value within this vector to make all of the times relative to the first time, which will be zero. This vector is called the timeImpulse.

Now, since 98 extra points were added due to the Hanning window, 98 points must be added to the timeImpulse such that each element in the unitImpulse response vector has an associated time.

To calculate new times, the differences between the timeImpulse elements were calculated and then all of the differences were averaged to calculate a time increment.

Next, a dummyTimeVector was created by creating 98 values of this time increment. To make the dummyTimeVector relative to the timeImpulse, a cumulative sum of the dummyTimeVector was calculated from the last time associated with the timeImpulse. The extra times was called additionalTime.

Therefore, the final time vector called, fullTimeImpulse, is the concatenation of the timeImpulse and the additionalTime vectors. The final output from the 'define_unit_impulse_response' function is the fullTimeImpulse vector and the unitImpulseTrim vector.

- The next main function is called 'calc_fractional_response_coefficient,' which calculates the fractional response coefficient using the impulse response, the change in the road elevation, the times interpolated at the halfuVector, and the times interpolated at the location of the road elevation points (zTimes). The operations of this function can be summed up by Equations (11),(22),(23), and(24).

    - Within this function, the times interpolated at the halfuVector are used for the duration of the impulse force, which is represented by Δt_i. The zTimes are used to define the absolute time at which road excitation occurs (the location of the road data elevation points). Thus, the time difference between two excitations is interpolated on the unitImpulse response calculated from the 'define_unit_impulse_response' function.
    - This 'calc_fractional_response_coefficient' function consists of two main 'for' loops. The first 'for' loop calculates the numerator of the fractional response coefficient equation. Once the internal 'for' loop is complete, the sum of the responses at the j^{th} response location is calculated.

- The second main ‘for’ loop divides each of the numerator terms calculated in the first main ‘for’ loop by the sum calculated in the first main ‘for’ loop.
- The output of this function is a matrix of fractional response coefficient values indicating the portion of the suspension travel at a particular response location due to a particular road elevation impulse excitation divided by the total suspension travel response at the particular response location from all existing excitations throughout the road profile.
- The fractional response coefficient provides a quantitative value indicating the percent contribution from an excitation to a response. The output of this function is a large square matrix of f_{ij} values. The size of the matrix depends on the number of sampled road elevation points. Therefore, a road profile with 200 sampled road elevation points would result in a 200 x 200 matrix of fractional response coefficient values. This function is the most memory intensive function of the program.

- The last function of the DRI algorithm is called ‘calc_dri.’ This function calculates the change in suspension travel per distance travelled. Essentially it divides (term by term division) the change in suspension travel vector by the halfuVector, which should be the same lengths.
  - Then, the DRI_i values are calculated by multiplying the change in suspension travel per distance travelled by the fractional response coefficient matrix values as shown in Equation (26). The result is also multiplied by 1000 to obtain the units of mm/m for the DRI values. The equation below summarizes the operation of the function (refer to Chapter 3 for further explanation of DRI significance).
  - Finally, the DRI_i values are averaged by the number of sampled road data points (i.e. the length of the change in suspension travel) to obtain the average DRI value, which in certain circumstances, will approach the IRI standard as shown in Equation (30).

Appendix E: Pseudo Damage Calculations

E.1 Normalized pseudo-fatigue damage estimate

Equation (8) is normalized by the distance of the road traveled L to obtain Equation (101). This estimation of damage is based on the previous estimates of damage [1],[2],[32].

$$P_D = \frac{C\sum_{i=1}^{k} n_i \left(F_{a_i}\right)^{-\frac{1}{b}}}{L} \tag{101}$$

In Equation (101), P_D is the calculated pseudo-fatigue damage, which is the accumulated damage per distance traveled. b is the fatigue strength exponent, which will be set to -0.2 (this is a material property) in the following pseudo damage calculations. F_{a_i} is the force amplitude cycles obtained from the rain-flow cycle counting algorithm, which is determined by the upper limit amplitude of a bin. k is the length of the amplitude vector obtained from the rain-flow counting. L is the distance of the road traveled.

E.2 Preliminary damage simulations for 5 road profiles

The pseudo fatigue damage estimate was initially calculated for 5 road profiles, each of which is summarized in Table 17. Included within the roads is a triangular pulse road profile used in ASTM E1926-08 [11] to calibrate the IRI algorithm. Each road profile was filtered by a 250 mm moving average filter. A quarter-car model with golden quarter car parameters was simulated on each of the road profiles to obtain the suspension response. A constant 80 kph velocity was used for the vehicle-terrain simulation. The road profiles (synthetic and measured) are listed in order of ascending IRI values along with the calculated suspension damage. The motivation behind this study was to observe the trends of the predicted pseudo damage estimates when compared with roads with different IRI values.

Road	ASTM IRI (m/km)	Accumulated Susp Travel (m)	Road Distance (m)	Suspension Damage per m
MNRp00d9a1909080	1.24	0.19	151.50	0.006
MNRp00d9a1909010	1.26	0.20	151.50	0.006
Pothole	2.60	0.39	151.50	0.315
Tripulse (ASTM E1926-08)	4.36	0.06	14.85	52.86
Square Bumps Road	6.75	2.71	402.20	1.50e5

Table 17. Preliminary investigation results

Figure 34 shows that the initial results do not show a direct, proportional relationship between the calculated pseudo fatigue suspension damage and the corresponding IRI of the road. This suggests that a linear assumption between damage and the IRI cannot be assumed from the IRI equation. Initially, it was implied that the since the accumulated suspension travel was proportional to the IRI, the damage associated with the IRI would also be proportional. Figure 34 suggests otherwise. The trend observed resembles the relationship shown in [1]. As shown from Table 17, the IRI and the accumulated suspension travel for the road profile named 'Pothole' are approximately twice in magnitude of the IRI and suspension travel for the 'MNRp00d9a1909010' road profile. This example shows that the IRI is directly proportional to the suspension travel for two roads that are of the same length, since the IRI doubles when the suspension travel doubles. The calculated suspension pseudo damage, however, is approximately 53 times greater in magnitude than what the vehicle encounters for the 'MNRp00d9a1909010' profile.

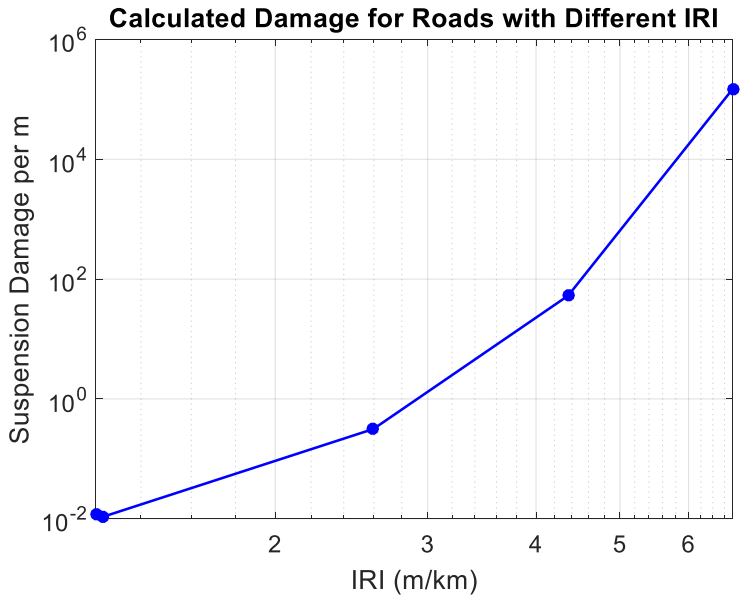

Figure 34. Damage results for road profiles shown in Table 17.

E.3 Investigation of the fatigue exponent on the calculated suspension damage

For the simulation results shown, a fatigue exponent, *b*, of -0.02 was used (typical value in the automotive industry). Depending on the magnitude of the fatigue exponent, the damage calculation will either be influenced by low or high-amplitude loads. A sweep of the inverse of the fatigue exponent ranging from 1 through 10 is shown in Figure 35 for the roads listed in Table 17. Figure 35 shows that the smaller the fatigue exponents (higher inverse) results in higher damage estimates for most of the roads with an IRI greater than 2. This can best be seen by the dashed black curve shown for the 'MNRp00d9a1909010' (IRI of 1.26) and 'Square Bumps Road' (IRI of 6.75) profiles. MNRp00d9a1909010 road was measured by the Vehicle Terrain Performance Laboratory (VTPL) at Virginia Tech and consists of relatively low-amplitude and scattered loads over a distance of 151.5m, resulting in a relatively smooth profile. On the other hand, 'Square Bumps Road', which was synthetically generated, consists of four 102 mm bumps on a flat road profile that spans approximately 403m. Thus, this road profile consists of isolated, high-amplitude loading events. Therefore, as shown in Figure 35, a higher damage estimate results for the 'Square Bumps Road' for an inverse fatigue exponent of 10 as opposed to a value of 1. At a fatigue exponent of 1, essentially all loading amplitude events are weighted equally, hence the relatively flat curve shown across all IRI values.

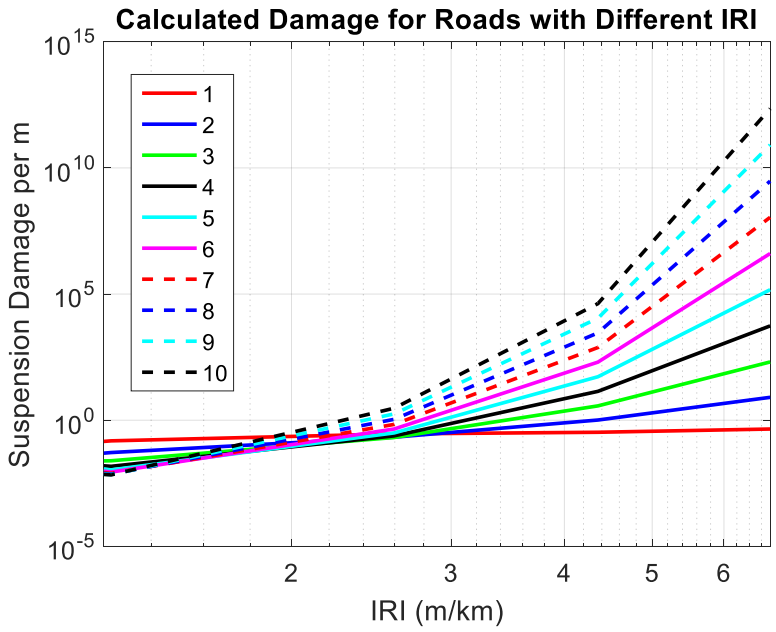

Figure 35. Damage results shown for inverted values of the fatigue exponent

E.4 Extended investigation of the correlation between damage and IRI

Further roads were used to calculate the pseudo fatigue damage. Additional roads were synthetically generated, each with distinguishing features. These additional road profiles are summarized in Table 18. Of particular interest is the road profile called 'Step Road' which consists of a long step excitation that is 102 mm high. When simulated on this road profile, the vehicle has two significant impact locations (beginning and end of the step excitation). For comparative purposes, each of the road profiles were designed the same length (approximately 402 m). All of the road profiles were pre-filtered with a 250 mm moving average filter prior to the vehicle simulation and a simulation constant speed of 80 kph was used.

Road	ASTM IRI (m/km)	Accumulated Suspension Travel (m)	Road Distance (m)	Suspension Damage per m
Step Road	1.52	0.61	402.20	37,706.1
Pothole Road	6.75	2.71	402.20	1.49e5
Sinusoidal Low Frequency	22.40	8.98	402.20	1,781.4
Sinusoidal High Frequency	42.65	17.04	402.20	62,877.8

Table 18. Additional road profiles

From Table 18, one interesting observation is that a large magnitude for the suspension damage was calculated for 'Step Road.' Despite a low accumulated suspension response and a correspondingly low IRI value, a significant amount of damage was calculated for the suspension. Other trends that were observed were that at larger IRI values, the calculated suspension damage does not proportionally increase according to the suspension travel. A visual representation of the previously simulated roads and additional roads are shown in Figure 36. Notice that the additional roads disrupt the trend observed earlier. This is due to the fact that the vehicle can endure significantly different amounts of damage for road profiles with similar IRI values. This shows that, in some cases, there does not exist a consistent correlation between the IRI (accumulated suspension travel) and the pseudo fatigue damage estimate.

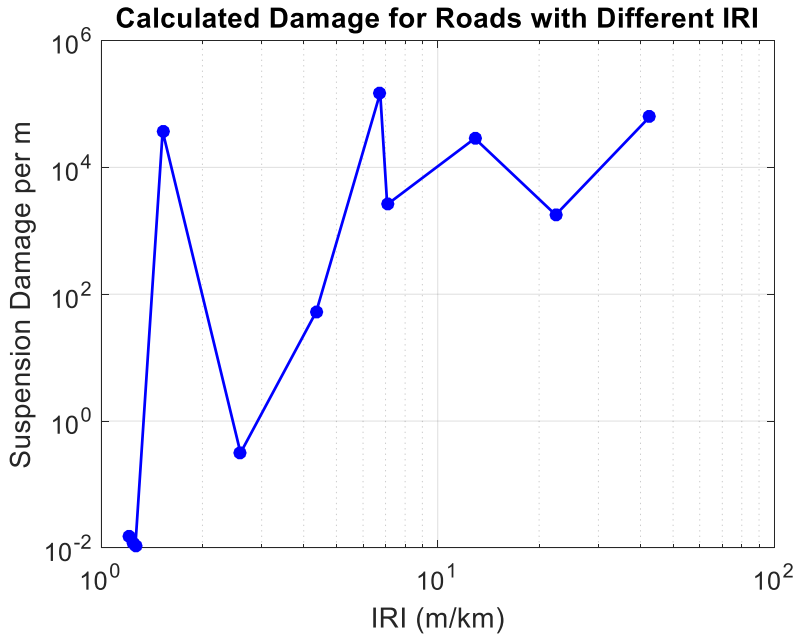

Figure 36. Extended damage results shown for an inverted value of the fatigue exponent of 5

E.4.1 Quarter car tabulated damage results

Table 19 and Table 20 show the results for the unfiltered road profiles and filtered road profiles with a moving average filter, respectively.

Road	ASTM IRI (m/km)	Accumulated Susp Travel (m)	Road Distance (m)	Susp PD per m	Spindle PD per m
MNRp00d9a1909020	1.25	0.19	151.7	0.008	0.336
MNRp00d9a1909080	1.28	0.20	151.7	0.006	0.297
MNRp00d9a1909010	1.3	0.20	151.7	0.007	0.359
Pothole	2.67	0.41	151.7	0.35	26.65
Tripulse ASTM	4.37	0.07	15	52.86	339.81
ILRaVTfac0914070	7.22	3.53	490.7	3035.7	602617.6
ILRaVTfac0914080	12.99	6.37	490.7	31322.3	748751.4

Table 19. Quarter car model simulation results (unfiltered)

From Table 19 and Table 20 one observation from results is that the pseudo damage does not increase proportionally with the IRI. For instance, in both unfiltered and filtered results for the quarter car model, the road profile named Pothole is approximately twice the IRI value as MNRp00d9a1909010. However, the suspension and spindle pseudo damage are approximately 50 and 74 times greater for the Pothole road profile, respectively. This goes to show that the accumulated suspension travel is not proportionally related to the amount of damage a vehicle may encounter since the accumulated suspension travel for the Pothole road was approximately 0.4 m, while 0.20 m of suspension travel was calculated for MNRp00d9a1909010 road.

Road	ASTM IRI (m/km)	Accumulated Susp Travel (m)	Road Distance (m)	Susp PD per m	Spindle PD per m
MNRp00d9a1909020	1.21	0.19	151.50	0.007	0.135
MNRp00d9a1909080	1.24	0.19	151.50	0.006	0.090
MNRp00d9a1909010	1.26	0.20	151.50	0.006	0.134
Pothole	2.60	0.39	151.50	0.315	8.065
Tripulse ASTM	4.36	0.06	14.85	52.86	309.5
ILRaVTfac0914070	7.08	3.45	490.5	2598.4	75,849.4
ILRaVTfac0914080	12.89	6.32	490.5	28,555.8	470,300.2

Table 20. Quarter car simulation results (filtered with 250 mm moving average filter)

For large IRI values (significantly rough road profiles), such as ILRaVTfac0914070 and ILRaVTfac0914080, the predicted pseudo damage dramatically increases due to the numerous excitations that load the suspension and spindle. For both of these road profiles, the spindle endures more damage than the suspension, especially for the unfiltered road profile. To recall, a spring follower is used for the tire model. Thus, there is no damping component that may absorb the impact from the road events. For ILRaVTfac0914070, the application of the moving average filter of 250 mm reduces the estimated pseudo damage per meter experienced by the vehicle by 8 times. As a general observation, the application of the moving average filter reduces the IRI, the suspension travel, and the predicted pseudo damage for the suspension and spindle.

E.4.2 Synthetic road profiles used in damage simulations

A second study was performed to observe which road events or characteristics of road profiles cause the most damage. Therefore, for this study, a total of 6 synthetic road profiles were generated as shown in Figure 37. The intention was to generate durability test profiles with significantly different IRI values. Each road profile is approximately 402 m (0.25 mi) long and the vehicle speed over these roads was 80 kph. The same golden quarter car parameters were used as in the previous simulations.

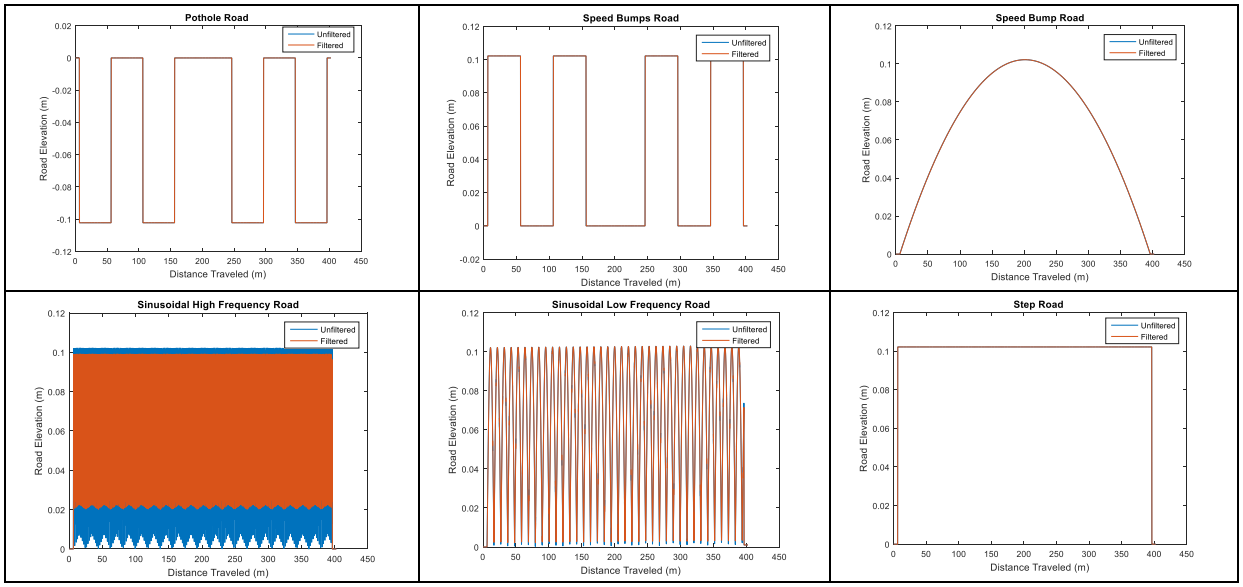

Figure 37. Synthetic road profiles

Pothole road consists of a series of 4 potholes, each 102 mm (4 in) deep. Square bumps road consists of a series of 4-102 mm high speed bumps, which is the identically the inverse of pothole road. Speed bump road consists of a long speed bump that is 102 mm high, but spans 390 meters of the profile. For the sinusoidal high frequency road profile, the 102 mm high speed bumps are positioned such that vehicle encounters the peak height of the bump every meter (3ft). For the sinusoidal low frequency road profile, the vehicle encounters the 102 mm high speed bumps every 10.4 m (34 ft). Step road is a single speed bump that spans 390 meters of the profile. For all the roads described, there are approximately 6 m of flat road before and after the main excitation. Table 21 and Table 22 show the results from the unfiltered and filtered durability-type roads.

Road	ASTM IRI (m/km)	Accumulated Suspension Travel (m)	Road Distance (m)	Susp PD per m	Spindle PD per m
Pothole Road	6.81	2.73	402.4	1.72e5	1.22e7
Square Bumps Road	6.81	2.73	402.4	1.71e5	1.22e7
Speed Bump Road	0.02	0.01	402.4	0.00	0.00
Sinusoidal High Frequency	48.33	19.30	402.4	1.08e5	8.14e7
Sinusoidal Low Frequency	22.47	9.01	402.4	1885.3	59,426.3
Step Road	1.54	0.62	402.4	42,797.1	3.07e6

Table 21. Quarter car durability simulation results (no moving average filter applied)

As shown from Table 21 and Table 22, 2 simulation sets of the road were run (one with the moving average filter applied and one without). For the filtered roads, the predicted pseudo damage estimates decreased, as expected. The road profile with the highest IRI was the sinusoidal high frequency road (42.65 m/km), which resulted in an accumulated suspension travel of 17.04 m. The road with the lowest IRI was the speed bump road, which resulted in an IRI of 0.02 m/km, indicating an overall smooth profile. No significant suspension or spindle damage was predicted for this road profile. On the other hand, the sinusoidal high frequency road resulted in the highest spindle pseudo damage. When the moving average filter was applied to this road profile, the suspension damage was reduced approximately by a factor of 2 and the spindle damage decreased by a factor of 2.7.

Road	ASTM IRI (m/km)	Accumulated Suspension Travel (m)	Road Distance (m)	Susp PD per m	Spindle PD per m
Pothole Road	6.75	2.71	402.20	1.49e5	7.30e6
Square Bumps Road	6.75	2.71	402.20	1.50e5	7.27e6
Speed Bump Road	0.02	0.01	402.20	0.00	0.00
Sinusoidal High Frequency	42.65	17.04	402.20	62,877.8	3.07e7
Sinusoidal Low Frequency	22.40	8.98	402.20	1,781.4	42,753.8
Step Road	1.52	0.61	402.20	37,706.1	1.83e6

Table 22. Quarter car durability simulation results (250 mm moving average filter applied)

E.4.3 Damage comparison of a synthetic road profile

Table 23 shows the calculated pseudo-fatigue damage estimates from the square bumps road from Figure 37. The heights of the speed bumps were varied from 12.8 mm to the originally designed height of 102.2 mm. Each of the profiles were filtered with a 250 mm moving average filter and was simulated with the golden quarter car parameters. As expected, the roughness of the road profile decreases since the suspension travel decreases. The objective of this study was to obtain road profiles with similar IRI values to view the corresponding pseudo-fatigue estimates.

Road	Bump Height (mm)	ASTM IRI (m/km)	Accumulated Suspension Travel (m)	Road Distance (m)	Susp PD per m	Spindle PD per m
Square Bumps Road	102.2	6.75	2.71	402.20	1.50e5	7.27e6
Half Square Bumps Road	51.1	3.37	1.36	402.20	4670.9	2.29e5
Quarter Square Bumps Road	25.6	1.69	0.68	402.20	150.1	7251.8
Fifth Square Bumps Road	20.4	1.35	0.54	402.20	50.1	2376.2
Sixth Square Bumps Road	17.0	1.12	0.45	402.20	20.5	946.9
Eighth Square Bumps Road	12.8	0.84	0.34	402.20	4.70	228.6

Table 23. Square Bumps Road Simulations (filtered with 250 mm moving average filter)

Of the roads tested, the quarter, fifth, and sixth square bumps road profiles have approximately similar IRI values ranging from 1.12 m/km to 1.69 m/km. Yet, the pseudo-fatigue damage estimates vary significantly, in particular the estimates for the spindle pseudo-fatigue damage.

E.4.4 Full Car (7DOF) Model Application

This investigation was conducted to show the applicability of the pseudo-fatigue damage estimate to a full car (7-DOF) model. For simplicity, the vehicle parameters were configured such that the parameters of each corner of the vehicle were scaled in a manner similar to the golden parameters used for the IRI. The vehicle parameters used for the simulations below are outlined in Table 24. Although identical parameters were used for all 4 corners, different parameters for each corner can be arbitrarily chosen.

	Corner			
Vehicle Parameters	**1 (Left Front)**	**2 (Right Front)**	**3 (Left Rear)**	**4 (Right Rear)**
Suspension Stiffness (N/m)	63300	63300	63300	63300
Suspension Damping (Ns/m)	6000	6000	6000	6000
Unsprung Mass (kg)	150	150	150	150
Tire Stiffness (N/m)	653000	653000	653000	653000

Table 24. 7-DOF vehicle corner parameters

Additional parameters of the vehicle are also are outlined in Table 25.

Vehicle Parameters	**Quantity**
Sprung Mass (kg)	1000
Wheelbase (m)	3.09
Track (m)	1.735
Ixx (kgm^2)	800
Iyy (kgm^2)	3300
Front to CoM length (m)	1.585

Table 25. 7-DOF vehicle additional parameters

Table 26 and Table 27 show the filtered road simulation results for the full car model discussed in Appendix B.3. Within the tables, under the road distance columns, there are two values. The value outside of the parenthesis signifies the actual road elevation content of the profile. However, to make sure that both axles of the vehicle cover the entire road elevation content of the original profile, the profile was extended to the distance shown in parenthesis.

This number is shown for reference purposes only since only the vehicle response for the 402.2 m (i.e. the distance outside of the parenthesis) was accounted for in the simulations. Additionally, the simulation calculates the pseudo-fatigue estimate for every corner, but for simplicity purposes, the max pseudo-fatigue damage estimate is shown on the table for a given corner. For instance, the two letters that precede the estimate signify the location of the corner of the vehicle (i.e. LF for left front).

Road	ASTM IRI (m/km)	VTPL IRI (m/km)	Road Distance (m)	Susp PD per m	Spindle PD per m
Pothole Road	6.75	5.46	402.2(405.30)	LR:8.73e4	LR:8.11e6
Square Bumps Road	6.75	5.46	402.2(405.30)	LR:8.73e4	LR:8.11e6
Speed Bump Road	0.02	0.01	402.2(405.30)	LF:0.000	LF:0.000
Sinusoidal High Frequency	42.65	40.13	402.2(405.30)	LR:5.12e4	LF:2.97e7
Sinusoidal Low Frequency	22.40	14.74	402.2(405.30)	LF: 2458.6	LF: 8.93e4
Step Road	1.52	1.35	402.2(405.30)	LR: 2.21e4	LR:2.02e6

Table 26. 7-DOF durability roads simulations

One noticeable difference in these results is the VTPL IRI. Although the standard ASTM IRI is based on a quarter car model, the VTPL IRI calculates the IRI by averaging the IRI calculated for each corner of the vehicle. Thus, for each corner, the accumulated suspension travel is divided by the distance. This averaged IRI is the VTPL IRI shown in the tables.

Road	ASTM IRI (m/km)	VTPL IRI (m/km)	Road Distance (m)	Susp PD per m	Spindle PD per m
MNRp00d9a1909020	1.21	1.01	151.7(154.6)	LF:0.003	LF:0.132
MNRp00d9a1909080	1.24	1.06	151.7(154.6)	LF:0.003	LF:0.105
MNRp00d9a1909010	1.26	1.10	151.7(154.6)	LR:0.003	LR:0.139
Pothole	2.60	2.59	151.7(154.6)	LR:0.280	LF:10.8
Tripulse ASTM	4.36	3.99	15(18.0)	LR:53.0	LR:785.0
ILRaVTfac0914070	7.08	6.66	490.7 (493.6)	LR:2878.4	LR:1.37e5
ILRaVTfac0914080	12.89	11.24	490.7 (493.6)	LR:1.97e4	LR: 9.69e5

Table 27. 7-DOF road simulations

From the 7-DOF simulation results, a similar trend is observed from the quarter car model simulations conducted previously. The pseudo-fatigue damage estimates do not increase or decrease proportionally with respect to an increase or decrease in the IRI values.

Appendix F: Implementation of Constraint Tire Model

F.1 Introduction

In this section, a constraint mode tire model proposed by Ferris and Ma is introduced [50]. This model was developed to predict the circumferential deformation of the tire and the resulting spindle force from vehicle-terrain simulations. The constraint mode tire model predicts a tire's low-frequency, nonlinear stiffness relationship. The tire is discretized into N segments that are used to model an axisymmetric and circumferentially isotropic stiffness relationship. The tire model is parameterized in a manner such that the deformation of the tire is independent of the overall stiffness of the tire and the forces imposed on the tire. Therefore, only an overall stiffness parameter and two shape parameters are necessary to parameterize the tire model.

The purpose of the constraint mode tire is to emulate the tire radial displacement and the corresponding spindle force from the terrain excitation. The tire center is adjusted, along the wheel path, until the spindle load reaches a specified constant load. One of the benefits of using the tire model is that it can be used as a morphological filter. The trajectory of the tire center is the filtered terrain profile and this filtered terrain can be used as an input into a simple tire model.

The calculated constraint modes of the tire capture the bridging and enveloping properties of the tire. These constraint modes are used to predict the tire deformation and the vertical spindle force. The objective of this model is to increase the ability to accurately predict spindle and chassis loads while maintaining the model computationally efficient. The mathematical development of the constraint tire model is discussed in [50].

F.2 Implementation of constraint tire model in simulation

The constraint mode tire model computational algorithm was restructured for ease of readability and was improved for efficiency and greater processing speed. A pseudo code of the

actual restructured code is outlined in this section for further explanation. Inputs of the constraint tire model algorithm are listed below:

- Spindle Height (zSpindle)
- K (stiffness matrix), already constructed-alpha1 and alpha2 assumed to be known from S data structure
- xRoad (the entire uVector according to the spatial increment of the sampled road points)
    - this is extended to ensure the wheel covers the road segment of interest
- zRoad (sampled road elevation heights for the entire road)
- roadPosition which is the x(5) from the states (longitudinal position of the spindle)
- nSegments (number of tire segments by which the tire discretized)
- radius (undeformed tire radius)

Outputs of the algorithm:

- Spindle Force, F

1st step: compute initial tire parameters function

Inputs: radius, nSegments, zSpindle, xRoad, zRoad

Outputs: rTire, segmentIndex, theta, xTire, zTire, zTireCenter, xTireCenter

Tasks of this function are to:

- compute the tire center in the z coordinate (zTireCenter)
    - zTireCenter=zSpindle+radius
- compute the tire center in the x coordinate (xTireCenter)
    - this is computed by the longitudinal distance of the wheel; given by the variable step ode45 uses (the 5th state)…assumed xTireCenter is the same as the road position
- compute the tire deflection (this is not being used right now)
- initialize the radial distance of each tire segment on the tire
    - set initially each one to the undeformed radius
    - called rTire
- define a tire segment index
    - increases counterclockwise
- define a theta vector corresponding to each segment as defined by the index.

    - 0 degrees is flat baseline, angle increases in counterclockwise direction
- calculate the x and z coordinate of each tire segment (these will be used to calculate the shape of the newly deformed tire)
    - xTire=xTireCenter+rTire*cos(theta)
    - zTire=zTireCenter+rTire*sin(theta)

2nd step: find the road longitudinal segments underneath the tire

Inputs: uVector,xTireCenter,radius

Outputs: xRangeIndex

Tasks of this function are to:

- find the distance behind the wheel (reach behind 1.5R)
    - a=xTireCenter-1.5*radius
- find the distance ahead of the wheel (forward 1.5R)
    - b=xTireCenter+1.5*radius
- find the indices of the xRoad (uVector) that is greater than or equal to a and less than or equal to b
- add an extra point to the beginning and the end of the indices whenever possible

3rd step: calculate the constraint modes

Tasks of this function and descriptions of the functionality of this function are to:

- Check to see if the tire is above, below, or on the road.
    - Run the function check_tire_perimeter_for_interference
        - Inputs: xRangeIndex,xRoad,zRoad,newXtire(i).matrix,newZtire(i).matrix
        - Outputs: tireContactIndex, roadContactIndex

Inside the check_tire_perimeter_for_interference function:

- Identify the indices used by the tire for the bottom quarter portion of the tire
- Discretize the road defined underneath the tire (xRangeIndex) into segments of B,D
- Discretize the tire contour for the bottom quarter of the tire in consecutive segments of A,C
- Take the first line segment defined by the tire contour and check if this line segment has an intersection within the segment defined by the xRangeIndex (B and D) along

the entire xRangeIndex segments. If the intersection is lies within the two line segments define, the intersection is good and therefore the intersection point is recorded. This means that there is interference between the tire contour and the terrain. If intersection is outside of the two line segments or bad, do not record the intersection point. One index of the tire contour is iteratively search through the xRangeIndex for an intersection point. The next iteration involves the following or consecutive tire contour index.

- Within this process the function compute_intersection(A,B,C,D) is used to compute the intersection of two lines.
  - To check if the intersection is 'good,' that is within both line segments, a separate function called check_intersection_point is executed
    - Distance formula techniques are used to check if the intersection point is within the segment boundaries
  - The compute_intersection function uses matrices and determinants to compute the intersection point. There is also a case for collinear lines.

- Now that all of the good intersection points have been identified by their x and z coordinates, determine the tire contact region.
  - The tire contact region index is determined by the indices that lie between the first most and last most intersection points
  - A road contact index is also found by finding the road indices that are greater in longitudinal position than the first intersection point and less than the last intersection point.

- Now if the tire contact index is empty, the tire is not in contact with the road for this step.
  - F=0, modeNumber=0, constraintNumber=0

    If tireContactIndex=0, this means that the tire is below the road surface.
  - F=inf, modeNumber=inf,constraintNumber=inf

    If none of these conditions are satisfied, compute the constraint modes.
- Begin the calculation of the constraint modes

- Check which tire contour indices intersect with the road portion underneath the tire
    - Check_tire_perimeter_for_interference
- Now that the specific tire contour indices have been found that interfere with the road, compute the distance from these indices to the tire center
    - Compute_tire_terrain_interference

Inside the Compute_tire_terrain_interference function:

- Create a line segment from the center of the tire (xTireCenter,zTireCenter) to the segment of the tire that is interfering (tireContactIndex).
- Create a line segment between consecutive road points. This road portion is the xRangeIndex.
- Check for the intersection of the first line segment throughout the entire xRangeIndex for good intersections. Repeat for the remaining tireContactIndex elements. This process uses the same compute_intersection function reviewed earlier to find the intersection points.
- If the intersection is good, store the x and z coordinates in a structure. The check_intersection_point function is used as reviewed earlier to verify that the intersection point is within the line segments.
- Compute the distance between the good intersection points and the tire center coordinates by using the distance formula.
- Output of this function is a structure called interference which contains the x and z coordinates of the intersection, and the distance of the intersection point to the tire center for each index/tire segment that is interfering with the terrain.

Next, the following tasks are performed:

- Proceed to calculate the 1st trial constraint mode, which is the undeformed shape of the tire (circle).

    Initially, for example, if the radius is 0.3, this represents no deformation. Therefore, the radialPosition is the original position (0.3- the output is the undeformed radius for each tire segment).

    - radialPosition= radius-constraintDeformation

- Calculate the circumferential deformation (**u**) at the tireContact indices by the following equation:
    - u=radialPosition(tireContactIndex)-interference.distance
- Out of the circumferential deformation calculated for all interfering tireContactIndices (tire segments) find the greatest u-->corresponding to the maximum circumferential deformation calculated in step 5
- Find the u index corresponding to the tireContactIndex of the maximum circumferential deformation
    - If there are multiple indices corresponding to the same deflection, sort the tireContactIndex from biggest to least. (i.e. fliplr). The output is called impingementIndex.
    - A separate data structure called activeTireIndexConstraint is formed to store the tire segment indices that cause the greatest impingement. These are therefore called the active tire constraints.
- Store the deformation caused by these active constraints tire index (indices) in an activeConstraintDeformation matrix structure
    - Radius (undeformed)-interference.distance(impingementIndex)
- Store the active tire constraints of the tireContactIndex in an activeConstraintHistory vector. These will be used in the sorting matrix.
- Create a sorting matrix (a separate function is used)
    - Inputs (number of tire segments,activeConstraintHistory)

    This matrix, after taking the transpose, lists the active constraints within the first rows and the omitted constraints after. This sorting matrix is used to reorder the stiffness matrix, such that the stiffness for the active constraints are also listed first.
- Then another function is run called calculate_coefficient_matrix, which calculates a matrix that is multiplied by the active constraints along with the sorting matrix to obtain the radial deformations for the particular constraint trial/mode (i.e. the constraint mode is calculated).

    - The calculated matrix from the calculate_coefficient_matrix function is generated from the guyan reduction.
    - This matrix is multiplied by the transpose of the transposed sorting matrix to get just [S] and is also multiplied by the active constraints deformations, and any previously active constraints if they exist.
- These radial deformations are used to calculate the new x and z coordinates for each tire segments. This is the definition of the new tire shape for the next constraint mode trial.
- If there exists significant impingement from this newly calculated tire shape, continue the constraint mode calculation iteration process. If there is no significant impingement, the iteration process ends.
    - To find the degree of impringement:
        - newZtire at the tireContactIndex is subtracted by the interference/intersection of the z coordinate computed in the compute interference function. A tolerance is specified to get it to end. A 0.001 tolerance is used.
        - Any impingement less than 0.001 in absolute magnitude is called zero. If impingement greater than this tolerance exists, the variable keepGoing is set to 1 to keep the calculation of the trial constraint modes continuing.
- The currently active constraints now are stored in the activeConstraintHistory vector to keep track of the previously active constraints in previous constraint mode trials.
- Outside of the iteration loop, the modeNumber is defined by the length of the data structure of the new tire shape (which is the same as the number of constraint trials)
- The constraint number is defined by the length of the activeConstraintHistory vector.
- Finally, calculate the tire force using the following function after the iteration ends:
    - Calculate_tire_force calculates the spindle force generated from the active constraints [50].
    - To get the vertical components from each force caused by each active constraint, the force vector obtained is multiplied by the corresponding sine of the angle of each tire segment that was active during the constraint mode

trials. The individual vertical forces are then summed to get the total force. The tire model outputs a spindle force for each step of the simulation (each horizontal or longitudinal position specified by the solver).

F.3 Preliminary spindle force estimation results

The estimation of the spindle force for a measured road profile is shown in Figure 38. The left plot of the Figure shows the elevation of the road profile and the plot on the right is the spindle load history calculated from the constraint tire model. A quarter car model was used with golden quarter car parameters at a constant speed of 80 kph.

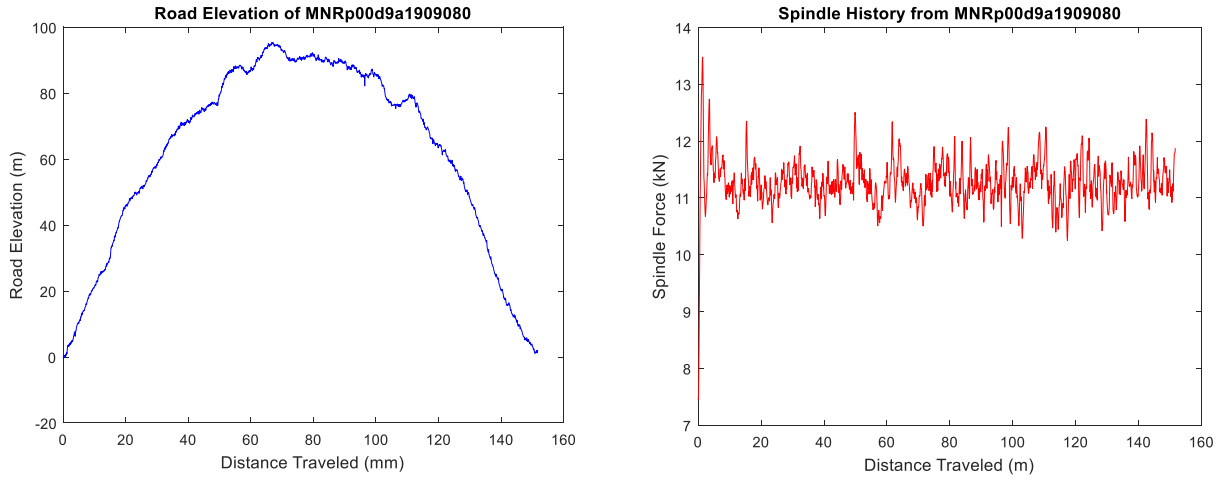

Figure 38. Estimation of spindle loads for MNRp00d9a1909080 road profile